異なる環境条件によるモルタルの細孔構造変化と劣化過程との関係

THE RELATIONSHIP BETWEEN PORE STRUCTURE CHANGE AND DETERIORATION PROCESS OF CEMENT-BASED MORTAR DUE TO THE DIFFERENT ENVIRONMENTAL CONDITIONS

異なる環境条件によるモルタルの細孔構造変化と劣化過程との関係

Nguyen Xuan Quy

Doctor of Philosophy

Division of Engineering

MURORAN INSTITUTE OF TECHNOLOGY

ABSTRACT

Service lifetime refers to the period during which a structure fulfills its performance requirements. Structures in areas that experience cold temperatures, such as Hokkaido in Japan, are exposed to freeze-thaw cycles which can cause frost damage, carbonation and reduce service lifetime. The modelling of service lifetime deterioration is the main aim of this research (Chapter 1). For this purpose (Chapter 2), the experimental program was designed in the following two series. In Series 1, mortar specimens subjected to drying conditions in the laboratory as one test set, and exposed to different natural climate conditions at three outdoor locations in 10 years as another test set. Next, in Series 2 a large tests was performed in the laboratory by adding not only different temperature but also different relative humidities and curing times. Mortar specimens were prepared using water, ordinary Portland cement, and sand. Pore structure of mortar specimens was evaluated using Mercury Intrusion Porosimetry method.

The results indicated that most of the pore structure change in the outdoor exposure test and the laboratory test showed the same tendency due to drying temperature. Test results confirmed that pore structure of mortar was coarsened and the pore volume with a diameter range of 40 to 2000 nm and 150-15000 nm were increased (Chapter 3, 4). Furthermore, this study reports evidence for the relationship between pore structure change and maturity, and an improved maturity function is proposed. The change in the pore structure is determined by the proposed maturity function, which considers the curing temperature history and the relative humidity. The relative humidity is an additional and novel factor forming the new maturity function for the prediction of pore structure change. Finally, the experimental results presented are useful information for understanding the pore structure of mortar changes due to environmental conditions.

In this study, by analyzing the influence of environmental conditions on the change of pore structure, quantifying the relationship of frost damage from pore structure change, conducting laboratory experiment and exposure to real environment, the method for forecasting frost damage deterioration calculated by ASTM equivalent cycle number including winter environment and dry condition in summer is proposed.

The service life of mortar is calculated for each region as forecasting method of frost damage by taking into consideration the effect of summer pore structure change on frost damage resistance in addition to prediction of frost damage by conventional cycle number corresponding to ASTM using the proposal of environmental indicator method (Chapter 5).

Keywords: Drying; Environmental condition; Pore Structure; Maturity; Mortar; Service Life; Frost Damage; Durability Factor; Carbonation

TABLE OF CONTENTS

LIST OF FIGURES

LIST OF TABLES

CHAPTER 1 INTRODUCTION

CHAPTER 1 INTRODUCTION

1.1. Background

Cement-based materials, such as mortar, are the most widely used building materials due to their excellent service performance. In recent years, despite the significant advances made in building material technology, the frequency of problems caused by the insufficient durability of structures is dramatically increasing.

The service life and long-term behaviour of cement-based materials are controlled by a number of transport processes in the cement-based materials pore system, (Choo and Newman 2003). Most of the changes and deterioration that occur in cement-based materials from transport processes in the pore system. The durability is also influenced or controlled by the number, type and size of pores present in the cement-based materials, (Richardson 2002). Due to the complex nature of environmental effects on cement-based materials, it is believed that controlling the nature and distribution of pores and cracks is essential. The modelling of these aspects of durability and service life has been in the background in standards and codes of practice, (Soutsos, n.d.).

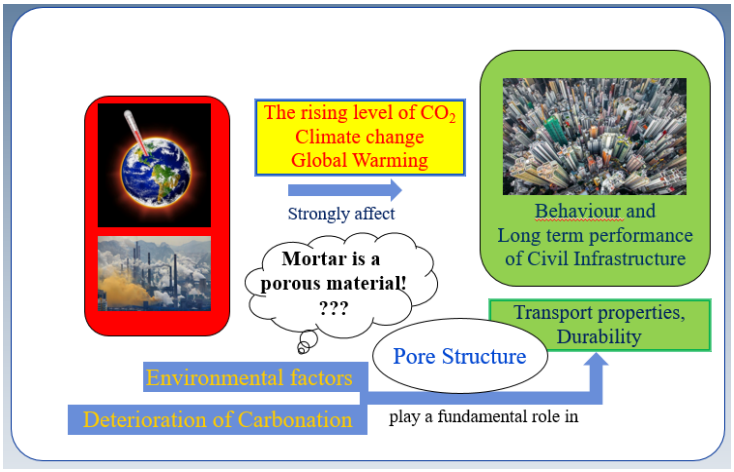

Figure 1.1 The background of research significance

The durability of the cement-based materials is basically affected by the processes involved in passing, entering or passing materials, of ions or molecules in the form of liquids and gases. Service life expectancy will depend on how fast these species can move through the materials. The radius of most ions and gas

molecules are smaller than the pores in cement-based materials, (Richardson 2002). Adoption of these potentially active organisms is primarily affected by the permeability of materials. Osmotic permeability can be defined as the ease with which an ion, molecule or liquid can move through the materials. The permeability of cement-based materials, such as carbon dioxide, is a function of the pore structure. However, the capillary pore structure is particularly significant, (P. Kumar Mehta and Paulo J.M. Monteiro 2014). These mechanisms are characterized by sorptive, permeable, and diffusible material properties, respectively. Figure 1.1 shows the cause and effect of environmental conditions change that strongly affect the behaviour and long-term performance of civil infrastructure, (Comité euro-international du béton. 1992).

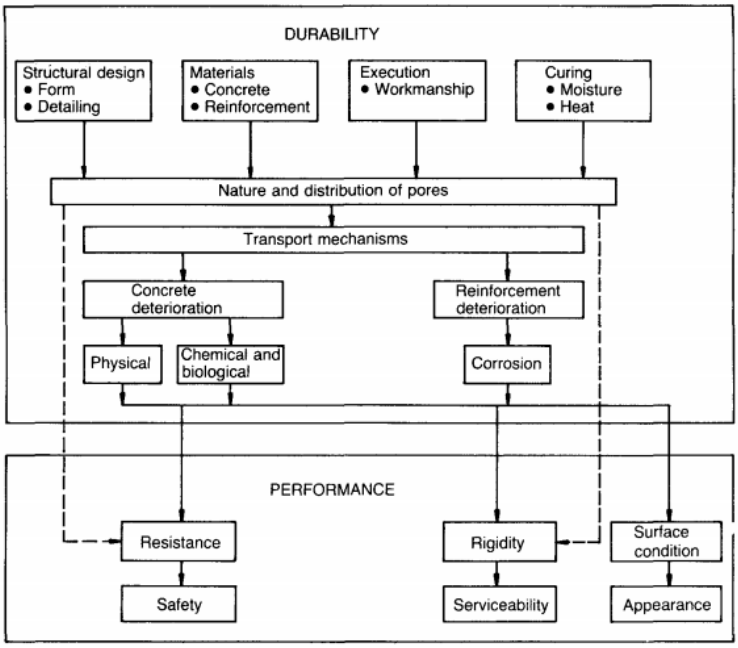

Figure 1.2 Relationship between the main factors influencing durability and performance, (Comité euro-international du béton. 1992)

Figure 1.2 shows the relationship between the main factors influencing durability and performance of cement-based materials.

A classification of pore sizes in cement-based materials is given in Table 1.1; it can be seen that the border lines between the different classes are not strict and there is an enormous range of pore sizes.

Table 1.1 Classification of pore sizes according to the general classification by IUPAC and cement-based materials science terminology, (Aligizaki 2006)

According to IUPAC, (IUPAC 1971)		According to Mehta, (P. Kumar Mehta and Paulo J.M. Monteiro 2014)		According to Mindess et al., (Mindess, Young, and Darwin 2003)		
Name	Diameter	Pore type	Size range	Name		Diameter
Micropores	<2 nm	Inter-particle space between C-S-H sheets	1-3 nm	Micropores inter layer	Gel pores	<0.5 nm
				Micropores		0.5-2.5 nm
Mesopores 2	2-50 nm			Small capillaries		2.5-10 nm
		Capillary pores (low water/cement ratio)	10-50 nm	Medium capillaries	Hollow-shell pores Capillary pores	10-50 nm
Macropores	>50 nm	Capillary pores (high water/cement ratio)	3-5 μm	Large capillaries		50 nm-10 μm
		Entrained air voids	50-1 mm	Entrained air		0.1-1 mm

Cement-based materials may deteriorate with time in an outdoor climate. Degradation can result from the environment to which it is exposed, such as carbonation or frost attack. In cold climates, damage to structures attributable to frost attack is one of the major problems, (Neville 2012). Furthermore, carbonation is the effect of carbon dioxide on cement-based materials and this phenomenon can lead to corrosion on structures. The causes of deterioration by carbonation or frost attack can be related to the pore structure of the cement-based materials. The deleterious effect depends not only on characteristics of the cement-based materials but also on the specific environmental conditions. As a result of environmental interactions the pore structure and so the properties change with time. Thus, in this study, the pore structure change by environmental conditions including temperature and humidity was carefully investigated and then established the relationship between pore structure change with carbonation and frost damage, and finally the corresponding prediction formula.

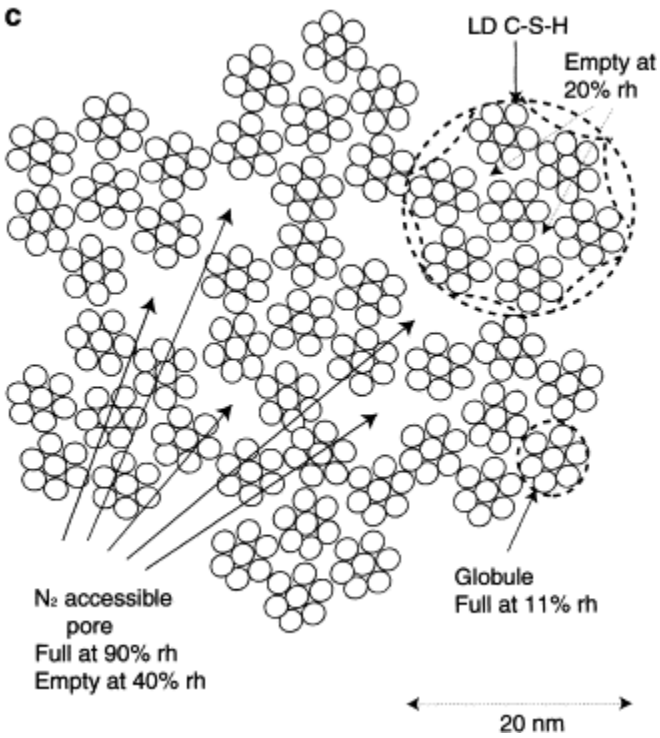

Figure 1.3 2-D schematic of C-S-H as formed by drying, (Tennis and Jennings 2000)

1.2. Service life concept

In 1997, Somerville proposed a quantitative approach to the design of structures for durability, similar to that adopted in structural design (Somerville, Glanville, and Neville 1997). He described it as an 'engineering approach' to durability design, and maintained that there were five aspects to be considered: "the predominant deterioration mechanisms which could be quantified using environmental 'loads'; performance criteria for a structure, e.g. notional service life or avoidance of deterioration; prediction models that consider the type and rate of deterioration; factors of safety that consider variability in environmental loads and the precision of models; and lastly specifications and quality assurance systems that verify compliance with the required performance". Figure 1.4 provides a schematic of the performance-based approach according to Somerville. Somerville was essentially proposing a 'performance-based' approach to durability design and specification, which should be based on quantitative predictions for durability from exposure conditions and measured material parameters. Therefore, quantitative predictions imply the ability to determine a service life, (Alexander and Thomas 2015).

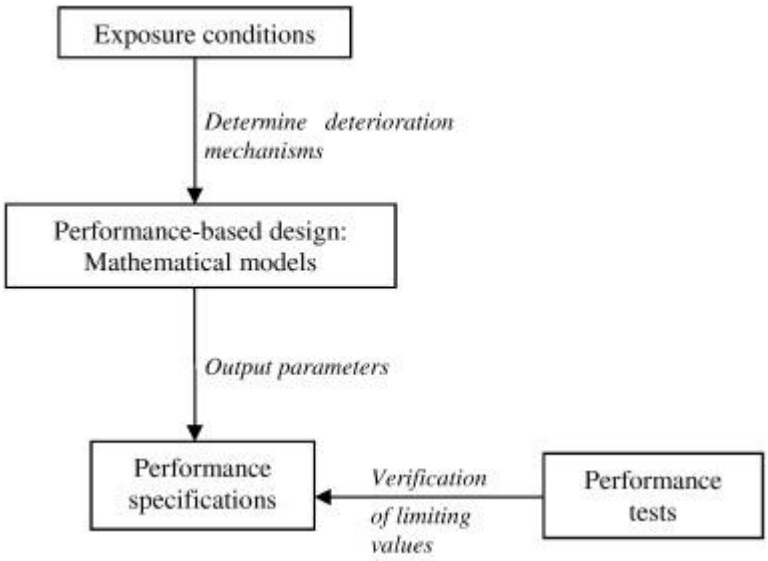

Figure 1.4 Schematic representation of the performance-based approach, (Somerville, Glanville, and Neville 1997)

Cement-based materials may have durability failures with time in an outdoor climate due to corrosion or frost attack. In special environment they may suffer from chemical attack by a reaction product absorbing water. The concept of durability is difficult to quantify because durability is not a property of a cement-based materials and need a proper definition. Service life is a quantitative concept for describing the durability of cement-based materials in which the performance of the cement-based materials must be identified and the performance requirements must be defined. The service life is defined as 'the time during which a cement-based materials fulfils its performance requirements', (Choo and Newman 2003). The definition of service life is shown in Figure 1.5.

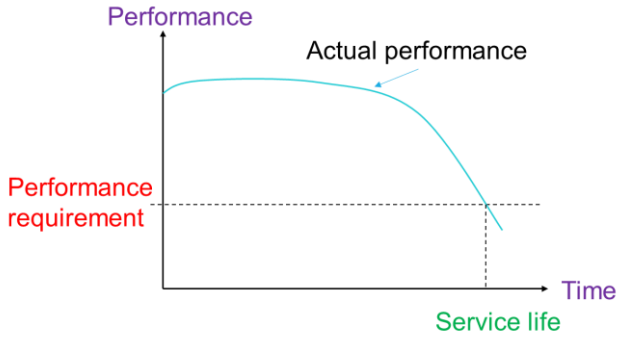

Figure 1.5 Service life design is based on predictions of future deterioration, (Choo and Newman 2003).

1.3. Problem definition

In the previous study, the volume of 40-2000 nm diameter pores changes depending on the temperature and the period, and proposes using the maturity temperature-time factor to predict performance. However, it is an empirical formula that does not take into consideration the influence of relative humidity on the maturity temperature-time factor representing 40-2000 nm diameter pore volume. In addition, the change in the volume of 40-2000 nm diameter pores differs for each water-cement ratio. Furthermore, the ambient conditions, such as the temperature and humidity during the in-laboratory drying period, might be different from actual ambient conditions in the outdoor exposure environment. In a real environment, cement-based materials age under various conditions, such as rain, high summer temperatures, and freezing temperatures in winter. Therefore, it is of great significance to evaluate the pore structure changes in outdoor exposure tests for mortar samples.

Although there are many studies related to this maturity method, they have mostly focused on strength–maturity relationships for cement-based materials; little attention has been paid to the pore structure–maturity relationships for mortar particularly. Literature on the relationship between the maturity and pore structure change is rare and little evidence is available.

Methods for predicting frost damage and change in pore structure have been proposed, but no predictive method that combines the prediction of frost damage deterioration and that of pore structure change in a real environment currently exists.

1.4. Objective and scope of this thesis

The purpose of this research is to propose an environmental indicator method, which predicts the change in durability factor based on conventional frost damage deterioration, and pore structure change in the summer; this in turn allows calculation of the service lifetime of cement-based materials. In conjunction with the proposal of environmental indicator method, an experiment that includes the relative humidity factor in the prediction of pore structure change using conventional maturity methods was conducted, and that proposes use of the modified maturity function.

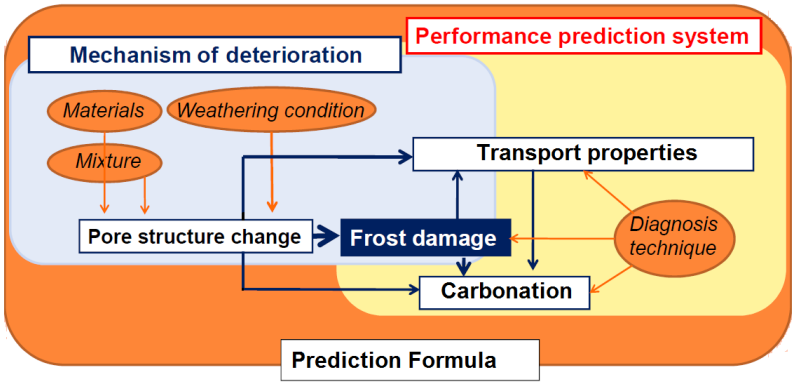

Figure 1.6 Objectives of this thesis

The main purpose of this thesis is to present a practical model for predicting service life in existing cement-based materials corespond to pore structure change due to environmental conditions. With this aim, the main objectives of the present thesis are focused on the following aspects:

- Pore structure change due to environmental conditions such as temperature, relative humidity.
- The pore size range affects the frost damage and carbonation.
- Maturity function base on temperature and relative humidity.
- The effect of pore structure change on frost resistance.
- The effect of pore structure change on carbonation.

- Cycle equivalent to ASTM using the Japanese climate data Japan Meteorological Agency from 1981 to 2000.
- The service life using meteorological indicator FD - CI for frost damage deterioration taking into consideration the influence of changes in pore structure during the summer on frost damage resistance.

1.5. Outline of this thesis

The present work is divided in six chapters. The first chapter, CHAPTER 1 is an introduction of the thesis and it summarizes the background of writing, literature review, the objectives and the aims. The second chapter, CHAPTER 2 deals primarily with the impact of the environmental conditions on the pore structure change of mortar. The third chapter, CHAPTER 3 provides the modified maturity function, which included temperature and relative humidity of environmental conditions that used the results in chapter 2 and shows the relationship between the pore structure change and frost damage. The fourth chapter, CHAPTER 4 investigates the effect of the pore size range from 150-15000 nm in diameter on carbonation due to environmental conditions. The fifth chapter, CHAPTER 5 provides the frost damage prediction method using ASTM equivalent cycle number and pore structure change, also proposes a meteorological indicator that briefly expresses the service life of each area. And the last chapter, CHAPTER 6 outlines the most important conclusions of this thesis.

A summary of the content of each chapter is presented in Figure 1.7.

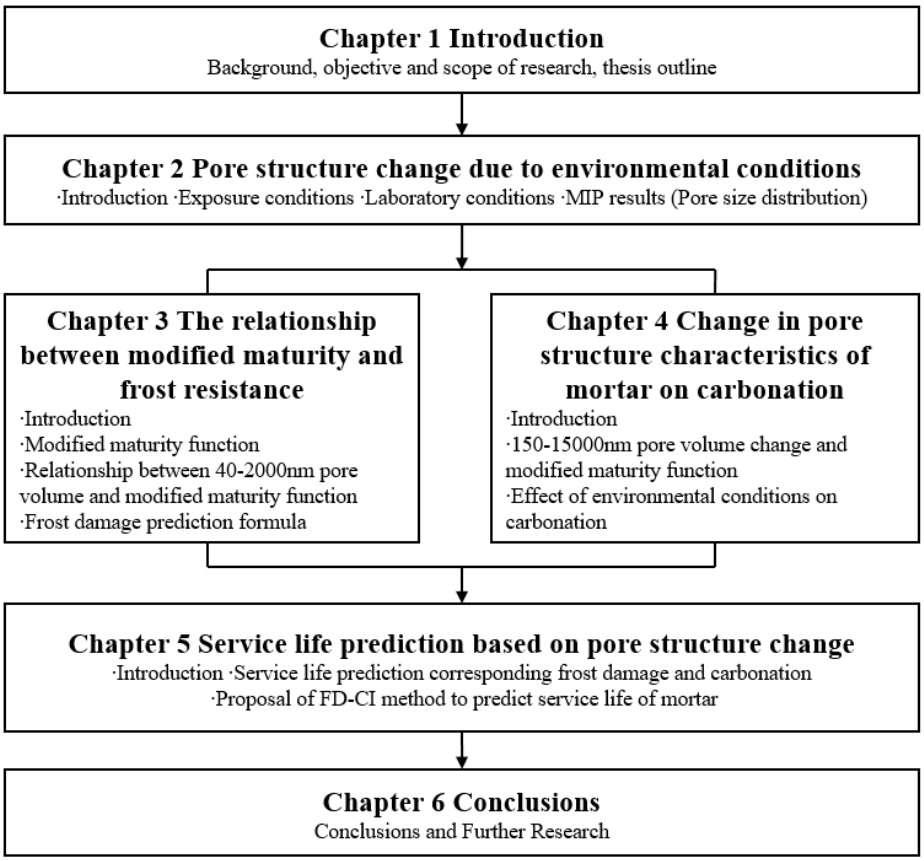

Figure 1.7 Outline of this thesis

CHAPTER 2

PORE STRUCTURE CHANGE DUE TO ENVIRONMENTAL CONDITIONS

CHAPTER 2 PORE STRUCTURE CHANGE DUE TO ENVIRONMENTAL CONDITIONS

2.1. Introduction

For a variety of reasons, pore structure has become the focus of modern building material science and has received much attention for many years. Cement-based materials are porous materials; thus, pore structure characteristics play a critical role in the engineering properties of cement-based materials [(P. Kumar Mehta and Paulo J.M. Monteiro 2014)]. Knowledge of the pore structure change is useful for exercising control on the durability properties and for predicting the deterioration behavior, such as frost damage and carbonation, of cement-based materials [(Neville 2012), (Taylor 1997)]. Figure 2.1 shows the capillary pores and macropores are particularly are the most relevant with regard to durability of cement-based materials.

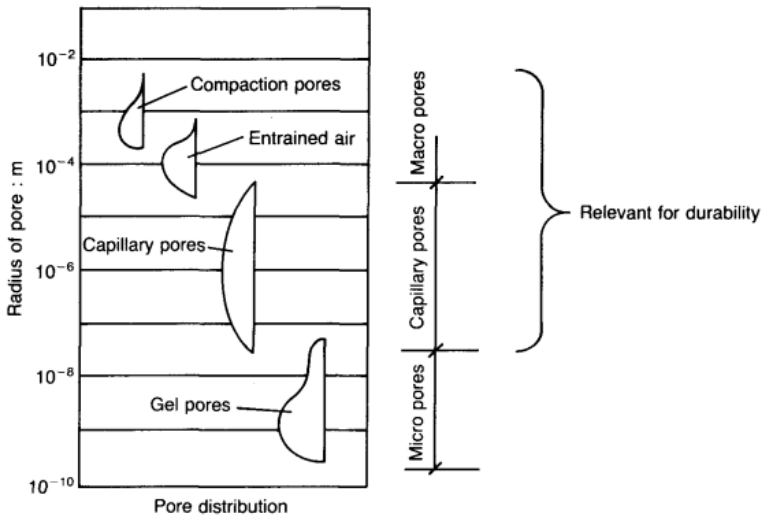

Figure 2.1 The sizes of pores in the cement paste range are particularly relevant with regard to durability, (Marchand, Pigeon, and Setzer 1997).

Much research in recent years has focused on the examination of the pore structure change of cement-based materials using the Mercury Intrusion Porosimetry (MIP) method [(Aono et al. 2007), (Atarashi et al. 2009), (Choi, Kim, and Choi 2017), (Diamond 2000), (Gallé 2001), (Gao, Wu, and Jiang 2016), (Nakamura, Hama, and Zakaria 2015), (Nakamura, Hama, and Taniguchi 2015), (Winslow and Liu 1990), which has become an important tool for studying pore structure (Aligizaki 2006), (Lamond and Pielert 2006), (Scrivener,

Snellings, and Lothenbach 2016)]. Changes in the pore structure of cement-based materials such as mortar can modify the engineering properties [(Marusin 1981), (Maruyama et al. 2017), (Parrott 1992)]. Previous results showed that the change in the pore structure of hardened cement paste is probably related to the change in the nanostructure of the C-S-H gel, which is a main constituent of the hardened cement paste [(E. Kamada et al. 1996), (Powers 1958), (Powers and Brownyard 1946)]. It was pointed out recently that the nanostructure of the C-S-H and the micro-pore structure of cement-based materials are remarkably changed by drying or drying–wetting cycles [(Chang et al. 2017), (Parrott 1981)]. In addition, the change in the micro-pore structure is due to the polymerization of silicate anions coordinated with a CaO layer developed when the C-S-H was subjected to drying [(Aono et al. 2007), (Espinosa and Franke 2006)]. In spite of these efforts, the effects of different environmental conditions on the pore structure change in the mortar are not fully understood. Moreover, the ambient conditions, such as the temperature and humidity during the in-laboratory drying period, might be different from actual ambient conditions in the outdoor exposure environment. Therefore, it is of great significance to evaluate the pore structure changes in outdoor exposure tests for mortar samples [(Tonoli et al. 2011), (S. Zhang and Zhang 2006)].

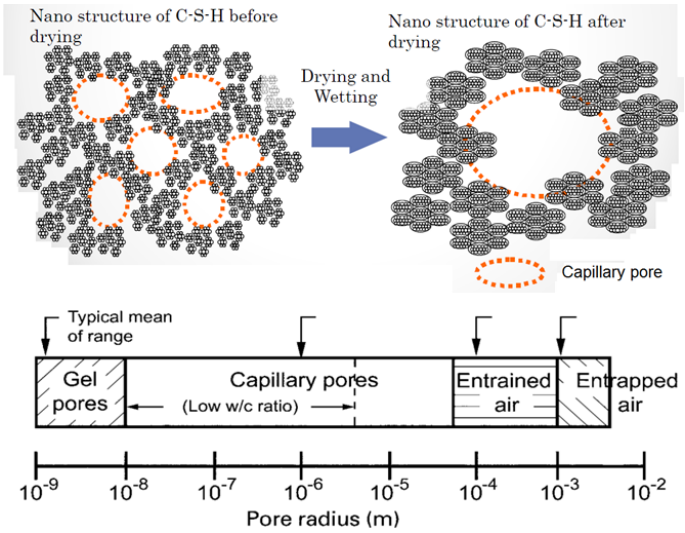

Figure 2.2 The coarsening of pore structure due to environmental conditions

The critical pore entry diameter is one of three important parameters characterizing the pore structure (which are: total percolated pore volume, threshold pore entry diameter and critical pore entry diameter) can be

determined from cumulative or differential curve of MIP results. Critical pore entry diameter is the pore diameter where the steepest slope of the cumulative curve is recorded. In the other way, critical pore entry diameter is the pore diameter corresponds to the highest peak of differential curve (see Figure 2.3).

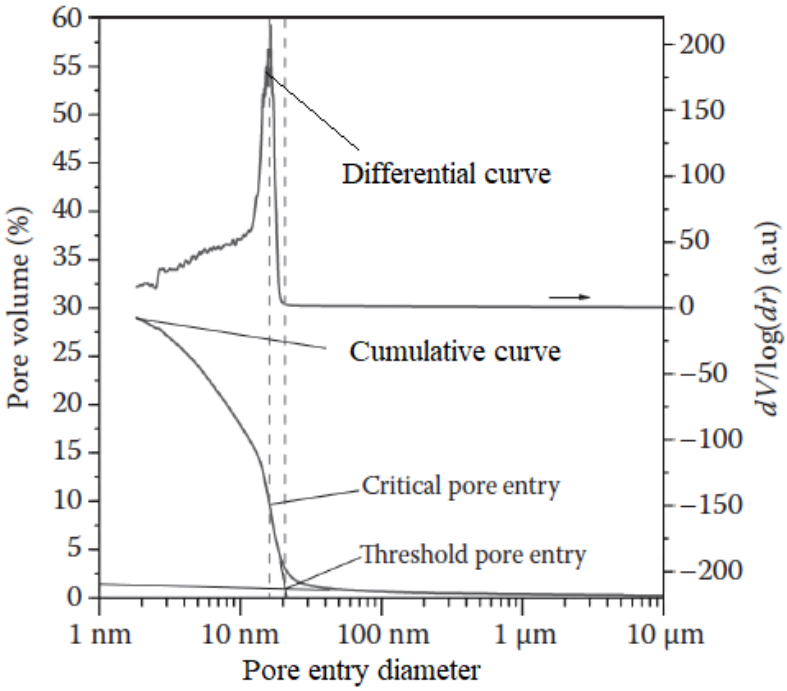

Figure 2.3 The determination of the critical pore entry diameter and threshold pore entry diameter from the cumulative and differential curve, (Scrivener, Snellings, and Lothenbach 2016).

Therefore, in this study, the influence of the environmental conditions, i.e., the temperature and relative humidity, on the pore structure of mortar is investigated. Mortar specimens were prepared and subjected to drying conditions in the laboratory and exposed to different real natural climate conditions. The experimental results show that the pore volume changed significantly due to changes in the environmental conditions.

2.2. Materials and methods

2.2.1 Materials

Ordinary Portland cement (OPC) in accordance with Japanese Industrial Standard was used to make the mortar in Series 1 and 2. The physical properties and mineral compositions are given in Table 2.1. The

mineral composition of the OPC was quantified by the X-ray diffraction (XRD) Rietveld method. The sand used as fine aggregate was obtained from a natural origin. The properties of the fine aggregates were determined as follows: the total water absorption was 1.52%, the density at a saturated and surface-dried condition (SSD) was 2698 kg/m^3, the bulk density was 1487 kg/m^3, and the fineness modulus was 2.6.

Table 2.1 Physical properties and chemical composition of OPC

Series	Specific gravity (g/cm^3)	Specific surface (cm^2/g)	Mineral composition (Rietveld) (%)				
			C_3S	C_2S	C_3A	C_4AF	Others
1	3.16	3460	60.2	16.2	4.7	5.4	13.5
2	3.15	3510	68.7	11.7	7.5	5.5	6.6

Table 2.2 shows the proportions to prepare the mortar samples in Series 1 and Series 2. In Series 1, the main mix variables were the free water-to-cement mass ratio (W/C) of 0.35 and 0.55 and the sand-to-cement ratio (S/C) of 2:1 without any chemical admixture. In Series 2, the main mix variables were W/C of 0.35, 0.45, and 0.55 and with the same S/C as that of Series 1.

Table 2.2 Mix proportions

Series	Water-cement ratio (W/C)	Sand-cement ratio (S/C)	Material contents (kg/m^3)			Flow (cm)
			Water	Cement	Sand	
1	0.35	2.0	248	709	1418	15
	0.55		342	621	1242	28
2	0.35	2.0	247	706	1412	16
	0.45		297	660	1320	23
	0.55		340	619	1238	29

2.2.2 Methods

1/ Preparation and curing of mortar specimens

The materials were mixed in a pan mixer. The cement and fine aggregate were mixed first. After the materials were uniformly dispersed, water was added and mixed until a consistent mixture was obtained.

For each mortar mixture, 40 × 40 × 160 mm prisms were cast. After casting, all the prisms were left in the casting room and covered with plastic sheeting for approximately 24 h. They were then demolded and cured in the laboratory and outdoor exposure sites according to the experimental program.

2/ Experimental program

The experimental program was designed for the following two series. In Series 1, one test set involved subjecting the mortar specimens to drying conditions in the laboratory and another test set involved exposing the specimens to different climate conditions at three outdoor locations. The experiment plan was conducted in the laboratory as shown in Table 2.4. After demolding, the specimens were cut into cubes of 40 × 40 × 40 mm and subjected to initial curing. First, the initial curing was performed in water at 20 °C for 4 weeks for all mortar specimens. Next, drying curing and drying–wetting curing were applied at 20 °C and 50 °C, respectively. In the case of drying at 50 °C in controlled chamber, different relative humidity levels (5%RH and 60%RH) were used. The 5%RH level set up by controlled chamber. The 60%RH level was performed using Potassium Iodide (KI) which is saturated salt aqueous solution, and the drying period was varied from 2 and 4 weeks as well.

Table 2.3 Saturated salt aqueous solution

	20 °C		35 °C	50 °C	
Saturated solution	CH_3COOK	NaCl	$CoCl_2$	KI	NaCl
Humidity (%RH)	23.1	75.7	61	59.9	74.9
Target of humidity (%RH)	23	75	60	60	75
Solubility (g/100g (H_2O))	269.4	35.89	53	168.8	36.67

Simultaneously, the outdoor exposure test was also performed. After 4 weeks of initial curing, the mortar specimens were exposed to different natural climate regions for 10 years at three outdoor sites in Japan: Muroran (M), Tokyo (T), and Okinawa (O) (see Figure 2.4). The latitude and longitude of M, T, and O are (42° N/141° E), (35° N/139° E), and (26° N/127° E), respectively. Muroran (a city is located in the northernmost of Japan) has a much cooler climate than Tokyo and Okinawa, long and heavy snowfalls dominate in winter. Tokyo (the Japanese capital) has the weather is temperate, hot, humid and rainy in summer; the winter is the sunniest and driest season of the year and snowfall is sporadic; sometimes can be affected by typhoons. The climate of Okinawa (southern island of Japan) is sub-tropical, with no snowfall

in winter, and long, hot, moist and rainy summers and especially is the most affected areas by typhoons. The annual mean temperature (°C) and the annual mean relative humidity (%RH) at the three outdoor sites were M (8.9 °C, 81%RH), T (16.4 °C, 60%RH), and O (23.4 °C, 71%RH). The total experimental time in Series 1 was 10 years, after which the experiments in Series 2 were performed.

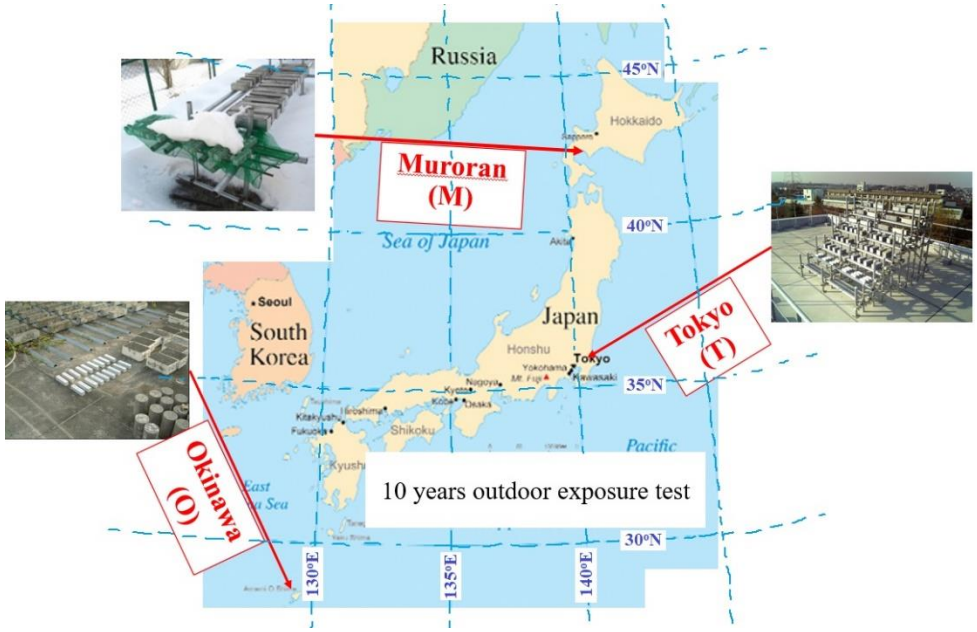

Figure 2.4 Locations of outdoor exposure test on a map of Japan.

In Series 2, the experiments were only performed in the laboratory (see Table 2.4). After demolding, the mortar specimens were cut into 40 mm cubes and subjected to the initial curing for 4 weeks at 20 °C in water. Next, the specimens were immediately placed in the secondary curing conditions in various environmental conditions for a period of 2, 4, 8, 13, or 26 weeks. In this stage, drying temperatures of 20 °C, 35 °C, and 50 °C were applied to mortar specimens; the relative humidity setting (%RH) corresponding to each drying temperature level were as follows: 23%RH, 60%RH, 75%RH, and 100%RH (in case of 20 °C); 13%RH and 60%RH (in case of 35 °C); and 6%RH, 23%RH, 60%RH, 75%RH, and 100%RH (in case 50 of °C). To reach 23%RH, 60%RH and 75%RH level, the saturated salt aqueous solutions were used: for 23%RH using Potassium Acetate (CH_3COOK); for 60%RH using Potassium Iodide (KI); for 75%RH using Sodium Chloride (NaCl). 100%RH condition was in water. The drying–wetting cycle was set at 50 °C and 6%RH for 3 days and then at 50 °C in water for 12 hours.

Table 2.4 Experimental in-laboratory plan

Series	Symbols	Initial curing	Environmental conditions after initial curing		Time interval (weeks)
			Temperature (°C)	Humidity (%)	
1	4WK	Water curing at 20 °C for 4 weeks	-	-	-
	20D-4W		20	60	4
	50DL-2W		50	5	2
	50DL-4W		50	5	4
	50DH-2W		50	60	2
	50DH-4W		50	60	4
	50DW-2W		Dry/Wet cycles (*)		2 (4cycles)
	50DW-4W				4 (8cycles)
2	20°C-23%RH	Water curing at 20 °C for 4 weeks	20	23	0, 2, 4, 8, 13, 26
	20°C-60%RH		20	60	
	20°C-75%RH		20	75	
	20°C-100%RH		20	100	
	35°C-13%RH		35	13	
	35°C-60%RH		35	60	
	50°C-6%RH		50	6	
	50°C-23%RH		50	23	
	50°C-60%RH		50	60	
	50°C-75%RH		50	75	
	50°C-100%RH		50	100	
	50°C-DW		Dry/Wet cycles (*)		

(*) 1 Dry/Wet cycle = Drying at 50 °C (5% RH) for 3 days then wetting at 50 °C for 0.5 day.

3/ Determination of pore structure

First, after curing under each environmental condition, the mortar specimens were cut into 5 × 5 × 5 mm cubes, excluding the material within 1 cm of the surface. Next, they were soaked in acetone for 24 hours immediately to stop the hydration reaction of cement and then kept in D-drying conditions for 24 hours. Figure 2.5 (a) shows the D-drying apparatus. The temperature of a dry ice–ethanol bath in the trap of this apparatus was kept at −78 °¬C, the temperature at which the water vapor pressure was about 0.5 μHg. Finally, the pore size distributions of the mortar specimens were characterized using MIP. The MIP test was performed using the Pore Master33 (U.S. Quantachrome Corp.) according to Japanese Industrial Standard (JIS R 1655) with operation pressures of up to 228 MPa, corresponding to 6 nm of minimum pore diameter. Figure 2.5 (b) shows the MIP apparatus. The contact angle between the mercury and pore wall was 140° and the surface tension of the mercury was 0.4854 N/m.

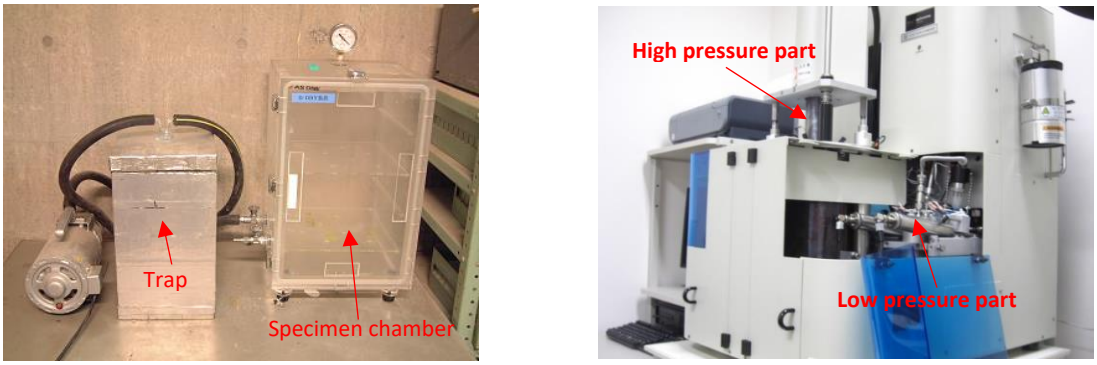

(a) (b)

Figure 2.5 Testing equipment: (a) D-drying apparatus (b) Mercury Intrusion Porosimetry (Pore Master33, U.S. Quantachrome Corp.).

MIP is a widely-used technique (Abell, Willis, and Lange 1999) for studying the distribution of pore sizes in cement-based materials, which applies Washburn's formula (Washburn 1921):

$$r = -\frac{2\sigma_m \cos\theta_m}{P}$$

Where P is the pressure; r is the capillary radius; θ_m is the contact angle between the mercury and the surface of the solid material tested; and σ_m is the surface tension of the mercury.

2.3. Effect of exposure and curing conditions on the pore size distribution of the mortar

As mentioned previously, the aim of the tests was to determine the pore size distribution using MIP. It was possible to obtain information about the pore structure change, which is observed in terms of the critical pore entry diameter of differential curves (Cook and Hover 1999). Figure 2.6 shows the curve of differential pore size distributions for OPC mortar (OPC-0.35 and OPC-0.55), which were measured at initial curing, and after 1.5, 5, and 10 years of exposure in Series 1. The pore size distribution curves of OPC-0.35 and OPC-0.55 typically exhibit at least two sharp peaks. The critical pore entry diameter corresponding to highest peak in differential curve was showed in Table 2.5. These diameter of pore increased with increasing the W/C ratio. There was a slowdown and downward trend in the increasing of the critical pore entry diameter after 5 years exposure. A clear difference can be observed for the 1.5-, 5-, and 10-year exposure testing samples (see Figure 2.6: OPC-0.35-M, OPC-0.35-T, and OPC-0.35-O, respectively). By comparing the differential curves of OPC-0.35-M and OPC-0.55-M (or OPC-0.35-T and OPC-0.55-T or OPC-0.35-O

and OPC-0.55-O, respectively) in Figure 2.6, it can be found that the highest peak is higher with increasing W/C ratio. Furthermore, the higher the temperature of the exposure area, the sharper the peak of the differential pore size distribution curves in case of OPC-0.35. The diameter envelopes and the increased pore volume show that the exposure samples have a coarser pore size than the initial curing samples. The coarsened pore structure most probably resulted from the increased temperature, as confirmed by the differences in the weather conditions of the exposure sites. The coarsening pore structure results are in general agreement with previous work (Rostásy, Weiβ, and Wiedemann 1980). The drying process causes the coarser the pore structure and a significant compression of the cement gel. In addition, the formation of large amounts of inkbottle pores due to the drying process reveals the change of the pore structure (Espinosa and Franke 2006). The amount of capillary pores, i.e, the 40-2000 nm pore size range, and the total pore volume increase mention a large coarsening of the pore structure.

Table 2.5 The change of the critical pore entry diameters

Sample	The critical pore entry diameters (nm)			
	Initial	1.5 years	5 years	10 years
OPC-0.35-M	32.19	9.19	9.64	9.83
OPC-0.35-T	32.19	43.2	46.48	145.58
OPC-0.35-O	32.19	85.03	95.22	69.2
OPC-0.55-M	62.15	57.92	155.41	162.09
OPC-0.55-T	62.15	65.64	171.81	29.06
OPC-0.55-O	62.15	153.21	195.41	205.28

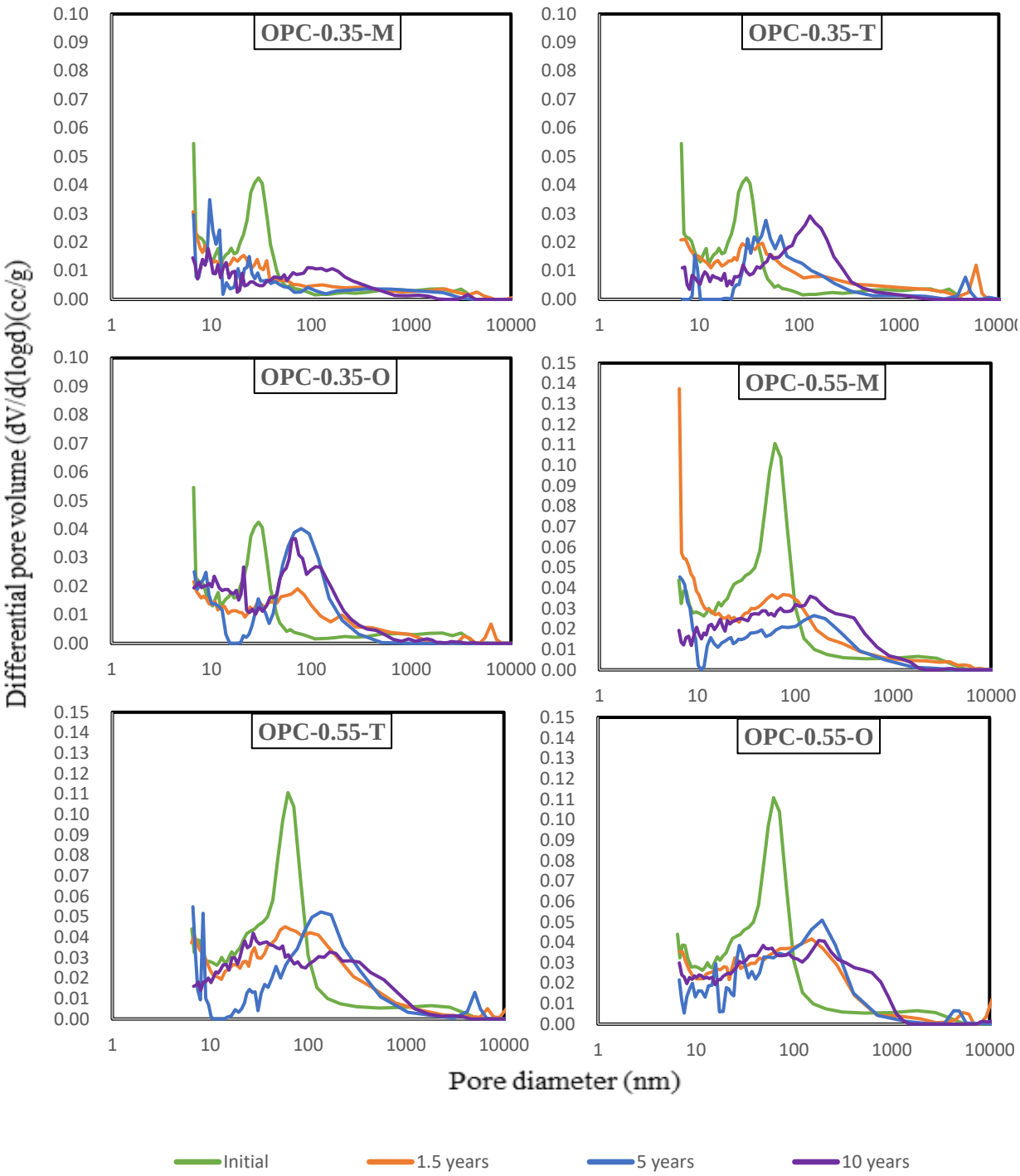

Figure 2.6 The characteristic curves of the differential pore volume as a function of pore diameter for cement-based mortars in Series 1. (Note: V is the pore volume and d is the equivalent pore diameter; OPC- identifies the cement type; 0.35 and 0.55 – are the water-to-cement ratio; M, T and O identify Muroran, Tokyo and Okinawa, respectively).

Results of the pore volume change for each pore size range are summarized in Figure 2.7. As can be seen in Figure 2.7, the effect of the curing and exposure conditions cause significant changes in the pore volume of mortar for Series 1. For OPC-0.55 mortar, the pore volumes of the 10-year exposure mortar samples (M, T, and O) are higher than in the case of initial curing only (4WK). On the other hand, the pore volume of the 10-year exposure mortar samples (M) decreases and is nearly lower than initial curing only (4WK) for OPC-0.35 mortar. Furthermore, the pore volumes of specimens OPC-0.55 and OPC-0.35, which were cured at 50 °C in the laboratory, are considerably higher than those of the 10-year exposure specimens (M, T, and O). High curing temperature does affect the pore structure change in a significant way, increasing the pore volume of large capillary pores. This effect is much more important in the range 40–2000 nm. Analysis of the incremental pore size distribution data shows that the laboratory curing mortar specimen has a much higher proportion of pore sizes with diameters in the range of 40–2000 nm than the 10-year exposure specimens (M, T, and O). The volume of these pores apparently increased with increasing W/C ratio. Previous studies [(Atarashi et al. 2009), (E. Kamada et al. 1996), (Nakamura, Hama, and Zakaria 2015), (Nakamura, Hama, and Taniguchi 2015)] have shown that the volume of pores of diameter 40–2000 nm significantly affects the mechanism of frost damage in cement-based materials. Therefore, pore sizes in this range must be taken into account when analyzing the pore structure change of cement-based materials. The change in volume of the aforementioned pores is presented in Section 3.4.

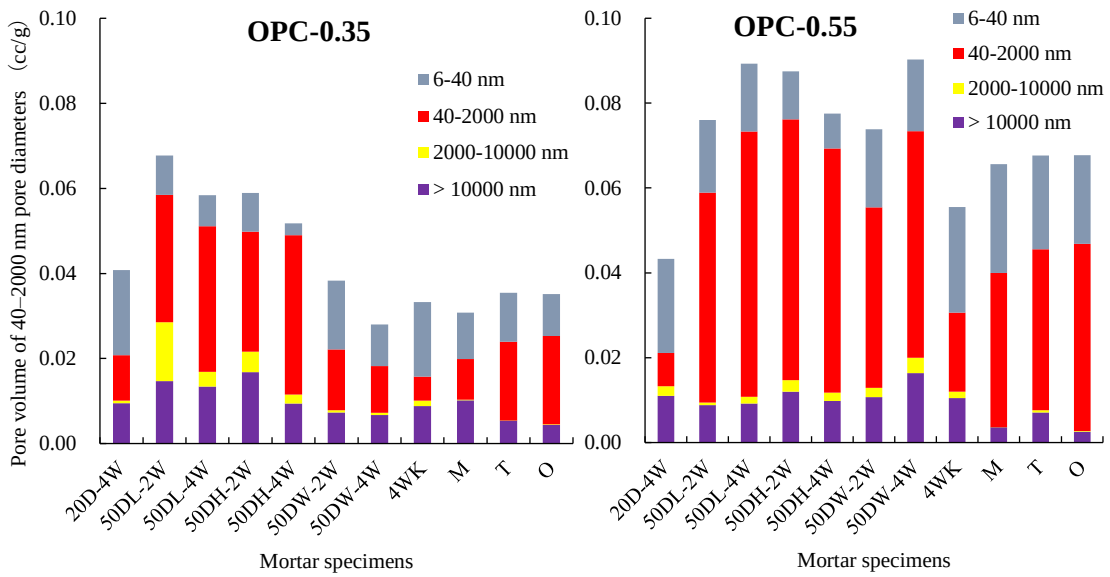

Figure 2.7 Influence of the environmental conditions on the pore volume of mortar in Series 1.

In Series 2, the effect of the relative humidity on the pore structure change was examined. Figure 2.8 shows the differential pore size distribution of mortar at 50 °C corresponding to the increase of the relative humidity. In general, the curves show the envelope of differential pore size distributions for OPC-0.35 mortars, which were measured at 0, 4, 8, 13, and 26 weeks. From the differential pore size distribution shown in Figure 2.8, the 26-w mortar presents the highest derivative peak with a pore diameter of approximately 100 nm (except for 75%RH and 100 %RH). By observing the pore size distribution, the critical pore entry diameter is found to be obviously larger, expanding from 10 nm at initial curing to 100 nm at 26-w curing. A larger critical pore entry diameter indicates that the pore is coarser. Furthermore, it is clear that the highest derivative peak strongly decreases as the relative humidity increases, especially for the 50 °C and 100%RH mortar. The results in Figure 2.8 clearly show that the highest derivative peak dropped sharply when the relative humidity reached 75%RH and it could not observe in case of in water (100%RH). It is interesting that the differential pore volume does not change in water. Based on these observations, it can be concluded that the relative humidity has a significant effect on the pore structure change of mortar. In other words, the pore structure change is a function of relative humidity. This conclusion agrees with that of other investigations (Adolphs, Setzer, and Heine 2002). The gel pores remain continuously water-filled. Furthermore, at intermediate and low relative humidity, the capillary pressure works in the water-filled pulling the pore

walls together. Beaudoin and Tamtsia (2004) pointed out that the microstructural change of C-S-H is influenced by drying at a low and intermediate humidity and the collapse of the C-S-H structure due to drying may occur (Beaudoin and Tamtsia 2004). This is the reason for the coarsening of the pore structure at lower relative humidity.

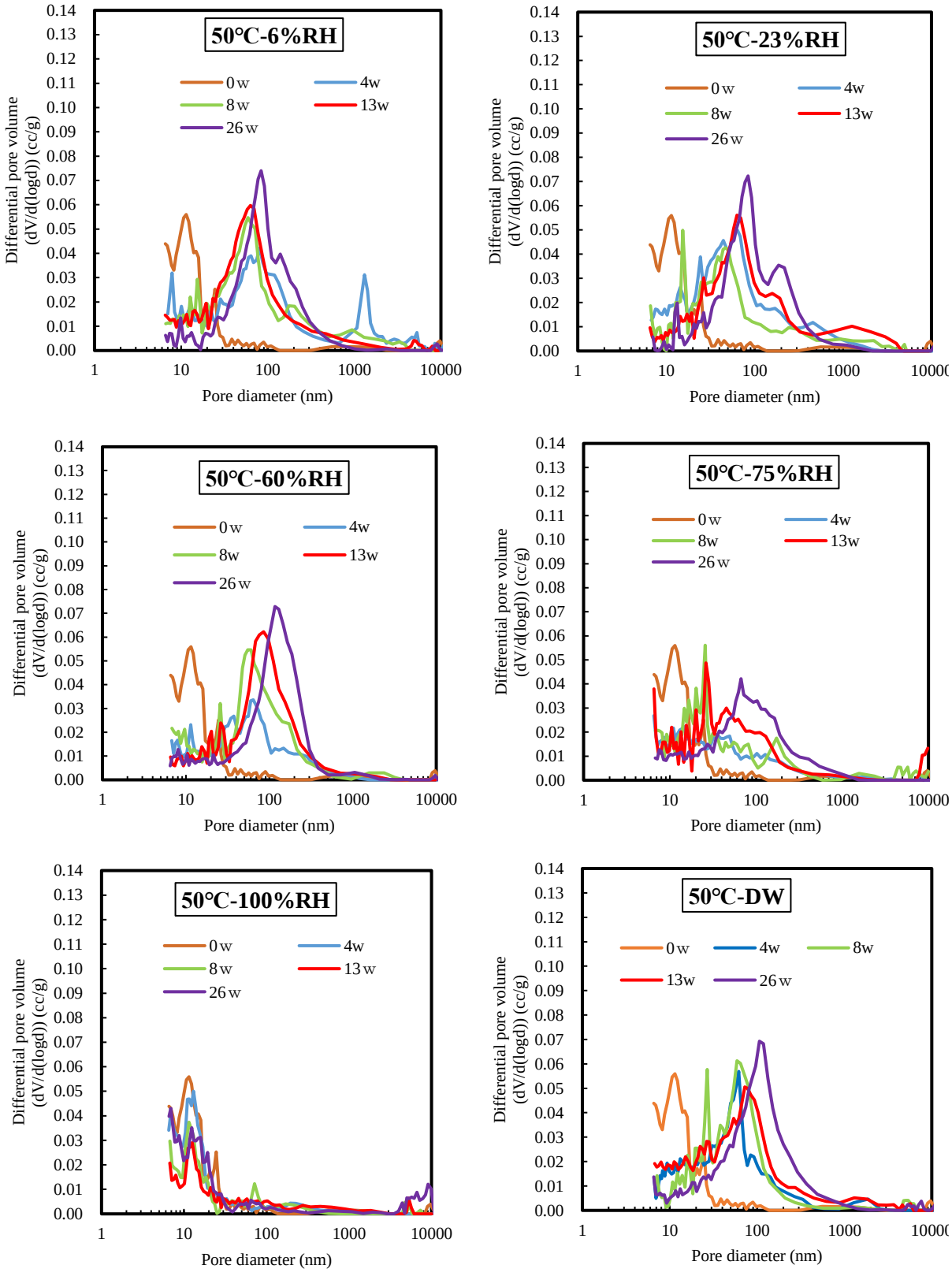

Figure 2.8 Differential pore size distribution for OPC-0.35 mortar in Series 2.

2.4. Pore structure change in the diameter range of 40 to 2000 nm due to temperature and relative humidity

First, comparing the volume of the pores of diameter 40–2000 nm in environmental conditions (PVd) and the volume of the pores of diameter 40–2000 nm in initial curing (PVi) in Series 1 shows that the change of the pore volume in the 40–2000 nm range tends to reach an upper limit due to exposure time in case of OPC-0.55 (see Figure 2.9 (b)). The significant increase rate of the changes in the pore volume for the O site samples are particularly faster than for the M and T climate exposure sites. A clear difference in the rate of volume change can be observed in the case of OPC-0.35 (see Figure 2.9 (a)). Figure 2.9 (a) shows an obviously faster rate of increase in volume change during the first 5 years of exposure, whereas the rate of increase slowed down for the following 5 years. For OPC-0.55 mortar, the pore volume of mortar in the 40–2000 nm diameter range at the O site increased by a factor of approximately 2 during the first 5 years of exposure, after which the increase significantly slowed down with almost no change for the subsequent 5 years. As such, it can be concluded that the higher the temperature, the greater the rate of pore volume change for the pore size range of 40–2000 nm. Furthermore, the pore volume in this range can reach a limiting value after long-term exposure.

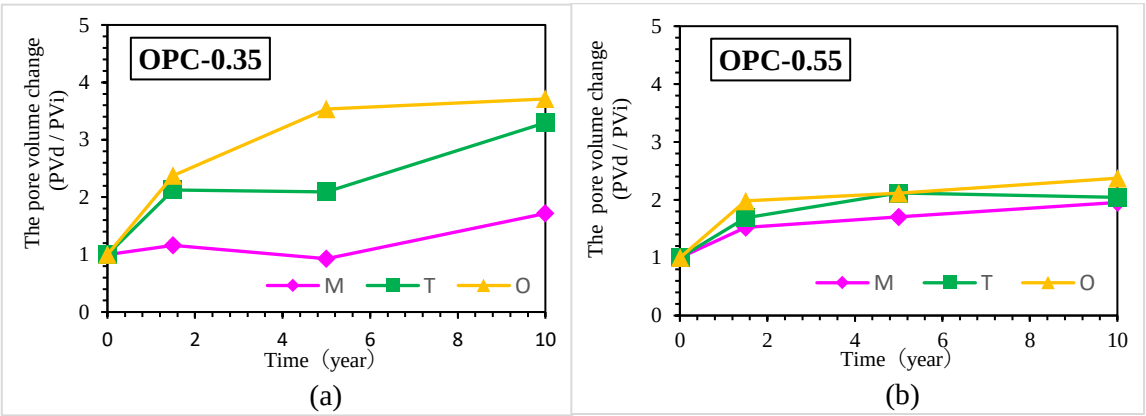

Figure 2.9 Pore volume change of the 40-2000 nm-diameter pores of mortar after 10 years of outdoor exposure in Series 1.

In addition, our results in Series 1 provide compelling evidence for the pore structure change of 40-2000 nm pore size range due to long-term exposure but they may still not be sufficient. An increase in

environmental temperature highly influences the deterioration processes of cement-based materials [(E. Bastidas-Arteaga et al. 2010), (Emilio Bastidas-Arteaga et al. 2013), (Stewart, Wang, and Nguyen 2011), (Yoon, Çopuroğlu, and Park 2007)]. The deterioration such as frost damage can be affected by the pore structure change of 40-2000 nm pore size range. The frost resistance is higher with lower amount of pore in the 40-2000 nm pore size range (E. Kamada et al. 1996). Therefore, this study provides a framework for future studies. Future work should therefore include a follow-up designed to evaluate the influence of the pore structure change of 40-2000 nm pore size range on frost resistance in the long term for different climate regions.

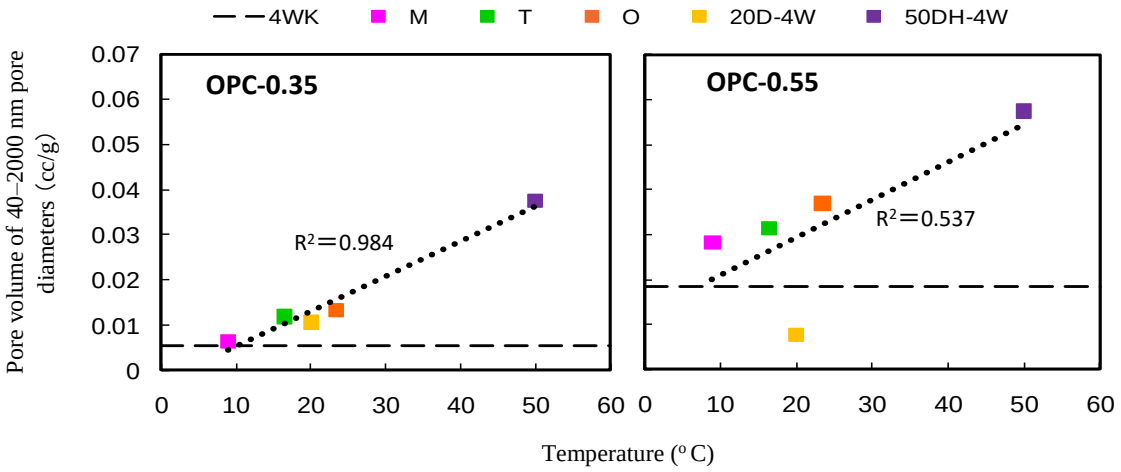

(a)

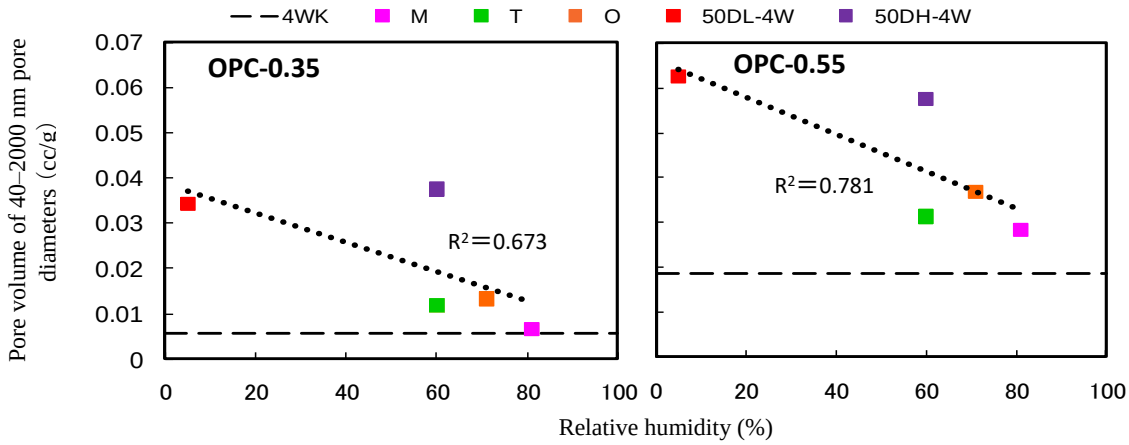

(b)

Figure 2.10 Change in pore volume of the 40-2000 nm-diameter pores due to (a) temperature and (b) humidity in Series 1.

Figure 2.10 shows the linear correlation between the change in the pore volume for 40–2000 nm pore diameters and the environmental conditions in Series 1, i.e., the temperature and relative humidity for outdoor exposure and for in-laboratory curing. Figure 2.10 also shows that there exists a meaningful correlation between the volume of pores in the 40–2000 nm diameter range and the temperature as well as between the same pore volume and the relative humidity. The tendency is clearly illustrated in Figure 2.10 (a) and (b). The linear correlation in Figure 2.10 (a) has the best fit for the experimental data. For the case of the OPC-0.35 mortar specimens, Figure 2.10 (a) indicates that the pore volume of the pores of diameter 40–2000 nm exhibits the highest correlation with the temperature, with a coefficient of determination R^2

reaching 0.984. For both OPC-0.35 and OPC-0.55, there is an upward trend in the volume of the pores of diameter 40–2000 nm with increasing temperature and increasing W/C (see Figure 2.10 (a), except for 20D-4W), which is in agreement with similar experiments performed by Nakamura et al. (2015), (Nakamura, Hama, and Zakaria 2015). However, unlike previous investigations that were only concerned about the effect of the temperature, in this study, the effect of the relative humidity on the volume of the pores of diameter 40–2000 nm is also observed. The results illustrated in Figure 2.10 (b) highlight that the pore volume decreases with an increase in the relative humidity. Alternatively, it can be anticipated that the linear correlation line may meet the 4WK line at 100%RH. Meanwhile, the volume of 40–2000 nm diameter pores does not change in water.

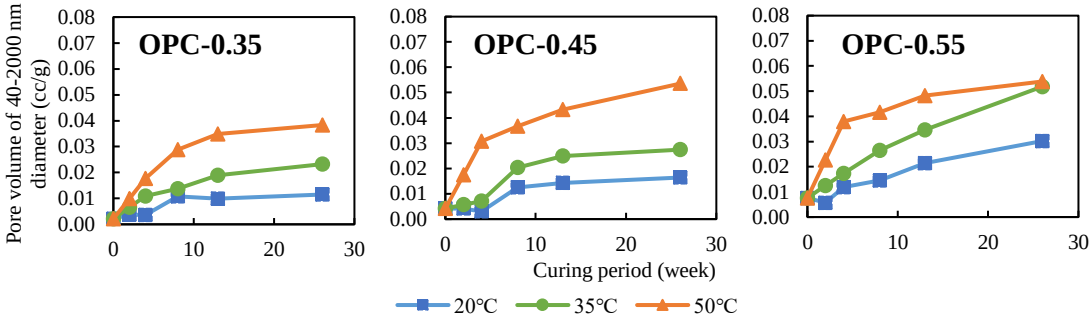

Figure 2.11 Effect of curing temperature on the pore volume of the 40–2000 nm-diameter pores of mortar in Series 2.

Finally, an interesting observation in this study is that the pore volume changes due to both temperature and relative humidity in Series 2, as shown in Figure 2.11 and Figure 2.12. The results in Figure 2.11 show that the temperature increases with increasing pore volume. In most cases, the 40–2000 nm pore volume started to increase after 2 weeks, then dramatically increased and reached the highest value, close to the upper limit, after about 13 weeks. This is similar to the trends seen in Nakamura et al. (2015), (Nakamura, Hama, and Zakaria 2015). These observations are important since they refine findings in the literature concerning the influence of temperature on the 40–2000 nm diameter pore volume. Previous studies [(Nakamura, Hama, and Taniguchi 2015), (Nakamura, Hama, and Zakaria 2015)] have identified the high drying temperature as a reason for the coarsening of pore structures. However, the results presented in this study show that the

relative humidity is another factor contributing to the coarseness of the pore structure, and as shown in Figure 2.12, this contribution can be significant. A significant difference in the pore volume change is observed, as seen in Figure 2.12, where the volume of the pores of diameter 40–2000 nm increases with decreasing relative humidity. For the 6%RH, 23%RH, 60%RH, and DW mortars, there was a very rapid increase in the pore volume after 2 weeks; the pore volume then slowly increased after 4 weeks and remained constant after about 13 weeks. The volume of the pores of diameter 40–2000 nm increased slightly for the 75%RH mortar for case OPC-0.35-50 °C. Interestingly, the pore volume does not change in most cases for the 100%RH mortar during the curing period. Therefore, the results in Figure 2.11 and Figure 2.12 show the need to consider both of relative humidity and temperature for predicting the change of pore volume of diameter 40–2000 nm pores in mortar. Based on the temperature and humidity dependency of the pore structure change, the datum humidity and datum temperature were considered.

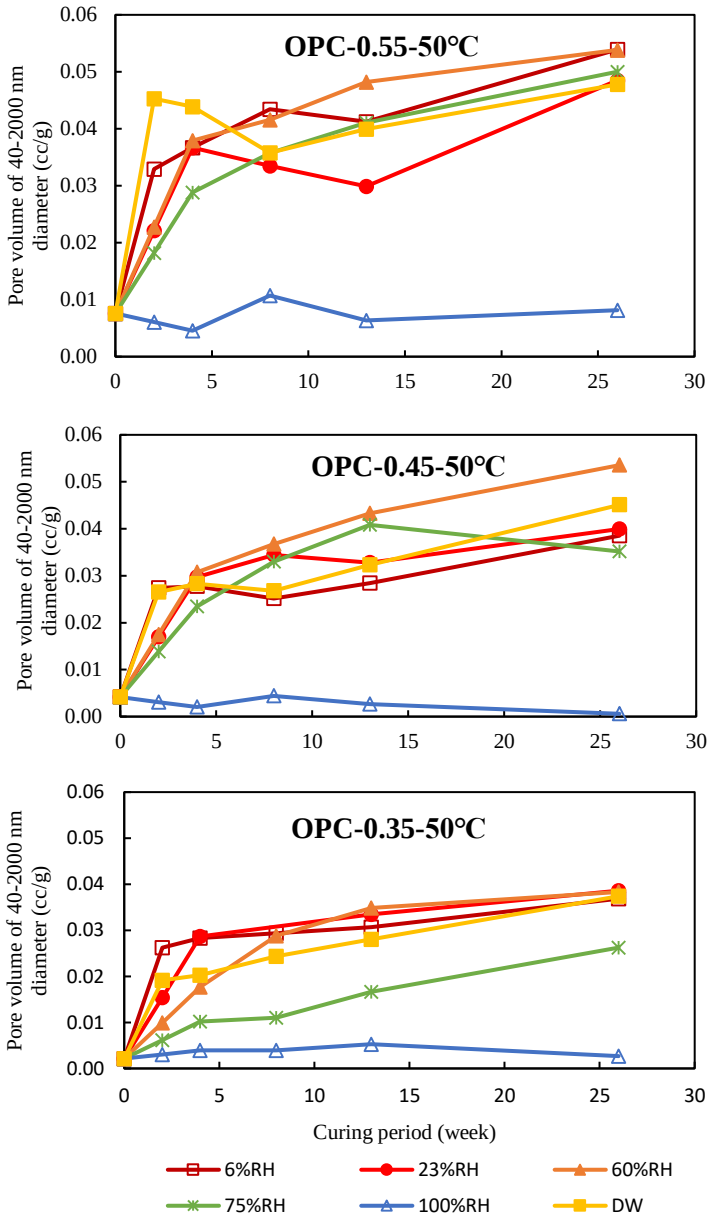

Figure 2.12 Effect of relative humidity on the pore volume of the 40–2000 nm-diameter pores of mortar in Series 2.

2.5. Conclusions

1. Both the laboratory and outdoor exposure tests revealed that the pore structure of mortar was coarsened due to temperature and relative humidity; the volume of the pores of diameter 40–2000 nm increased and reached an upper limit value.
2. The drying temperature was more critical to the coarsening of the pore structure. The influence of drying on the pore structure change at 50 °C was more severe than the effects of the outdoor exposure test on the mortar specimens.

3. The relative humidity had a significant effect on the pore structure change of mortar. The pore volume of the 40–2000 nm diameter pores increased with decreasing relative humidity. The pore volume after initial curing did not change in water content.

CHAPTER 3

THE RELATIONSHIP BETWEEN MODIFIED MATURITY AND FROST RESISTANCE

CHAPTER 3 THE RELATIONSHIP BETWEEN MODIFIED MATURITY AND FROST RESISTANCE

3.1. Introduction

The main factors affecting the pore structure change of mortar are age, relative humidity, mix proportion parameters, and curing temperature. Espinosa and Franke (2006) showed that the surface area of hardened Portland cement paste reduces after chemical aging while the pore structure becomes coarser due to the drying process, (Espinosa and Franke 2006). Adolphs et al. (2002) found that the changes in the mesoporous range (10 nm to 100 nm) of hardened cement paste exhibits a strong dependency on relative humidity (RH), (Adolphs, Setzer, and Heine 2002). Hamami et al. (2012) determined that the water-to-cement mass ratio and paste volume fraction were the main mix parameters affecting porosity, (Hamami, Turcry, and Aït-Mokhtar 2012). Moukwa and Aïtcin (1998) pointed out that the oven-drying temperature affects the pore structure of hardened cement paste by opening pores in the range of 0.02 and 0.1 μm, (Moukwa and Aïtcin 1988). The influence of heat curing on the pore structure was also identified by Reinhardt and Stegmaier (2006) and Galan et al. (2016), [(Reinhardt and Stegmaier 2006), (Galan et al. 2016)]. Furthermore, a maturity function is defined in ASTM C1074 - 11 as follows: "a mathematical expression that uses the measured temperature history of a cementitious mixture during the curing period to calculate an index that is indicative of the maturity at the end of that period", ("ASTM C1074 - 11 Standard Practice for Estimating Cement-based materials Strength by the Maturity Method," n.d.). In addition, the maturity is a function of the product of the temperature multiplied by time (ACI 116R, n.d.). As a result, it is believed that the pore structure change is closely related to the maturity function [(Nakamura, Hama, and Taniguchi 2015), (Nakamura, Hama, and Zakaria 2015)].

The term "maturity" was introduced for the first time in 1951 (Saul 1951), and is calculated from the temperature history according to the Nurse-Saul maturity function shown in Equation (1):

$$M = \sum_{0}^{t} (T - T_0)\Delta t \qquad (1)$$

where M is the maturity index (°C-days), T is the average cement-based materials temperature (°C), T_o is the datum temperature (°C), t is the elapsed time (days), and Δt is the time interval (days).

This equation also called the Nurse-Saul function. This function takes only the effect of temperature on the strength development of cement-based materials into account and has mostly been used with the cold weather concreting.

Although there are many studies related to this maturity method [(Abdel-Jawad 2006), (Carino and Tank 1992), (Galobardes et al. 2015), (Jin et al. 2017), (Liao, Lee, and Kang 2008), (Malhotra and Carino 2004), (Meneghetti and Meneghetti 1985), (Topçu and Toprak 2005), (Voigt, Sun, and Shah 2006), (Volz et al. 1981), (Xuan, Zhan, and Poon 2018), (Yikici and Chen 2015)], they have mostly focused on strength–maturity relationships for cement-based materials; little attention has been paid to the pore structure–maturity relationships for mortar particularly (Nakamura, Hama, and Zakaria 2015). Moreover, literature on the relationship between the maturity and pore structure change is rare and little evidence is available.

Based on the pore volume change of the pores of diameter 40–2000 nm, a modified maturity function that is able to predict the change in the mortar pore structure caused by environmental conditions is proposed. The results of this study strongly confirm previous predictions about the relationship between maturity and pore structure change.

Frost damage is the most serious durability issue to affect structures. This phenomenon can occur when moisture within the material freezes and expands causing deep cracks in a structure. Many studies on the frost damage deterioration of cement-based materials in real environments have been conducted. Hama et al. [(Hama, Y., Senbu, O., Tomosawa 2002), (Hama et al. 1999), (Hama, Y., Aono, Y., and Shibata 2004), (Hama, Y., Kamada, E., Han 1997)] showed that the frost resistance of high performance cement-based materials without an air-entraining admixture decreased after several years of outdoor exposure. Hasegawa et al. (Hasegawa, K. 1979) classified the risk map by calculating the frost damage risk based on external

factors (weather conditions such as freezing and thawing temperatures, freeze and thaw speed, and precipitation).

Conversely, frost damage deterioration of cement-based materials is known to depend on pore structure. According to Kamada et al. (E. Kamada et al. 1996), the greater the volume of 40-2000 nm diameter pores, the lower the frost resistance of the cement-based materials for various water-cement ratios and curing temperatures.

3.2. Materials and methods

Ordinary Portland cement (OPC) was used to make the mortar. The sand used as fine aggregate was obtained from a natural origin. The proportions to prepare the mortar samples in Series 1 and Series 2 are given in Table 2.2. In Series 1, the main mix variables were the free water-to-cement mass ratio (W/C) of 0.35 and 0.55 and the sand-to-cement ratio (S/C) of 2:1 without any chemical admixture. In Series 2, the main mix variables were W/C of 0.35, 0.45, and 0.55 and with the same S/C as that of Series 1.

3.3. Relationship between the structure change of 40-2000 nm pores and the modified maturity function

As is well known, according to the origins of the maturity method [(Nurse 1949), (Saul 1951)], maturity is calculated using the Nurse-Saul maturity equation (see Equation (1); nevertheless, this equation is only applied for the strength prediction of cement-based materials. It was suggested in the introduction that the pore structure change is closely related to the maturity function. There are very few results in the scientific literature about this relation. Nakamura et al. (2015) found an empirical formula expressing the relation between the pore structure change and the maturity, [(Nakamura, Hama, and Taniguchi 2015), (Nakamura, Hama, and Zakaria 2015)]:

$$\begin{aligned} P_d &= 0.0012\sqrt{M_p} + 0.0097 \quad \left(0 \le M_p < 598\right) \\ P_d &= 0.0391 \quad \left(M_p \ge 598\right) \end{aligned} \tag{2}$$

where P_d is the pore volume of pores with 40–2000 nm diameters after drying (cc/g) and M_p is the maturity (°C·days). M_p, which is a function of the drying temperature corresponding to the pore structure change, is given as:

$$M_p = \sum_{t=1}^{n} \left(\theta_{d,t} - 31\right)\Delta t \tag{3}$$

where $\theta_{d,t}$ is the curing temperature (°C) and t is the time (days).

The function in Equation (2) shows a strong correlation between the drying temperature and the pore structure change. Nonetheless, the maturity in Equations (2) and (3) does not include the relative humidity, as Equation (3) considers time and temperature as the only main factors. It is clear that the environmental conditions, including both temperature and humidity, strongly affect the pore structure change. The results in this study point to the need to consider the effect of relative humidity on the pore structure change as an equally major factor. This is in agreement with a study by Liao et al. (2008) in which it was concluded that the relative humidity needs to be accounted for when using a maturity function for cement-based materials strength prediction, (Liao, Lee, and Kang 2008). Therefore, it is necessary to improve these equations to establish proper and complete expressions of the pore structure change.

The correlation between the change in the volume of the pores of diameter 40–2000 nm and the modified maturity can be illustrated in general by the following formula:

$$\begin{aligned} PV_d &= \alpha\sqrt{M_{ph}} + \beta \quad \left(0 \le \sqrt{M_{ph}} < \sqrt{a}\right) \\ P_d &= \gamma \quad \sqrt{M_{ph}} \ge \sqrt{a} \end{aligned} \tag{4}$$

where α is the slope of a straight line to the upper limit, β is the initial pore volume (cc/g) value before drying, γ is the upper limit of the pore volume (cc/g), and a is an empirical constant. Based on the experimental results in Series 2, all of these parameters can be expressed by a linear equation from a linear correlation with the W/C ratio:

$$\alpha = 0.002(\frac{W}{C}) + 0.0005 \quad (5)$$

$$\beta = 0.027(\frac{W}{C}) - 0.0076 \quad (6)$$

$$\gamma = 0.0695(\frac{W}{C}) + 0.0062 \quad (7)$$

$$a = 372.4(\frac{W}{C}) + 307.67 \quad (8)$$

In this study, the modified maturity function (M_{ph}) based on the results in Series 2 was propose, which is a function of temperature and humidity, expressed as the following equation:

$$M_{ph} = \sum_{t=1}^{n} \Delta RH_t \left(\theta_{d,t} - D_t\right)\Delta t \quad (9)$$

where $\theta_{d,t}$ is the curing environment temperature (°C), D_t is the datum temperature at which the further increase of the volume of the pores of diameter 40–2000 nm does not occur (°C), t is the time (days), and ΔRH_t is the added humidity factor. ΔRH_t is:

$$\Delta RH_t = \left(H_t - \varphi_{d,t}\right) \quad (10)$$

where $\varphi_{d,t}$ is the curing environment humidity and H_t is the datum humidity at which the further increase of the volume of the pores of diameter 40–2000 nm does not occur (%RH).

The datum temperature and datum humidity in Equations (9) and (10) were obtained based on Figure 3.1. The datum temperature in Equation (9) is the temperature corresponding to the highest coefficient of determination at which the further increase of the volume of the pores of diameter 40–2000 nm does not occur, as shown in Figure 3.1 (a). The coefficient of determination was obtained by the correlation between the change in the volume of the pores of diameter 40–2000 nm and the modified maturity. It is interesting to see that the datum temperature in Equation (9) is 16 °C for all W/C cases (see Figure 3.1 (a)). Similarly, the datum humidity in Equation (10) is the humidity corresponding to the highest coefficient of determination at which the further increase of the volume of the pores of diameter 40–2000 nm does not

occur was determined for each W/C. For W/C = 0.35, 0.45, and 0.55, the datum humidity was 76%RH, 80%RH, and 83%RH, respectively (see Figure 3.1 (b)).

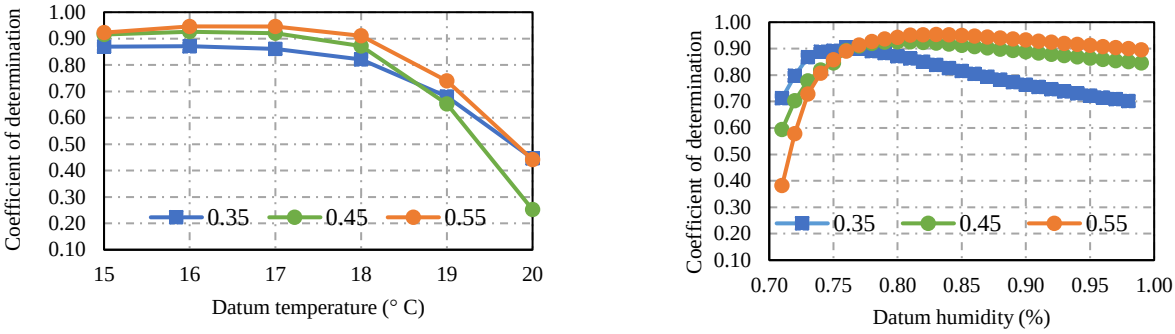

Figure 3.1 Coefficient of determination of the modified maturity formula for each datum temperature and datum humidity.

Figure 3.2 indicates the relationship between the volume of the pores of diameter 40–2000 nm and the modified maturity which as a function of temperature and relative humidity. It can be clearly seen that the line has a steep slope, which was measured over the square root of the modified maturity. An empirical formula can be obtained from the initial slope of the line, which shows a good correlation between the pore volume and the modified maturity of each W/C ratio (see Equation (4)). The volume of the pores of diameter 40–2000 nm soon reached a maximal value (the so-called upper limit), at which most of the data converges to a straight line with a different upper limit value. The higher the W/C ratio, the larger the upper limit. As can be seen from Figure 3.2, it is clear that the coefficient of determination R^2 reached a higher value with increasing W/C ratio. It can be concluded that the W/C ratio has a significant impact on the volume of the pores of diameter 40–2000 nm. In agreement with the literature [(Nakamura, Hama, and Taniguchi 2015), (Nakamura, Hama, and Zakaria 2015)], this study found that the modified maturity has a close relationship with the pore structure of mortar. The relationship between the change of volume of the pores of diameter 40–2000 nm and the modified maturity due to laboratory and exposure condition is shown in Figure 3.3. It can be seen that the correlation is good in both case of laboratory and exposure condition. The change of volume of the pores of diameter 40–2000 nm due to laboratory is higher than the change of volume of the pores of diameter 40–2000 nm due to exposure condition. Similar upward trends of the change of volume

of the pores of diameter 40–2000 nm are observed here for OPC-0.35 and OPC-0.55. Therefore, it can be understood that the pores of diameter 40–2000 nm was coarsened due to environment condition.

To sum up, the application of Equation (4) to predict the change of volume of the pores of diameter 40–2000 nm based on modified maturity and the limits of this work open new perspectives for the future work. The prediction equation of the current study investigated pore structure with only 40 – 2000 nm range. However, this pore size range strongly affects the frost resistance of cement-based materials according to Kamada (1996). Therefore, the application of Equation (4) to predict frost damage needs to be taken into consideration.

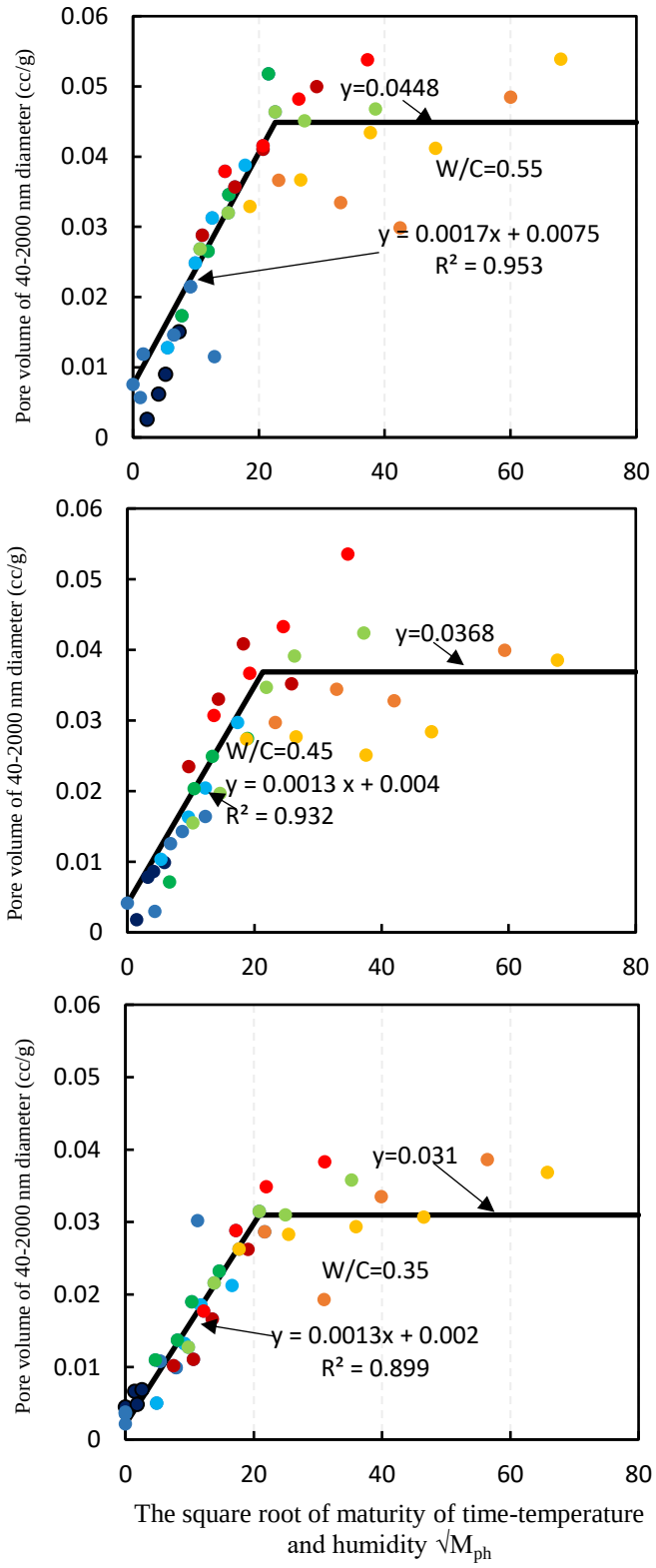

Figure 3.2 The pore volume of the 40-2000 nm-diameter pores changing as a function of the square root of the modified maturity.

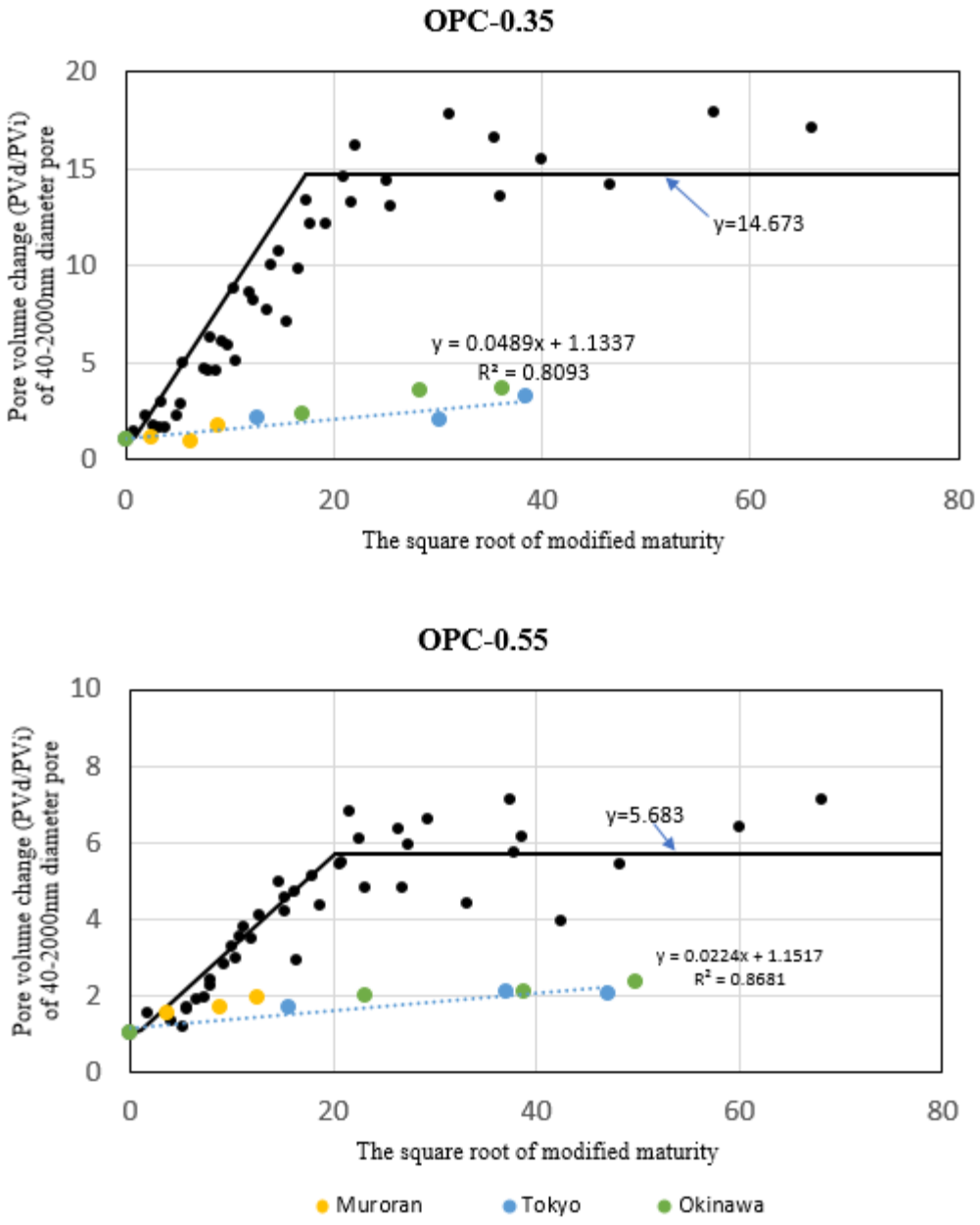

Figure 3.3 The relationship between the change of pore volume of the 40-2000 nm-diameter pores and the modified maturity of mortar due to laboratory and exposure condition. (Black dot corresponds to laboratory condition and Color dot corresponds to exposure condition)

3.4. Effect of pore structure change on frost resistance corresponding to modified maturity

In this study, the modified maturity function, that is a function of temperature and humidity, can be expressed as in Equation (11):

$$M_{ph} = \sum_{t=1}^{n} (\theta_{d,t} - D_t)(H_t - \varphi_{d,t})\Delta t \quad (11)$$

Where M_{ph} is the modified maturity function using temperature and humidity (°C.days); $\theta_{d,t}$ is the curing temperature (°C); D_t is the datum temperature at which an increase in volume of 40-2000 nm diameter pores does not occur (°C); H_t is the humidity of the curing environment (% RH); and $\varphi_{d,t}$ is the datum humidity at which an increase in pore volume does not occur.

The characteristic of pore structure change (PV_d/PV_i) is expressed as the ratio of the volume of 40-2000 nm diameter micro pore in drying condition, PV_d, to its volume after initial curing condition, PV_i, (in water at 20 ^{0}C for 4weeks). The relationship between the pore structure change (PV_d/PV_i) and the modified maturity (Mph) can be shown by a linear regression. The correlation was good in the case of the square root of modified maturity ($\sqrt{Mph}$) and natural logarithm of pore structure change ($Ln(PV_d/PV_i)$). It was found that the line of regression corresponds well to the experimental data in Figure 3.2.

$$\begin{aligned} \ln\left(\frac{PV_d}{PV_i}\right) &= w\sqrt{M_{ph}} \quad \left(0 \le \sqrt{M_{ph}} < \sqrt{b}\right) \\ &= m \qquad \left(\sqrt{M_{ph}} \ge \sqrt{b}\right) \end{aligned} \quad (12)$$

where, (PV_d/PV_i) is the pore structure change in drying condition, b is constant value.

The relationship between the volume of 40-2000 nm diameter pores, the air content-paste ratio and the durability index are represented in Equation (13); while the relationship between drying conditions and the change in pore structure is calculated with Equation (14) using the parameters obtained from the exposure test results. If the initial durability factor is DF_i, and the durability factor after drying is DF_d, the ratio of the

durability factor before and after changing the pore structure calculated from Equations (13), (14), and (15) can also be expressed as Equation (16).

$$\log(\mathrm{DF}) = -0.317 - 1.209\log(\mathrm{PV}) + 1.799\frac{\mathrm{A}}{\mathrm{P}} \tag{13}$$

$$\frac{\mathrm{PV_d}}{\mathrm{PV_i}} = 0.99\mathrm{Temp.} - 0.151\frac{\mathrm{W}}{\mathrm{B}} + 1.564\mathrm{FB} + 6.81 \tag{14}$$

$$\frac{\mathrm{DF_d}}{\mathrm{DF_i}} = \left(\frac{\mathrm{PV_d}}{\mathrm{PV_i}}\right)^{-1.209} \tag{15}$$

Where: DF is the durability factor; DF_d is the durability factor after drying; DF_i is the durability factor at initial conditions (water curing at 20°C for 4 weeks is the standard); PV is the 40 to 2000 nm diameter pore volume (cc/g); A/P is the air content-paste ratio (%); PV_i is the volume of 40-2000 nm diameter pores after initial curing (cc/g); PV_d is the volume of 40-2000 nm diameter pores after drying (cc/g); Temp. is the maximum temperature reached during the drying period (°C); W/B is the water-binder ratio (%); and FB is the cement type (N = 0, FB = 1).

By substituting Equation (12) into Equation (15), it is possible to obtain the durability factor ratio given in Equation (16).

$$\frac{\mathrm{DF_d}}{\mathrm{DF_i}} = \left(\frac{\mathrm{PV_d}}{\mathrm{PV_i}}\right)^{-1.209} = \left(exp\left(\alpha\sqrt{\mathrm{M_{ph}}}\right)\right)^{-1.209} \tag{16}$$

On the other hand, frost resistance is evaluated by durability factor. The durability factor of CIF test was calculated by the modified ASTM C666 Equation (17):

$$\mathrm{DF} = \frac{\mathrm{P} \times \mathrm{N}}{\mathrm{M}} \tag{17}$$

where, DF durability factor of the test specimen, P relative dynamic modulus of elasticity at N cycles, %, N number of cycles at which P reaches the specified minimum value for discontinuing the test or the specified number of cycles at which the exposure is to be terminated, whichever is less and M specified number of cycles at which the exposure is to be terminated.

As a result, it is clear that can predict the frost damage by the modified maturity function. In addition to the risk of frost damage in cold regions, in the high temperature dry condition mainly in summer, the initial durability index as shown in Equation (16), drops sharply as shown in Figure 3.4 as the amount of pores with a diameter of 40-2000 nm increases. Therefore, in addition to the conventional number of cycles Equivalent to ASTM, the influence of maturity is also considered as an important factor. The slope w of the equation representing the pore structure change is a linear Equation concerning the water cement ratio.

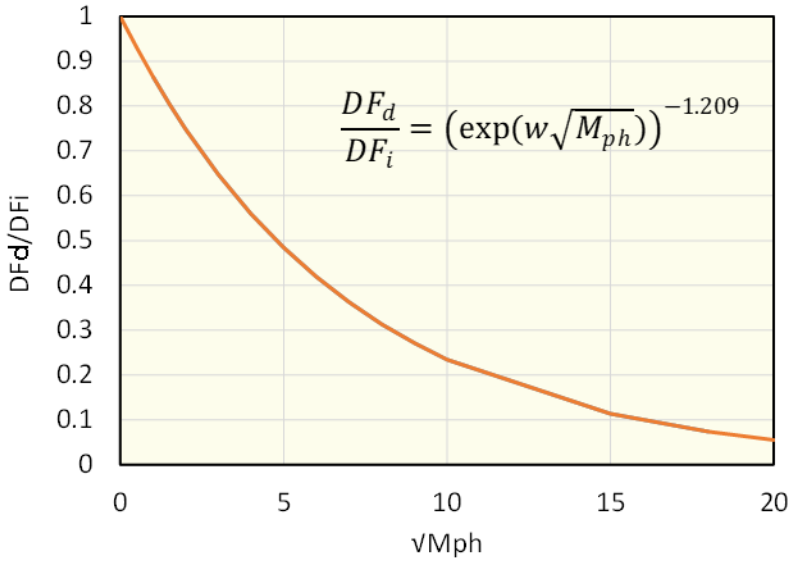

Figure 3.4 Relationship between maturity and durability index

3.5. Conclusions

Based on the experimental results of this work, the following conclusions can be drawn:

1. It was confirmed that as the drying temperature was higher, the amount of pores with diameters of 40-2000 nm increased. Regardless of the water cement ratio, the tendency of the pore structure to coarsen with the age in all curing conditions except 20 ℃ 100% RH and 50 ℃ 100% RH was confirmed.
2. The modified maturity can be use for proper and complete expression of pore struture change. Using the Equation expressing the temperature-humidity time product, it is possible to predict the amount of pores with a diameter of 40-2000 nm corresponding to the temperature, humidity and the water cement ratio.
3. Frost damage can be predicted by modified maturity corresponding to durability factor.

CHAPTER 4

CHANGE IN PORE STRUCTURE CHARACTERISTICS OF MORTAR ON CARBONATION

CHAPTER 4 CHANGE IN PORE STRUCTURE CHARACTERISTICS OF MORTAR ON CARBONATION

4.1. Introduction

Carbonation is one of the most well-discussed research topics and a common type of attack in cement-based materials, (Šavija and Luković 2016). Cement-based materials have to undergo a certain extent of carbonation reaction during their service life. The process begins when cement-based materials exposed to the environment, atmospheric carbon dioxide penetrates into the cement matrix, dissolving in the pore solution to precipitate as various forms of calcium carbonate. This reaction affects both the pore structure and durability of cement-based materials. Carbonation reaction reduces the alkalinity of cement-based materials and thus the reinforcement initiates to corrosion. Carbonation of portlandite and the C-S-H phase can result in a significant reduction of pH and in the increase of volume of calcium carbonate in the pore network. Therefore, at a certain level the the protective oxide film on the steel bars surface can be destroyed, (Ashraf 2016).

According to Borges et al., when the porosity in cement pastes is high hence the atmospheric carbon dioxide diffusion can happen, the portlandite is further depleted and the interlayer calcium from C-S-H phase also reacts with atmospheric carbon dioxide. Therefore, atmospheric carbon dioxide attack causes polymerisation in C–S–H phase, cracking and coarsening the porosity. And Borges conluded that the coarsening of the pore structure of cement-based materials related with the formation of silica gel, (Borges et al. 2010).

The pore-size distributions of cement-based materials can compare before and after carbonation by using MIP results. Ngala et al. showed that carbonation reaction changes the pore size distribution by increasing the proportion of capillary pores in the pore sizes greater than 30 nm, (Ngala and Page 1997). Temperature increase led to a significant reduction in the water retained at equilibrium and the “monomolecular layer edification of capillary condensation within a meso-porous medium” is clearly visible (Henriksen 1993) .

Therefore, carbonation of cement-based materials is one of the principal causes of deterioration can lead to corrosion of the steel bars in cement-based materials. Many studies have attempted to investigate the effect of carbonation on microstructure of cement-based materials. Moreover, in many studies the pore size range that affect the carbonation is unknown. This study aimed to investigate the variation of pore size 150-15000 nm in diameter and carbonation resistance in mortar subjected to environmental conditions and exposure times. This pore size range is within the capillary pores types.

4.2. Materials and method

Ordinary Portland cement (OPC) and the sand used as fine aggregate was obtained from a natural origin were used to make the mortar. The properties of the fine aggregates were determined as follows: the total water absorption was 1.52%, the density at a saturated and surface-dried condition (SSD) was 2698 kg/m^3, the bulk density was 1487 kg/m^3, and the fineness modulus was 2.6. Table 4.1 shows the proportions to prepare the mortar samples. The main mix variables were W/C of 0.35, 0.45, and 0.55 and the sand-to-cement ratio (S/C) of 2:1 without any chemical admixture.

Table 4.1 Mix proportions

Water-cement ratio (W/C)	Sand-cement ratio (S/C)	Material contents (kg/m^3)			Flow (cm)
		Water	Cement	Sand	
0.35	2.0	247	706	1412	16
0.45		297	660	1320	23
0.55		340	619	1238	29

The pore size distributions of the mortar specimens were characterized using the Mercury Intrusion Porosimetry. The Mercury Intrusion Porosimetry test was performed using the Pore Master33 with operation pressures of up to 228 MPa, corresponding to 6 nm of minimum pore diameter.

4.3. Pore structure change of 150-15000 nm pores diameter

4.3.1 Effect of temperature on the pore structure change of 150-15000 nm pores diameter

Figure 4.1, Figure 4.2, Figure 4.3, Figure 4.4 show the relationship between the diameter of 150-15000 nm for each water-cement ratio and the curing period in different temperature conditions.

The influence of the temperature on the relationship between the diameter of 150-15000 nm pore and the curing period was confirmed. The overall tendency is that the higher the temperature, the larger the diameter of pore diameter 150-15000 nm. In underwater curing, the amount of pores with a diameter of 150-15000 nm has not changed due to period, regardless of temperature (see Figure 4.2, Figure 4.3, Figure 4.4).

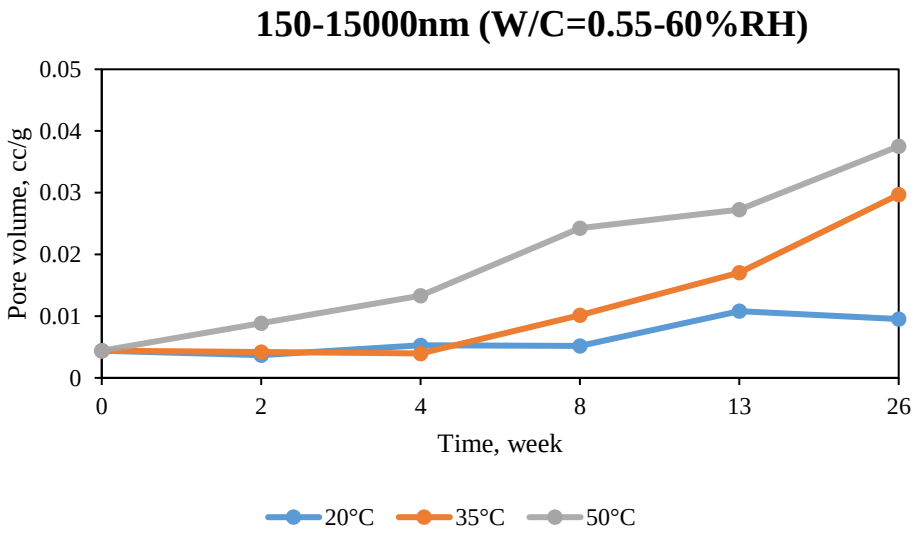

Figure 4.1 Relationship between pore volume diameter 150-15000 nm and curing period in case of 60%RH

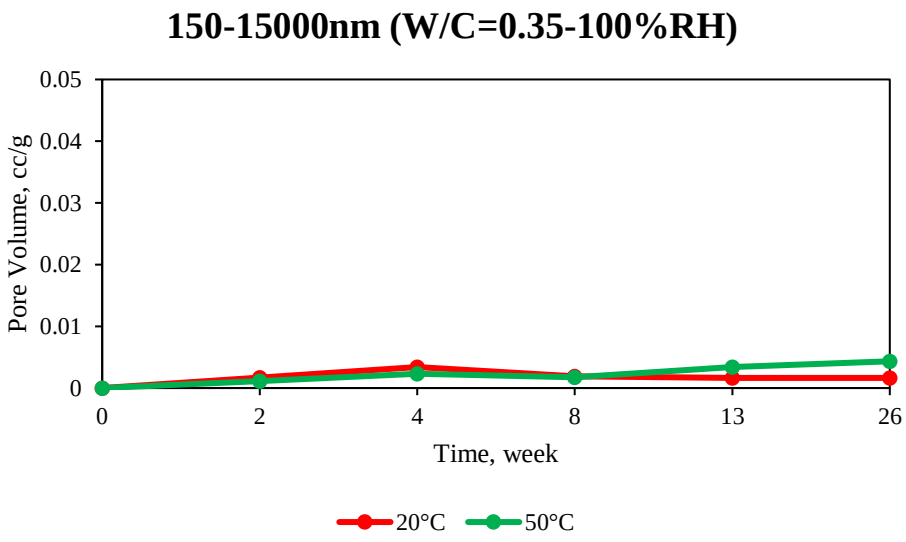

Figure 4.2 Relationship between pore volume diameter 150-15000 nm and curing period in case of OPC0.35 in water

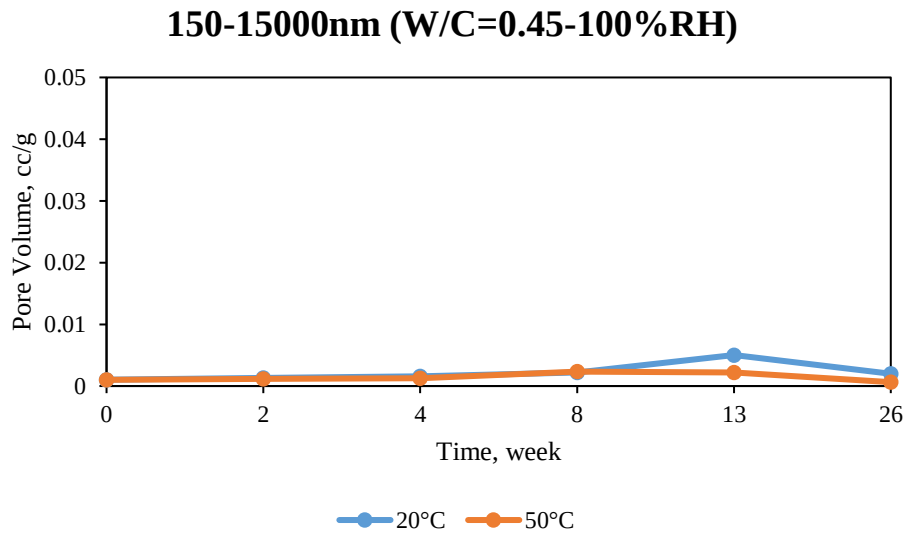

Figure 4.3 Relationship between pore volume diameter 150-15000 nm and curing period in case of OPC0.45 in water

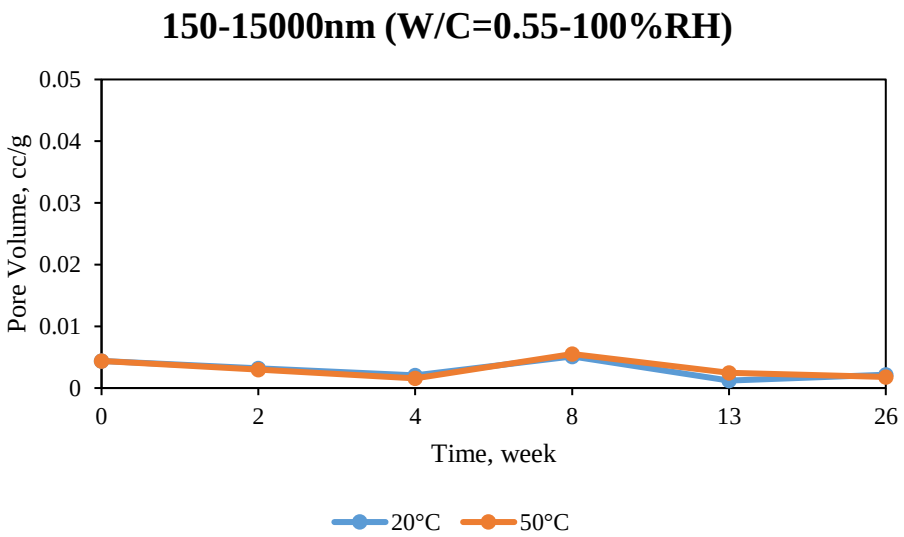

Figure 4.4 Relationship between pore volume diameter 150-15000 nm and curing period in case of OPC0.55 in water

4.3.2 Effect of relative humidity on the pore structure change of 150-15000 nm pores diameter

Figure 4.5, Figure 4.6, show the relationship between the diameter of 150-15000 nm for each water cement ratio and the period in different relative humidity conditions. For each temperature, as a whole trend, the slope of increase increases as the humidity decreases. In addition, the amount of pores with a diameter of 150-15000 nm also increases. At 50 ^{o}C and 60%RH and 75% RH, the amount of pores with a diameter of 150-15000 nm significantly increased due to the curing period increased. In underwater curing, the amount of pores with a diameter of 150-15000 nm has not changed due to period, regardless of temperature.

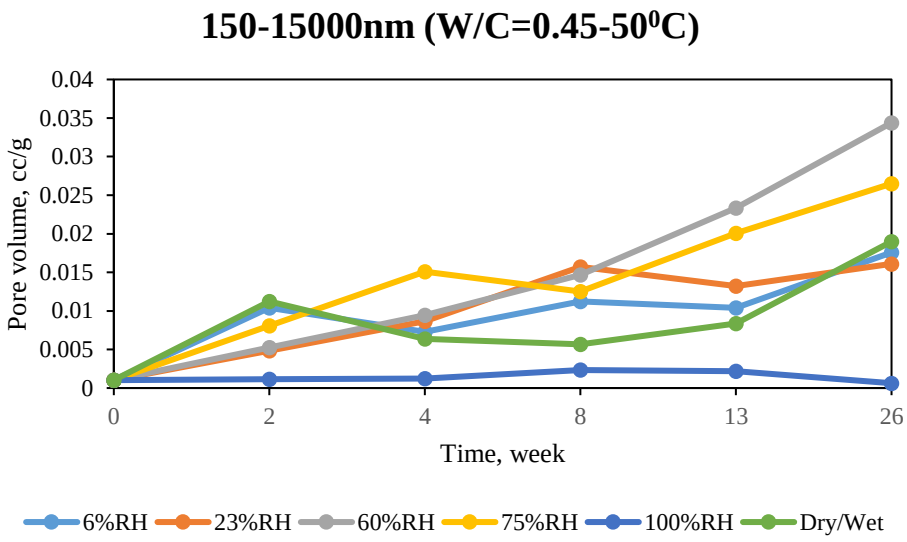

Figure 4.5 Relationship between pore volume diameter 150-15000 nm and curing period in case of OPC0.45

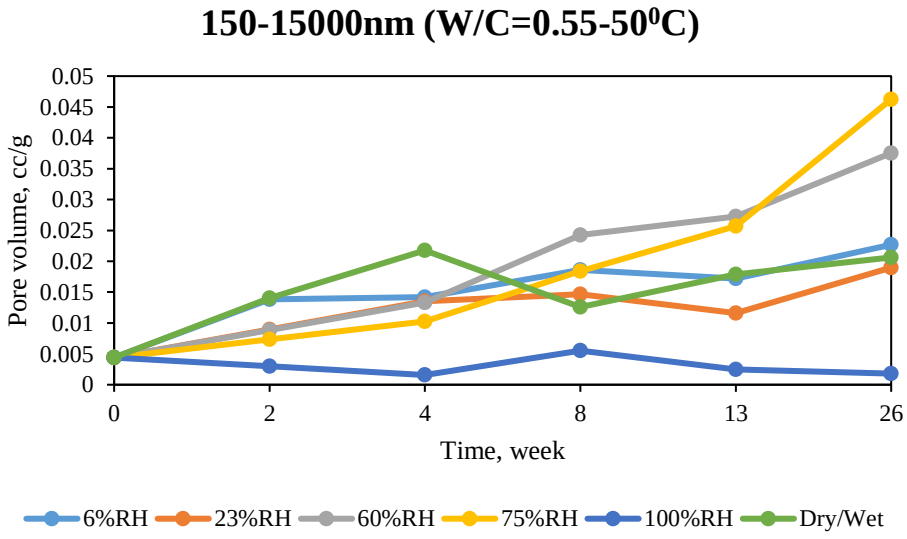

Figure 4.6 Relationship between pore volume diameter 150-15000 nm and curing period in case of OPC0.55

Figure 4.7, Figure 4.8 and Figure 4.9 show the pore structure change strongly in the range of relative humidity of 60-70% in most cases.

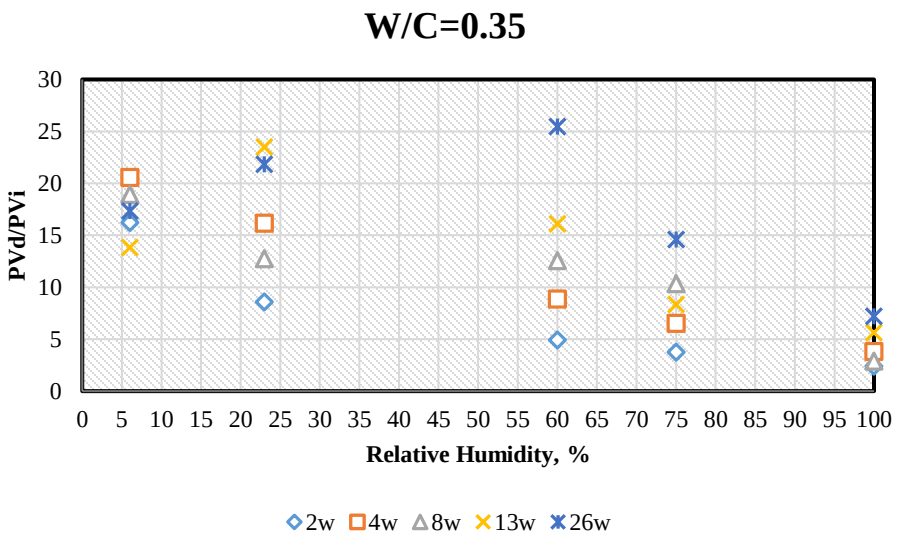

Figure 4.7 Relationship between pore structure change of 150-15000 nm pores diameter and relative humidity in case of OPC0.35

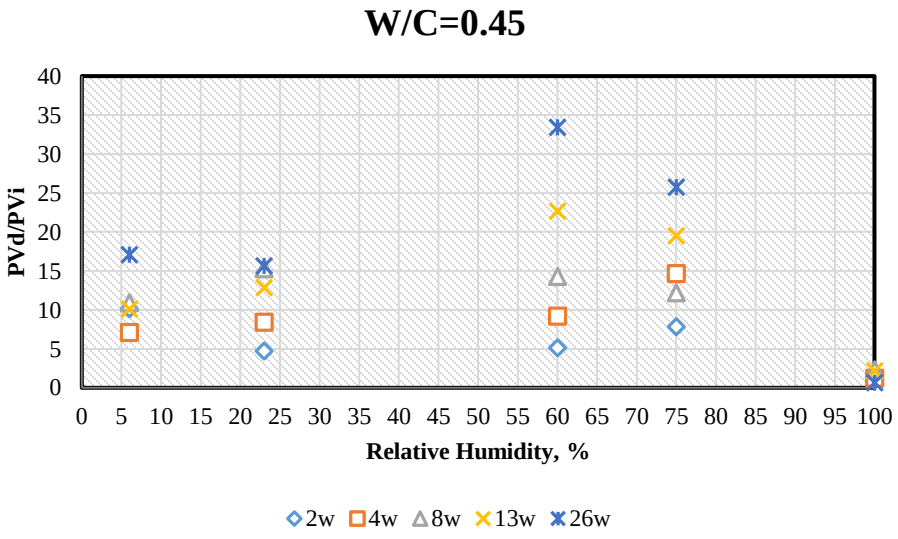

Figure 4.8 Relationship between pore structure change of 150-15000 nm pores diameter and relative humidity in case of OPC0.45

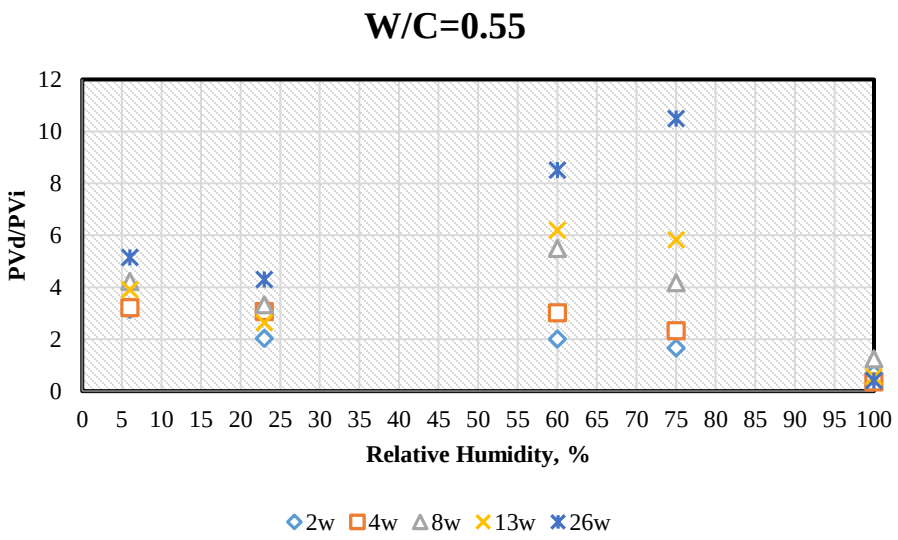

Figure 4.9 Relationship between pore structure change of 150-15000 nm pores diameter and relative humidity in case of OPC0.55

4.3.3 Effect of water-cement ratio on the pore structure change of 150-15000 nm pores diameter

Comparing each temperature and humidity with water cement ratio, it was confirmed that the initial value becomes larger as the water cement ratio is higher. Also, as the water cement ratio is higher, the increase in the amount of pores with a diameter of 150-15000 nm tends to be larger. Thus, it is considered that the higher the water cement ratio, the coarsening of the pore diameter of the diameter of 150-15000 nm due to the period tends to be increased.

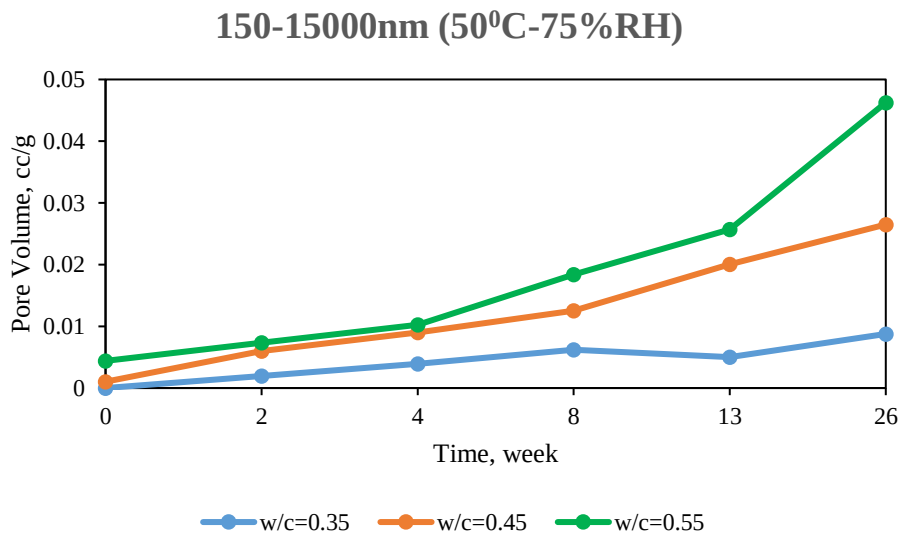

Figure 4.10 The pore volume due to respective environment curing for each water-cement ratio

In the case of underwater curing, there is almost no change in the amount of pores with a diameter of 150-15000 nm regardless of the water cement ratio.

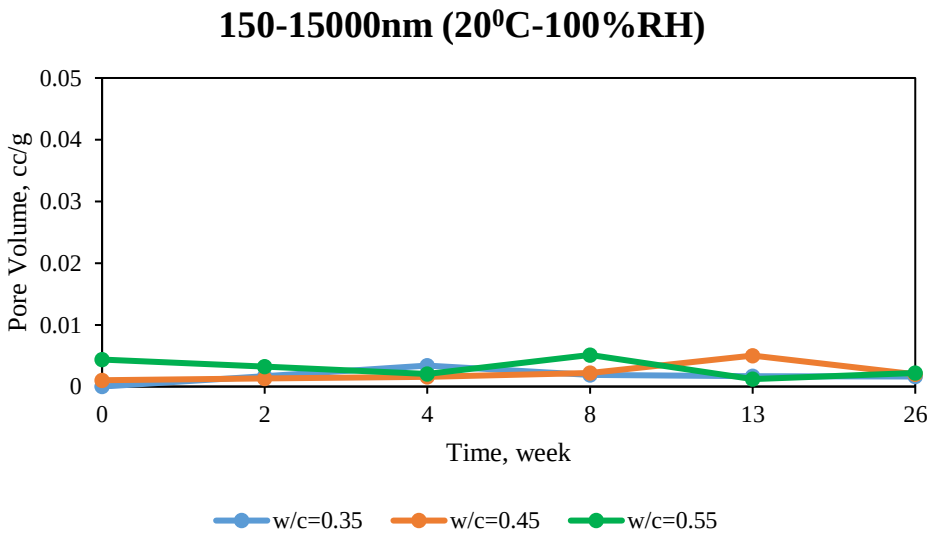

Figure 4.11 The pore volume due to respective environment curing in water for each water-cement ratio in case of 20^0C

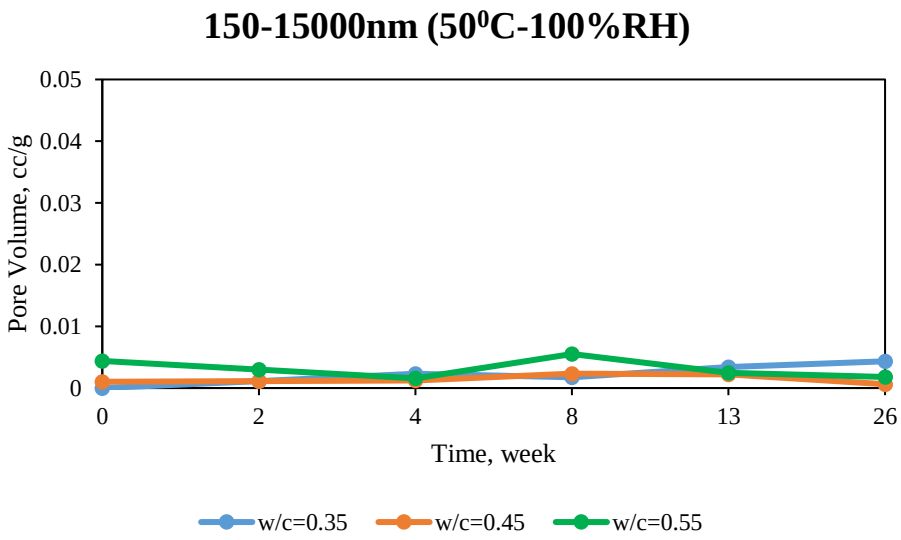

Figure 4.12 The pore volume due to respective environment curing in water for each water-cement ratio in case of 50^0C

4.4. Relationship between pore structure of 150-15000 nm pores diameter and maturity of carbonation

Previous study have shown that the temperature, humidity and time is related to pore structure change. In addition, in this study, it is shown in Chapter 3 that water cement ratio and relative humidity are also related. Here, it can be considered that an empirical formula of the change in pore volume (PVd) can be derived as shown in Equation (18) using these as elements.

$$PV_d = f(\text{Temp.}, \text{Time}, W/C, RH) \quad (18)$$

Where, PVd: Diameter 150 - 15000 nm pore volume after drying; Temp.: Curing temperature (℃); Time: Time (days); W/C: Water cement ratio; RH: Relative humidity.

Moreover, the modified maturity is proposed in chapter 3, it is clarified that temperature and time are related to pore structure change and it can be expressed by the Equation (19), in which M_{phc} is the modified maturity function of time-temperature and humidity relating the pore size from 150 to 15000nm in diameter corresponding carbonation.

$$M_{phc} = f(\text{Temp.}, \text{Time}, \text{RH}) \quad (19)$$

Therefore, the pore structure change using Equations (18) and (19) obtained above is shown in Equation (20):

$$PV_d = f(M_{phc}, W/C) \quad (20)$$

4.4.1 Datum temperature

The height of the coefficient of determination is investigated by a linear equation using the square root of the time-temperature-humidity time product and the pore volume (PVd) with a diameter of 150 to 15000 nm. Here, it is conceivable that those which do not correctly indicate the slope of the straight line due to the variation of the measurement result. Data is selected and the reference temperature and the reference relative humidity are examined. For the selection method, only curing conditions with two or more data are used between the initial value.

Firstly, from the result of Section 4.3, at 20 ° C and 50 ° C, the amount of pores with a diameter of 150 to 15000 nm does not increase in water, and increases at a relative humidity of 75% RH, so the reference relative humidity is 75%. It is assumed that the semi-relative humidity is 85% RH, and the temperature with the highest coefficient of determination is taken as the reference temperature and indicated by a yellow frame. Based on the above results, the reference temperature was not dependent on water cement ratio, and the coefficient of determination was high at 17 ° C. Table 4.2 and Figure 4.13, Figure 4.14, Figure 4.15 show the coefficient of determination of the reference temperature when the reference relative humidity is assumed.

Table 4.2 Coefficient of determination of reference temperature at reference relative humidity of 80% RH

Temperature (℃)	OPC0.35	OPC0.45	OPC0.55
1	0.908845421	0.892244361	0.890730038
2	0.909560333	0.893028555	0.891852006
3	0.910219754	0.893867999	0.892972564
4	0.910933587	0.89465077	0.894147639
5	0.911592014	0.895488693	0.895265324
6	0.912304774	0.896325834	0.896493168
7	0.913016977	0.897162193	0.897663634
8	0.913728625	0.897997773	0.898888202
9	0.914385039	0.898832576	0.900055554
10	0.915040983	0.899666605	0.901276872
11	0.915696456	0.900444335	0.902441134
12	0.916351461	0.901221393	0.90354856
13	0.916896941	0.901942348	0.90465463
14	0.917387595	0.902607334	0.905593728
15	0.917823512	0.903161115	0.906476696
16	0.918095856	0.90354856	0.907083238
17	0.918259223	0.903714557	0.907358804
18	0.918095856	0.903493221	0.907138358
19	0.917551088	0.902551938	0.905869748
20	0.914658406	0.897217922	0.898721314

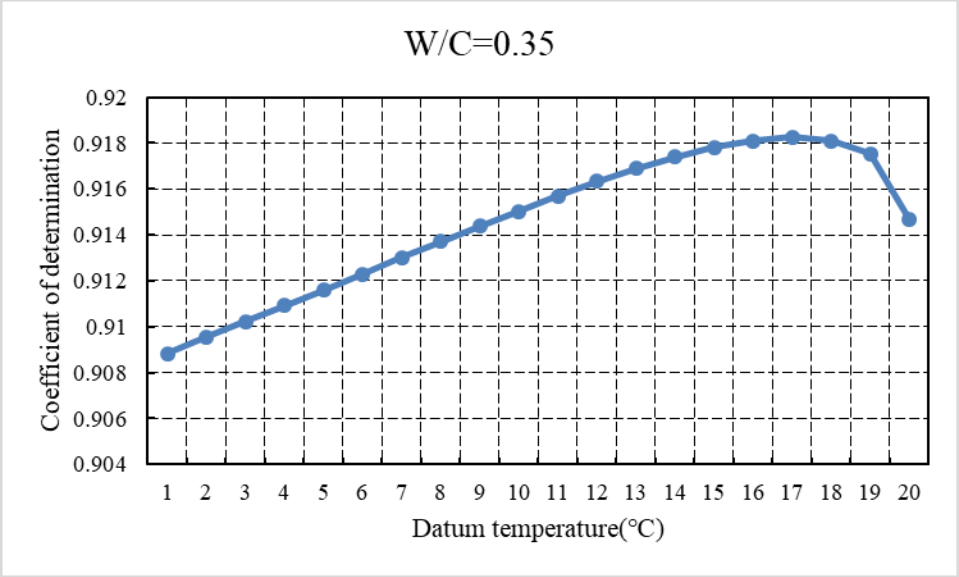

Figure 4.13 Coefficient of determination of regression formula for each datum temperature for OPC0.35

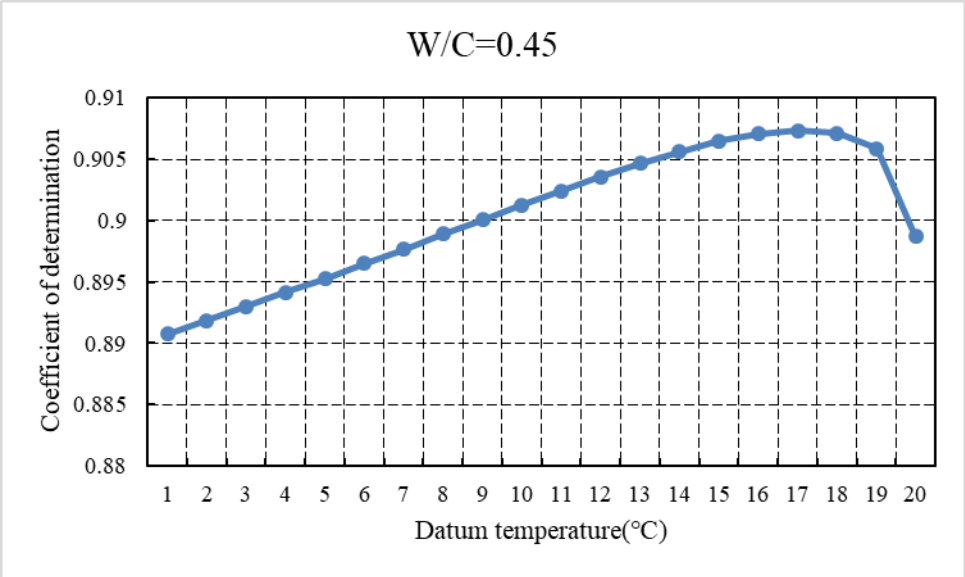

Figure 4.14 Coefficient of determination of regression formula for each datum temperature for OPC0.45

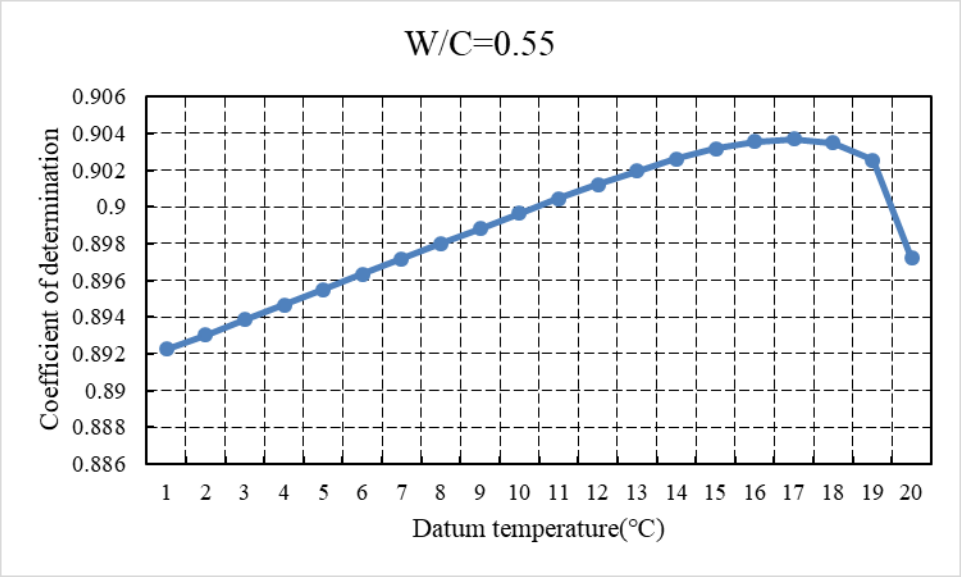

Figure 4.15 Coefficient of determination of regression formula for each datum temperature for OPC0.55

4.4.2 Datum humidity

Table 4.3 and Figure 4.16, Figure 4.17, Figure 4.18 show the coefficient of determination of the reference relative humidity. The reference temperature was set to 17 ° C and the coefficient of determination of the reference relative humidity was calculated. As for the reference relative humidity, W / C = 35% is (Ht = 85% RH), W / C = 45% is (Ht = 95% RH), W / C = 55% is (Ht = 95% RH) and the result with high correlation coefficient was obtained.

From this, it is found that the minimum temperature (Dt) at which the pore structure occurs is constant at 17 ° C regardless of the water cement ratio, and the reference relative humidity (Ht) at which the pore structure occurs differs depending on the water cement ratio.

Table 4.3 Coefficient of determination of reference relative humidity at reference temperature 17 °C

Relative Humidity	Coefficient of determination		
	OPC0.35	OPC0.45	OPC0.55
0.75	0.82176639	0.896548939	0.882043083
0.76	0.86844689	0.901387819	0.889381808
0.77	0.884985876	0.903050386	0.892412461
0.78	0.895767827	0.904157066	0.89465077
0.79	0.903382532	0.904930937	0.896493168
0.8	0.908845421	0.905593728	0.898053451
0.81	0.912743118	0.906090503	0.899444273
0.82	0.915368778	0.906531853	0.90066642
0.83	0.917005998	0.906862724	0.901776025
0.84	0.917932459	0.907138358	0.902773504
0.85	0.918150314	0.907358804	0.903714557
0.86	0.917877988	0.907579198	0.904599359
0.87	0.917224073	0.907689374	0.905372851
0.88	0.916133178	0.907799537	0.906090503
0.89	0.914822387	0.907909687	0.906752447
0.9	0.913181253	0.907964757	0.907413908
0.91	0.911427452	0.908019824	0.907964757
0.92	0.909450383	0.908019824	0.908515272
0.93	0.907358804	0.908019824	0.909010451
0.94	0.905151921	0.908019824	0.90950536
0.95	0.902884267	0.908019824	0.909945053
0.96	0.900555384	0.907964757	0.910384534
0.97	0.898164796	0.907909687	0.910823803
0.98	0.895712007	0.907854614	0.911153116
0.99	0.893252484	0.907799537	0.911537163

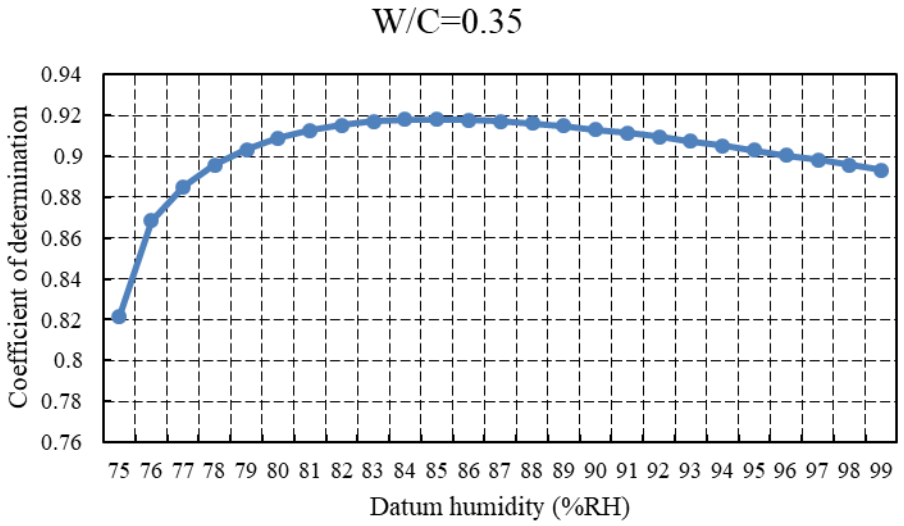

Figure 4.16 Coefficient of determination of regression formula for datum humidity of OPC0.35

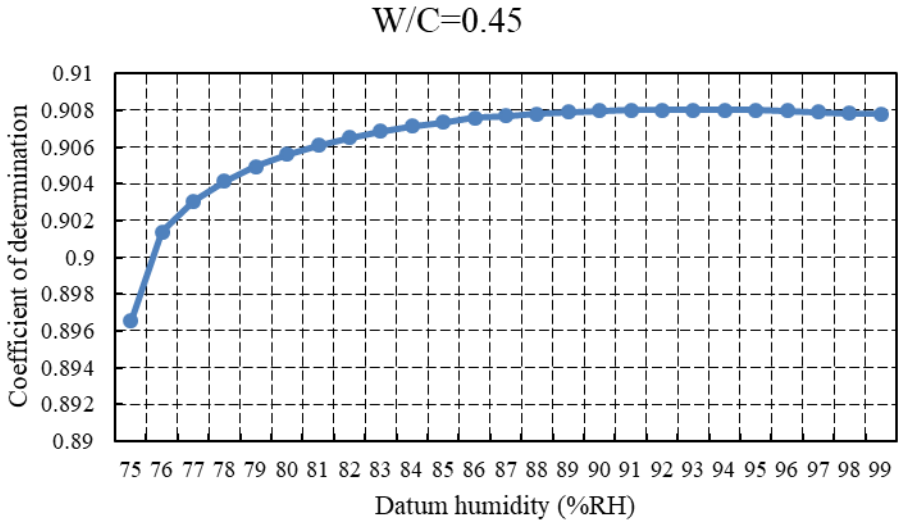

Figure 4.17 Coefficient of determination of regression formula for datum humidity of OPC0.45

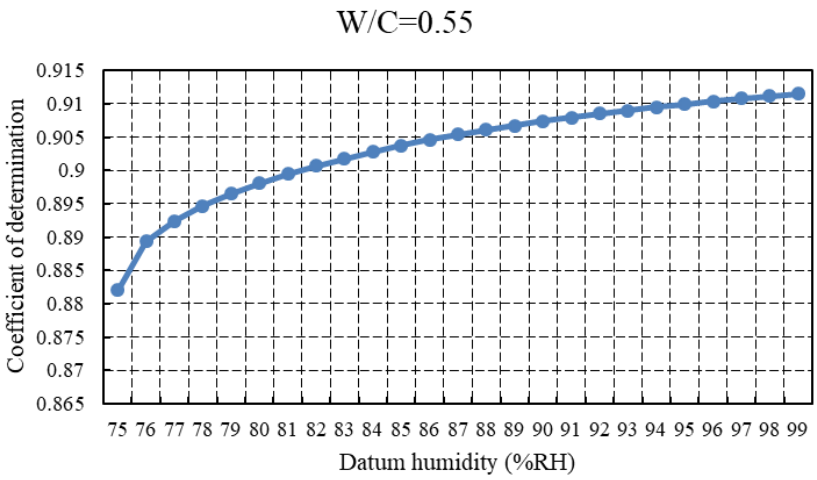

Figure 4.18 Coefficient of determination of regression formula for datum humidity of OPC0.55

4.4.3 Relationship between the pore volume of 150-15000 nm diameter pores and the modified maturity

The relationship between the square root of the temperature and humidity time product calculated using the reference temperature (17^0C) obtained from the above results and each reference relative humidity and the pore volume PVd with a diameter of 150 to 15000 nm is shown in Figure 4.19, Figure 4.20, Figure 4.21. It can be confirmed that considering the water cement ratio, temperature and humidity, the pore volume PVd with a diameter of 150 to 15000 nm. A good correlation was obtained for each water cement ratio for each straight line. The proposed function was fitted with the experimental data.

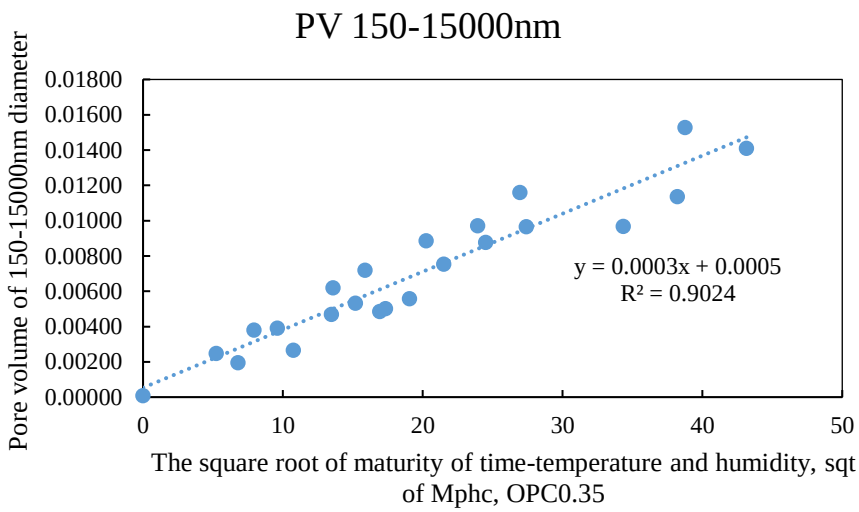

Figure 4.19 Relationship between the pore volume of 150-15000 nm diameter pores and the modified maturity of OPC0.35

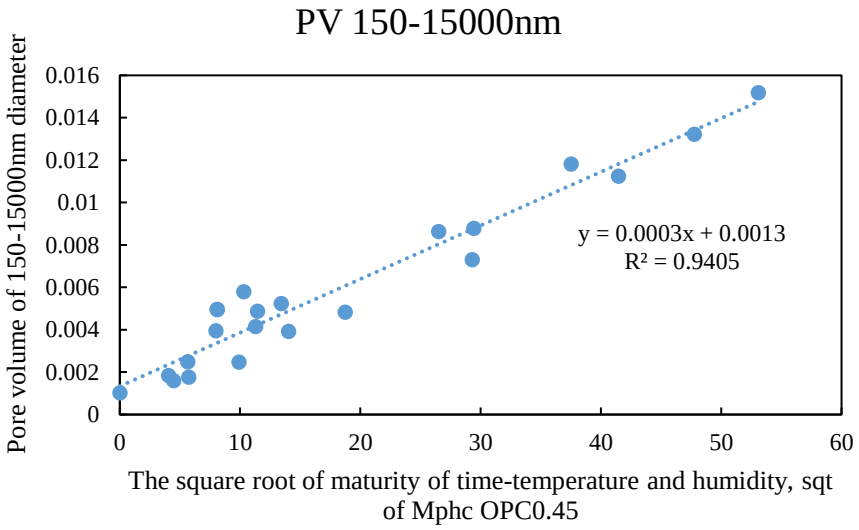

Figure 4.20 Relationship between the pore volume of 150-15000 nm diameter pores and the modified maturity of OPC0.45

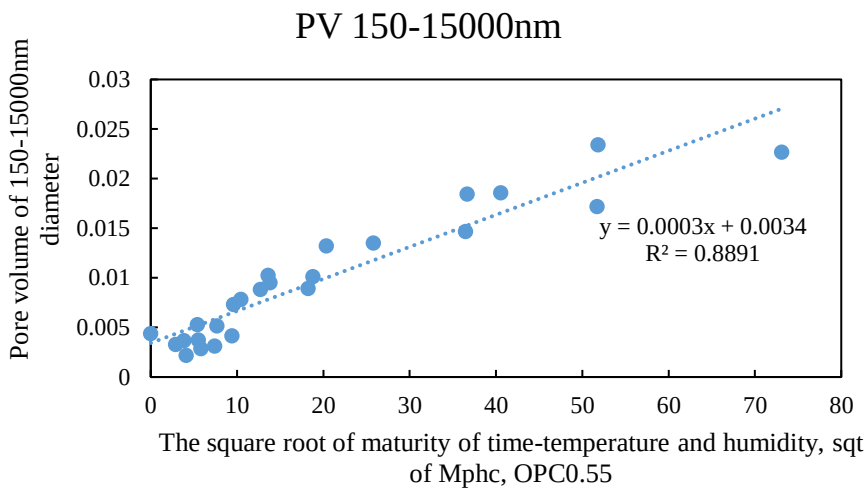

Figure 4.21 Relationship between the pore volume of 150-15000 nm diameter pores and the modified maturity of OPC0.55

Experimental equation (21), (22) and (23) represent the relationship between the time-temperature-humidity product and the diameter of the pores with a diameter of 150-15000 nm obtained. Figure 4.22 shows the relationship between different reference relative humidities Ht for each water cement ratio. The reference humidity is in a linear relationship with the water cement ratio, and as the water cement ratio increases, the amount of pores with a diameter of 150-15000 nm increases at a high relative humidity.

$$\text{W/C=35\%}: PV_{dc} = 0.0003 \times \sqrt{\sum(\theta_{d,t} - 17) \times (0.85 - \varphi_{d,t}) \times t + \beta} \quad (21)$$

$$\text{W/C=45\%}: PV_{dc} = 0.0003 \times \sqrt{\sum(\theta_{d,t} - 17) \times (0.95 - \varphi_{d,t}) \times t + \beta} \quad (22)$$

$$\text{W/C=55\%}: PV_{dc} = 0.0003 \times \sqrt{\sum(\theta_{d,t} - 17) \times (0.99 - \varphi_{d,t}) \times t + \beta} \quad (23)$$

From equation (21), (22), (23) and Figure 4.22, Figure 4.23, the relationship between pore volume of 150 – 15000 nm in pore diameter can be expressed by equation (35):

$$PV_{dc} = 0.0003 \times \sqrt{\sum(\theta_{d,t} - 17) \times (Ht - \varphi_{d,t}) \times t + \beta} \quad (24)$$

The modified maturity function that expressing the relationship between pore volume of 150-15000nm in diameter and the environmental conditions in which affect carbonation, is:

$$M_{phc} = \sum(\theta_{d,t} - 17) \times (Ht - \varphi_{d,t}) \times t \quad (25)$$

Where:

The datum humidity Ht is:

$$Ht = 0.7 \times (\frac{W}{C}) + 0.615 \quad (26)$$

And the initial value is:

$$\beta = 0.0145 \times \left(\frac{W}{C}\right) - 0.0048 \quad (27)$$

W/C is water-cement ratio. Therefore, in general, the pore structrure change regarding carbonation can be expressed by equation (33):

$$PV_{dc} = 0.0003 \times \sqrt{M_{phc}} + \beta \quad (28)$$

Where, M_{phc} is the modified maturity of 150-15000 nm pore size regarding carbonation.

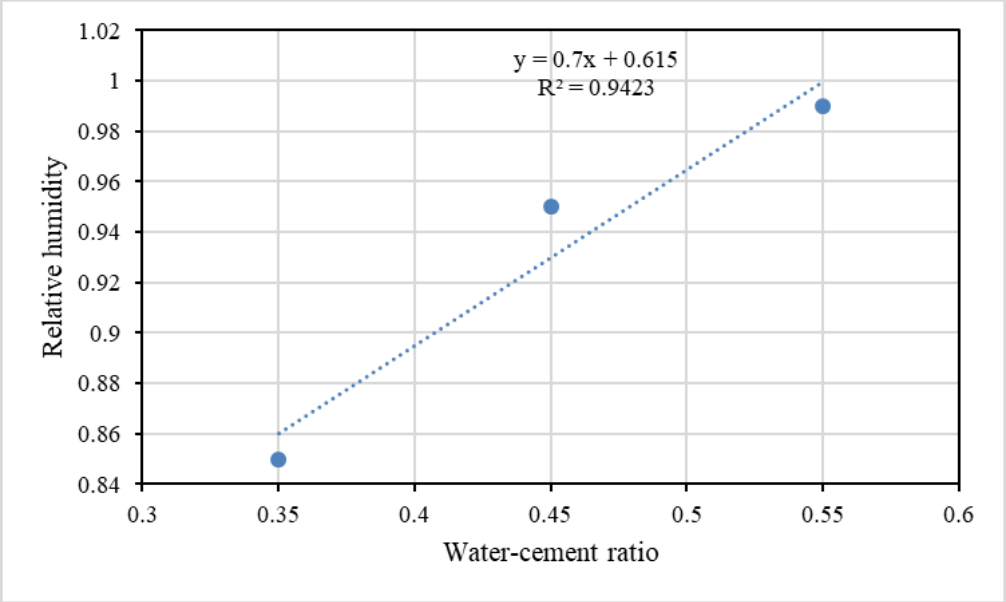

Figure 4.22 Relationship between different reference relative humidities Ht for each water cement ratio

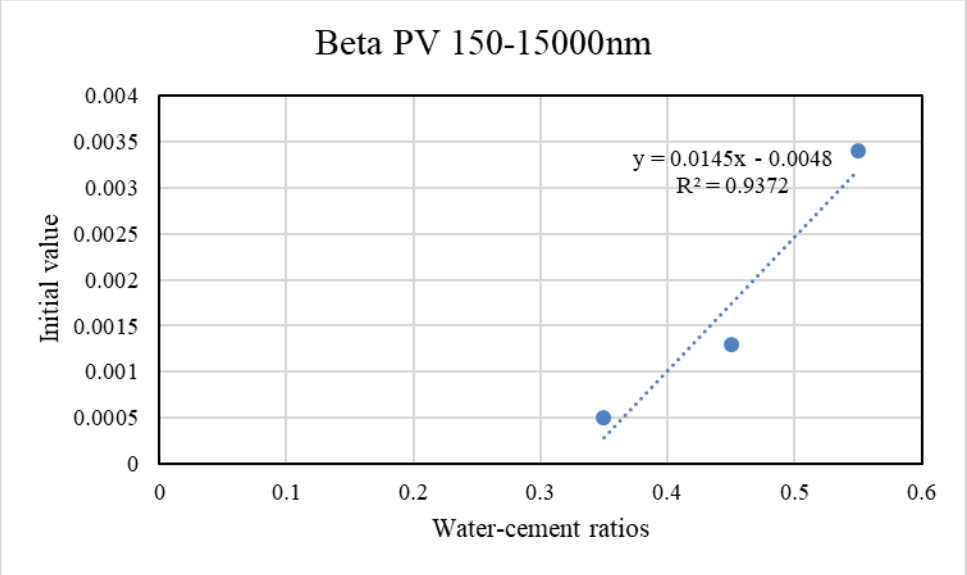

Figure 4.23 Relationship between different initial value for each water cement ratio

4.5. Service life prediction equation regarding carbonation due to pore structure change

The pore structure change can be predicted regarding temperature and relative humidity is give by equation (28).

In terms of carbonation exposure, a non-linear differential equation is developed by Papadakis et al. (Papadakis, Fardis, and Vayenas 1992), (Demis, Efstathiou, and Papadakis 2014). This equation permits the calculation of the carbonation depth according to the following equation (29):

$$X_c = \sqrt{\frac{2D_{e,CO_2}\left(\frac{CO_2}{100}\right)t}{0.33CH + 0.214CSH}} \tag{29}$$

where CO_2 is the CO_2-content in the ambient air at the cement-based materials surface (%), CH and CSH are the contents of calcium hydroxide and calcium–silicate–hydrate in cement-based materials volume (kg/m^3), the effective diffusivity of CO_2 in carbonated part (m^2/s), is calculated as:

$$D_{e,CO_2} = (1.64 \times 10^{-6}) \times (PV)^{1.8} \times \left[1 - \left(\frac{RH}{100}\right)\right]^{2.2} \tag{30}$$

where RH is an ambient relative humidity, RH (%), and PV is the pore volume of cement-based materials is calculated from equation (28)

In addition, Henriksen, (Henriksen 1993), presents a service life model due to the deterioration of carbonation as shown in equation (34):

$$T = \left(\frac{\sqrt{T_a}}{X_c} \times C\right)^2 \tag{31}$$

Where, T is service life (years); T_a is age at time of inspection (years); X_c is measured carbonation depth at time of inspection (mm) and C is cover (mm).

Therefore, by combining equation (28), (29) and (31), the service life prediction equation regarding carbonation due to pore structure change can be obtained.

4.6. Conclusions

As a result, the reference humidity and the reference relative humidity were reset and an empirical formula was obtained. The reference temperature at which the pore structure change occurs is 17 °C regardless of the water cement ratio. In addition, it was revealed that the pore volume increases as the humidity decreases and the pore volume increases as the water cement ratio increases. The pore structure changes strongly at 60%RH and 75%RH. A pore volume of 150 to 15000 nm in diameter and a time-product of temperature and humidity were in good relation.

CHAPTER 5

SERVICE LIFE PREDICTION BASED ON PORE STRUCTURE CHANGE

CHAPTER 5 SERVICE LIFE PREDICTION BASED ON PORE STRUCTURE CHANGE

5.1. Introduction

Frost damage of cement-based materials is an important issue for cement-based materials structures in cold climates, up to now, some frost damage deterioration prediction methods have been proposed. Among them, the number of cycles Equivalent to ASTM is treated as an index considering a relatively large number of parameters such as weather conditions and curing conditions. It is well known that the frost damage resistance of cement-based materials depends on the pore structure, and the amount of pores with a diameter of 40 to 2000 nm has a large influence on frost damage resistance.

On the other hand, as also in Chapter 2 and Chapter 3, it is known that the amount of pores with a diameter of 40-2000 nm coarsens the amount of pores under high-temperature drying conditions. Here, if the frost damage resistance is reduced by coarsening the pores under high temperature drying conditions, there is a risk that frost damage will occur not only in cold area, which is a representative of cold districts, but also in all areas. For example, in regions where dry conditions tend to be high in summer, the amount of pores with diameters of 40 to 2000 nm increases in the summer and the risk of frost damage may be higher than in cold region such as Hokkaido in Japan due to freezing and thawing in winter.

Many different mathematical methods for service life prediction have been presented. The mathematical model expressed in this study is based on pore structure change, combined with previous laboratory tests and empirical results from existing exposure mortar samples. The model can be used to predict service life in practical situations. In the previous study, the volume of 40-2000 nm diameter pores changes depending on the temperature and the period, and proposes using the maturity temperature-time factor to predict performance. However, it is an empirical formula that does not take into consideration the influence of relative humidity on the maturity temperature-time factor representing 40-2000 nm diameter pore volume. In addition, the change in the volume of 40-2000 nm diameter pores differs for each water-cement ratio. Methods for predicting frost damage and change in pore structure have been proposed, but no predictive

method that combines the prediction of frost damage deterioration and that of pore structure change in a real environment currently exists.

In this chapter, a method that adds the potential change of frost damage of cement-based materials by maturity function proposed in Chapter 3, in order to predict frost damage deterioration, to the risk of frost damage by the region in winter by ASTM Equivalent cycle number. In addition, The ASTM Equivalent cycle number is the index proposed in 1999 that calculation based on Japan climate in 1982. This study will reexamine it using the daily average year value of the Meteorological Agency of 1981 to 2010 with the standard year extended AMeDAS weather data from 2000 to 2010.

Furthermore, the purpose of this research is to propose an environmental indicator method, which predicts the change in durability factor based on conventional frost damage deterioration, and pore structure change in the summer; this allows calculation of the service lifetime of cement-based materials. In conjunction with the proposal of environmental indicator method, an experiment that includes the relative humidity factor in the prediction of pore structure change using conventional maturity methods was conducted, and that proposes use of the modified maturity function. A theory is presented for the estimation of the service life of mortar exposed to frost action.

5.2. Materials and method

The physical properties and mineral compositions are given in Table 2.1. The mineral composition of the OPC was quantified by the X-ray diffraction (XRD) Rietveld method. The main mix was water-cement ratio (W/C) of 0.45 and the sand-to-cement ratio (S/C) of 2:1 without any chemical admixture.

Table 5.1 Mix proportions

Water-cement ratio (W/C)	Sand-cement ratio (S/C)	Material contents (kg/m^3)			Flow (cm)
		Water	Cement	Sand	
0.45	2.0	297	660	1320	23

5.3. Frost damage deterioration prediction based on ASTM Equivalent cycles number

ASTM Equivalent cycle number (Y.Hama et al. 1993) is a method to estimate the effect of freezing temperatures on the extent of frost damage, and the effective number of freeze/thaw cycles corrected to ASTM Equivalent cycles, was proposed as shown in Equation (32) and Table 5.2.

$$Cy_{ASTM-sp} = C.F.s.p.Ra_{90} \tag{32}$$

Where, $Cy_{ASTM-sp}$ is the number of ASTM Equivalent cycles (cycle/year); C is the coefficient of the curing condition; F is the coefficient of the freeze-thaw condition; s is the coefficient of the sunlight condition; p is the coefficient of the degradation process; Ra_{90} is the effective number of ASTM Equivalent cycles by air temperature (cycles/year).

The number of cycles corresponding to ASTM Ra_{90} by air temperature is calculated using the region coefficient, T (Equation (33) and (34)). Furthermore, it is shown in Equation (35) that there is a relationship between the Equivalent ASTM cycles of Ra_{60} and Ra_{90}.

$$T = -t_a min\left(1 - \frac{D_f}{D_w}\right) \tag{33}$$

$$Ra_{90} = \sum\left(-\frac{t_a}{18}\right)^{\beta} = 4.2T - 5.4 \tag{34}$$

$$Ra_{60} = 1.64Ra_{90} \tag{35}$$

Where, $t_a min$ is the annual minimum freezing temperature (°C); D_f is the freeze duration in days; D_w is the total number of freezing and thawing days; t_a is the freezing temperature (°C); and β is a constant.

Regional coefficient T used for ASTM Equivalent cycle number was calculated from the Japanese climate data in 1982. Therefore, this study will reconsider using the daily average value of Japan Meteorological Agency in 1981 to 2010.

In calculating ASTM Equivalent cycle number $Cy_{ASTM\text{-}sp}$ shown in Equation (32), it is necessary to determine C, F, s, P, R_{a90}. R_{a90} can be expressed by the region coefficient T and can be obtained by knowing the annual extreme of day minimum temperature, freezing duration (number of days), freezing and thawing (total days).

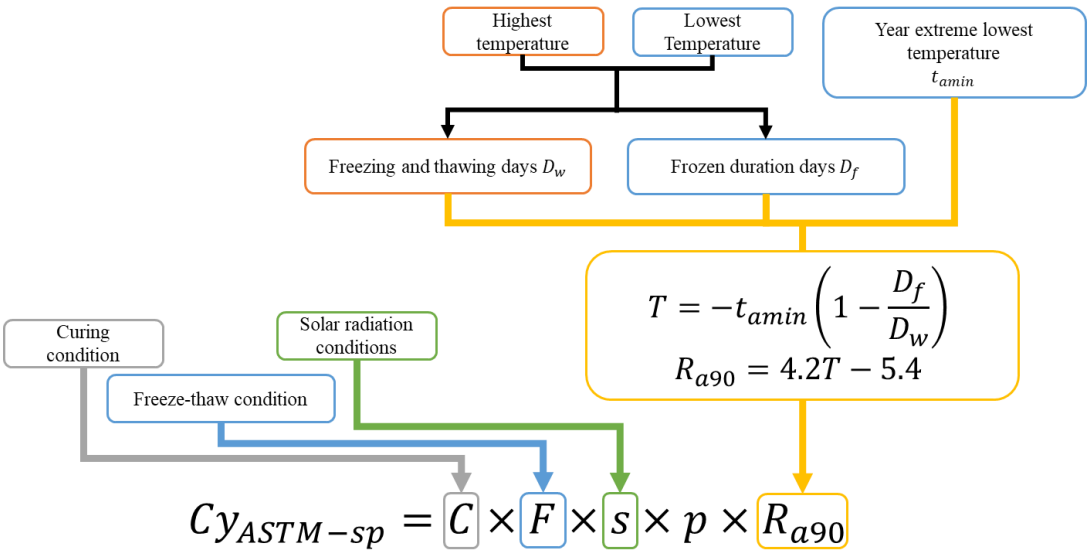

Figure 5.1 Examination of meteorological statistical data

The annual extreme value t_{amin} of the day minimum temperature was set to the lowest value in every hour of the year. In addition, the freezing temperature of concrete is generally slightly lower than 0 °C, as the lowest temperature ranges from -0.1 °C to -0.9 °C, the effect on frost damage is small. So, the minimum day temperature is -1.0 or less and the maximum day temperature is equal to or higher than 0 °C is defined as one freeze-thaw cycle; and the freeze duration D_f, the freezing and thawing total number of days D_w were calculated.

The ASTM Equivalent cycle number uses the relative dynamic elastic modulus as an index showing the process of deterioration of concrete in the freeze-thaw test. The process of frost damage deterioration is

thought separately into two stages, the process in which signs of deterioration appear at a relative dynamic elastic modulus of 90% and the process in which the deterioration after that appears clearly.

As a result of examining correspondence between deterioration prediction using ASTM Equivalent cycle number and deterioration of actual structure, it became clear that the temperature and humidity in concrete varies depending on environmental conditions such as snow cover and site. Regarding the humidity, the horizontal member was higher in humidity than the vertical member, and it was found that the humidity in the concrete correlated with the deepest snow; although, there was variation. In addition, due to differences in moisture supply conditions, there is a difference in damage amount due to freezing and thawing between indoor acceleration test and actual structure.

By studying the correspondence between the prediction of degradation using ASTM Equivalent cycles, and the deterioration of an actual structure, with differences in the level of moisture supply, the indoor acceleration test and actual structure show different extents of damage due to freeze-thaw cycles. It was found that the deterioration speed in the ASTM Equivalent cycle is faster than the actual degradation speed.

Table 5.2 Coefficient of ASTM Equivalent cycle formula

ASTM Equivalent cycle Cy_{ASTM}=C.F.s.p.Ra90			Process of frost damage	
			Signal 100%≥Ed>90%	Clear 90%≥Ed>60%
Degradation coefficient, p			1.00	1.64
Conditions Coefficient	Solar radiation, s	North face	1.00	1.00
		South face	1.45	1.45
	Curing and Drying, C	In water	1.00	1.00
		In air	0.66	1.41
		Drying at 20^0C	0.26	0.80
		Drying at 30^0C	0.14	0.45
	Freeze-thaw, F	In water	1.00	1.00
		In air	0.21	0.23

Furthermore, if the accelerated test result of the targeted cement-based material is known, it is possible to predict deterioration and estimate the service lifetime using Equation (36) with ASTM Equivalent cycles and considering the effect of weather conditions using the coefficients in Table 5.2.

$$X_{Ed} = \frac{N_{Ed}}{Cy_{ASTM-sp}} \tag{36}$$

Where, X_{Ed} and N_{Ed} are the number of years or cycles, respectively, that pass before the relative dynamic modulus of elasticity decreases to 90 or 60% of its initial value in an accelerated test; and X90 and X60 are the number of years in which the relative dynamic modulus of elasticity is 90% or between 90 and 60%, respectively, of its initial value in a natural environment.

Further, if $Cy_{ASTM\text{-}sp}$ which is annual number of freezing-thawing cycles and the number of cycles at which the relative dynamic modulus in the freezing-thawing test of the target cement-based materials become 90% and 60% are known, the service life for frost damage deterioration can be calculated. Therefore, service life for frost damage deterioration in this study has been defined as the number of years until the relative dynamic modulus falls below 60%. Although it is possible to estimate the service life depending on the number of cycles Equivalent to ASTM, it is considered that cement-based materials does not change the frost hazard as potential, so consideration should be given to the frost resistance accompanying the change in pore structure due to drying is an issue.

5.4. Prediction method of service life of mortar by environmental indicator process

5.4.1 Proposal of environmental indicator for frost damage of mortar considering the effect of drying

One of degradation phenomena of cement-based materials in cold areas is frost damage due to freeze-thaw action. In order to extend the life of cement-based materials structures, it is necessary to properly predict deterioration due to frost damage. Regarding the influence of external factors on the frost damage deterioration of cement-based materials, Hasegawa et al. calculated the frost damage risks in various parts of the country from the weather conditions such as temperature, solar radiation, precipitation, and snow melting amount, and the regional difference of the occurrence probability of freezing damage. It is done by classification of frost damage risk map. Hama et al. have proposed a method to estimate frost damage of actual structures, proposing "ASTM Equivalent cycle number" representing the freeze-thaw action of the cement-based materials structure under regional coefficient and real environment as an index showing the severity of freezing and thawing action in the cold region, (Y.Hama et al. 1993).

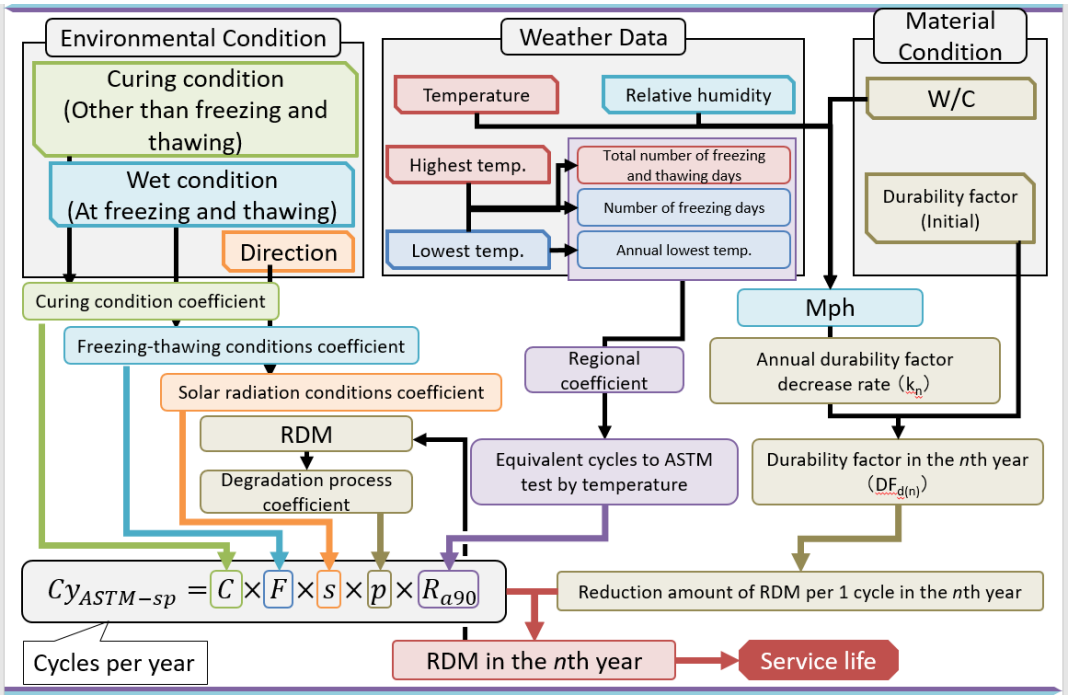

Figure 5.2 Overall flowchart of calculation process

On the other hand, relating to the pore structure that affects the frost resistance, Kamata et al. analyzed the results of the freeze-thaw test and the measurement of the pore structure of hardened cement paste and found that the good correlation between the pore volume of 40-2000 nm in diameter and the frost resistance. Aono et al. found that the structure of C - S - H of the paste with low water cement ratio changed due to the effect of drying, it is revealed that the pores become coarse so that the amount of pores having a diameter from 40 to 2000 nm increases and the frost resistance decreases. In addition, Nakamura et al. proposed a temperature-time product representing the change in the pore volume of 40 to 2000 nm in diameter due to the drying temperature and period. Conventional frost damage deterioration prediction method has been shown that cement-based materials has no change in potential frost damage, but it seems to be necessary to consider deterioration of frost process relating to pore structure change due to drying. Therefore, in this research, proposing environmental indicator method, which is a frost damage environment index which can take into consideration changes in freezing hazard due to drying; also is a frost damage prediction method considering the influence of pore structure change by drying and aim to calculate the service life of each region.

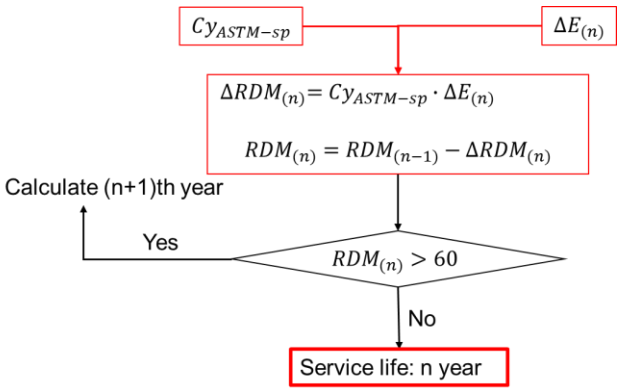

Figure 5.3 Process flowchart

In this study, the environmental indicator method, which is a frost damage deterioration prediction method considering the influence of pore structure change due to summer high temperature drying condition on frost resistance and ASTM Equivalent cycle number as an index of prediction of frost damage of cement-based materials was proposed. Calculation of the service life of cement-based materials by environmental indicator method revealed that the number of years is shorter than the service life calculated by ASTM Equivalent cycle number, even in areas where the influence of winter seasons was small and the risk of frost damage deterioration was underestimated. It was confirmed that there is the risk of frost damage deterioration by considering the influence of pore structure change during the summer season.

In order to predict frost damage deterioration, this study proposes a method which adds the potential change of frost damage of cement-based materials by the maturity formula proposed in Chapter 3 to the risk of frost damage by the winter region according to ASTM Equivalent cycle number. In order to calculate regionality by environmental indicator method, need to consider fixed water cement ratio. In the experiment conducted in Chapter 2, water cement ratio is 0.35, 0.45, 0.55, but in calculation of Chapter 5 water cement ratio of 0.45 is used.

As described in Equation (16), it is considered that the service life of concrete structures can be estimated by using the number of cycles equivalent to ASTM if the antifreeze property of cement-based materials is known. On the other hand, the durability index is generally calculated by the Equation (17). Next, in Equation (16), if the initial durability DFi is known, the durability index when the pore structure is changed

by drying can be expressed as DF_d by the Equation (16). In addition, when the temperature-humidity time product exceeds the upper limit, it is calculated using the upper limit value.

Therefore, even if do not know the frost harmfulness of concrete, it still can calculate the service life if N is known. Examination is made using Equations (16) and (17). The durability index DF_d changed by the pore structure change differs in the calculation formula between both case of when the relative dynamic elastic modulus is greater than or equal to 60 at 300 cycles and when the relative dynamic elastic modulus is less than 60. In addition, in ASTM Equivalent cycle number, it is considered that the slope is different in the process of signs of deterioration with a relative dynamic elastic modulus of 90% or more, and clear deterioration of 90% to 60% is observed. However, general concrete structures are unlikely to have small initial durability index. Therefore, in this research, consider the gradient of degradation as constant.

As forecast of frost damage deterioration taking into consideration change of pore structure in summer, prediction of change of potential against frost damage by cement-based materials by temperature / humidity time product. In addition to forecasting method of frost damage by region in winter by ASTM Equivalent cycle number, it is possible to calculate the service life. In the actual environment, under freezing and thawing calculated from the ASTM Equivalent cycle number in winter as it in summer, the durability index decreases due to the pore structure change, so the relative dynamic modulus of cement-based materials can not be represented by a simple straight line. Therefore, from the ratio of the durability index, the decrease in the durability index for each year is calculated. Because the temperature and humidity time product increases every year, the evaluation of the durability index changes year by year as the 1st year, 2nd year, nth year and years increase. Therefore, as shown in Figure 5.4, a process which changes with aging is calculated as a ratio k to the previous year. Since the initial durability index is maintained, the axis deviates as it is reevaluated the following year. Therefore, considering the ratio k for each year, it is possible to predict the current future as shown by the broken line in Figure 5.4. The ratio k (n) to the previous year in the nth year is expressed by the Equation (37), and the durability index in the year is represented by the Equation (38) by using k (n).

$$k_n = \frac{DF_{d(n)}/DF_i}{DF_{d(n-1)}/DF_i} \tag{37}$$

$$DF_{d(n)} = DF_i \cdot \prod_{j=1}^{n} k_{(j)} \tag{38}$$

Where, k_n represents the ratio of the durability index to the previous year at the nth year, and $DF_{d(n)}$ represents the durability index of the n^{th} year.

Next, the reduction amount of the relative dynamic elastic modulus for each cycle is calculated. With relate to the durability index DF, since the calculation method is different when DF ≧ 60 and DF <60, the reduction amounts are respectively calculated by Equations (39) and (40) separately for the case.

$$\Delta E_{(n)} = \frac{100 - DF_{d(n-1)}}{300} \ (DF \geq 60) \tag{39}$$

$$\Delta E_{(n)} = \frac{100 - 60}{N} \ (DF < 60) \tag{40}$$

Where, ΔE (n) represents the decrease amount of 1 cycle relative dynamic elastic modulus in the n^{th} year.

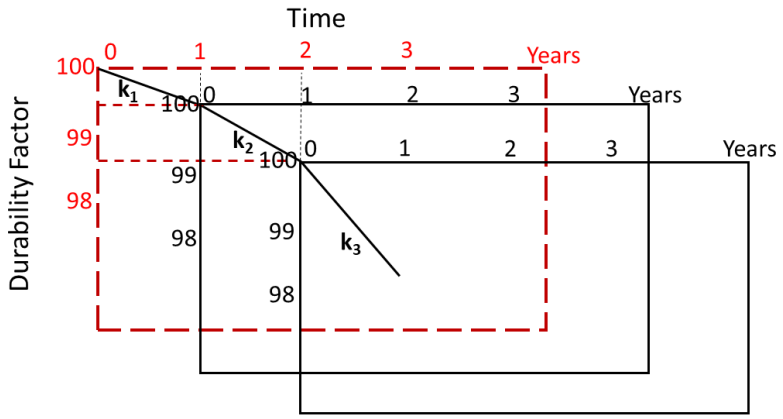

Figure 5.4 Conceptual diagram of relationship between durability index and elapsed years

As shown in Figure 5.5, ΔE (n) represents the slope of the relative dynamic elastic modulus with respect to the number of cycles, and the way is different when DF ≧ 60 and DF <60. Moreover, considering the process of actual frost damage deterioration, it seems that the relative dynamic modulus coefficient does not decrease with a certain value as shown in Figure 5.5. In this study, however, cement-based materials is supposed to deteriorate constantly every cycle in order to simplify calculation.

Equations (40) can be rewritten to Equation (42) by substituting Equation (17) into Equation (41) and substituting into Equations (40).

$$N = \frac{M \cdot DF_{(n-1)}}{P} \tag{41}$$

$$\Delta E_{(n)} = \frac{100 - 60}{\frac{M \cdot DF_{(n-1)}}{P}} = \frac{8}{DF_{(n-1)}} \tag{42}$$

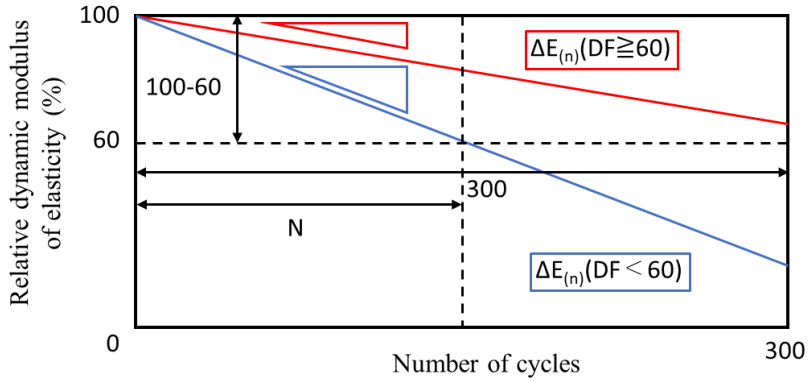

Figure 5.5 Relative dynamic modulus of elasticity decreasing per cycle

Using the calculated amount of decrease in relative dynamic elastic modulus per cycle and the number of cycles Equivalent to ASTM, the amount of decrease in the relative dynamic elastic modulus at each year is calculated. The relative dynamic elastic modulus is calculated in each year from the decrease amount of the relative dynamic elastic modulus by the Equation (43). By integrating the relative dynamic elastic modulus which decreases every year in real environments, it is possible to express the relationship between elapsed years and relative dynamic elastic modulus. The service life is the number of years until the relative dynamic elastic modulus falls below 60%. If the relative dynamic elastic modulus falls below 60% in a certain number of years, the number of years before that year is the service life.

$$RDM_{(n)} = 100 - \sum_{j=1}^{n} Cy_{ASTM-sp} \cdot \Delta E_{(j)} \tag{43}$$

where, RDM (n) represents the relative dynamic elastic modulus at the nth year.

5.4.2 Service life of each region

Regarding the weather data used for the calculation, the number of cycles Equivalent to ASTM proposed in the past research is the Japan climate data in 1982). In this study, the temperature-humidity time product using the Japan Meteorological Agency's day-to-day flat average value from 1981 to 2010 for ASTM Equivalent cycle number, calculated from the standard year extended AMeDAS weather data from 2000 to 2010. Figure 5.6 shows the relationship between the relative dynamic modulus of elasticity and the elapsed years in each temperature / humidity time product, ASTM Equivalent cycle number.

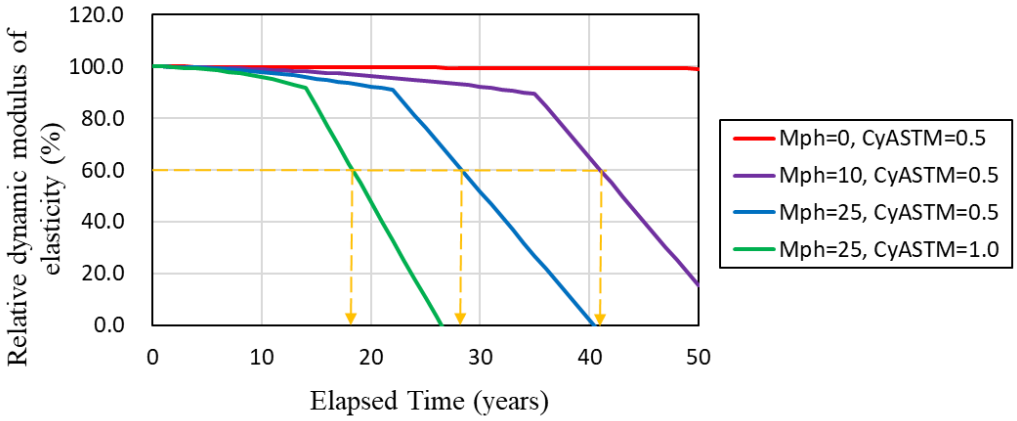

Figure 5.6 Relationship between relative dynamic modulus of elasticity and elapsed time

If the number of years in which the relative dynamic elastic modulus is 60% is taken as the service life, in the case of the same weather condition in winter, the service life is shorter as the influence of summer becomes larger. In the case where the influence of summer is the same, it can be confirmed that the severe weather condition in winter becomes tolerable and the number of years becomes shorter. Therefore, it is possible to calculate the service life by using the environmental indicator method (FD-CI).

ASTM Equivalent cycle number, the value obtained by substituting each coefficient necessary for each area used for temperature and humidity time product, and the relative dynamic elastic modulus respectively calculated from the calculation method using environmental indicator method. The service life up to 60% is shown in Table 5.3. Regarding the number of cycles equivalent to ASTM, the solar

radiation condition s is the north surface, the curing / drying condition C is 20 ° C, drying, the freezing and melting condition F is the melting in air frozen water.

The service life was calculated as cement-based materials in which the number of cycles at which the relative dynamic elastic modulus in the accelerated test was 90% was 300 cycles and the number of cycles at which the relative dynamic modulus coefficient became 60% was 600 cycles.

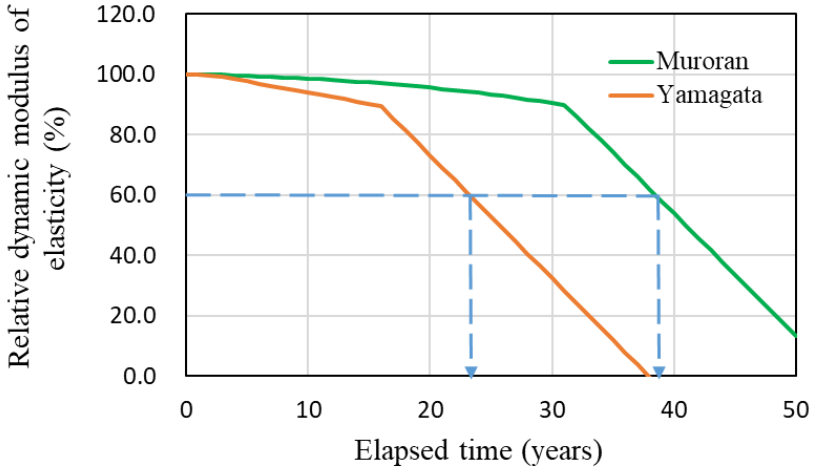

Figure 5.7 Relationship between relative dynamic modulus and elapsed time in Muroran city and Yamagata city

For the temperature-humidity time product, the service life was calculated with the water binder ratio 45% and the initial durability index 90. Compared with the service life calculated from the conventional number of cycles Equivalent to ASTM, the service life calculated using environmental indicator method proposed in this research is found to be shorter. This is thought to be due to a decrease in durability index due to pore structure change during the summer season.

Here, as an example, comparing the two areas of Muroran City in Hokkaido and Yamagata City in Honshu, the ASTM Equivalent cycle number shows almost the same value in both areas, but the temperature / humidity time product of Yamagata city is higher than Muroran city. As shown in Figure 5.7, by the relationship between relative elastic modulus and elapsed years, the service life of Yamagata city is shorter than that of Muroran City. Since Yamagata city, which has a large temperature-humidity time product,

shows a small value of service life, it can be seen that even if the same ASTM Equivalent cycle number is taken into consideration, the service life is shortened.

Also, the service life of each place calculated using environmental index is mapped. Figure 5.8 shows a map calculated from the number of cycles Equivalent to ASTM and by environmental indicator method.

Although the service life is 100 years or more regardless of Hokkaido and Honshu at ASTM Equivalent cycle number, it can be seen that the service life is shortened in most areas by environmental indicator method. Although the risk of frost damage deterioration has been evaluated solely by the influence of winter, from the environmental indicator method, considering the influence of the summer seems to be necessary for anti - freezing measures even in temperate areas.

Table 5.3 Service life of each region

Region		Number of cycles Equivalent to ASTM (times / year)		Modified maturity Mph (° D · day)	Number of cycles Equivalent to ASTM Service life (years)※1	According to FD-CI Service life (years)※2
		$Cy_{ASTM-90}$	$Cy_{ASTM-60}$			
Hokkaido	Wakkanai	0.3	1.4	14.2	510	62
	Kitami	0.6	3.2	37.7	222	27
	Asahikawa	1.1	6.2	81.9	115	13
	Abashiri	0.8	4.2	35.3	171	22
	Sapporo	0.9	4.8	76.2	147	17
	Obihiro	1.7	9.3	62.8	76	11
	Nemuro	0.7	3.8	6.9	186	43
	Suttsu	0.5	3.0	34.6	238	29
	Muroran	0.6	3.3	10.3	216	38
	Urakawa	1.2	6.9	5.3	104	35
	Hakodate	1.3	7.0	57.7	102	13
Honshu	Aomori	0.7	4.1	71.0	175	19
	Hachinohe	0.8	4.5	50.1	160	20
	Akita	0.4	2.0	100.7	349	36
	Morioka	1.1	6.2	85.4	114	13
	Miyako	0.7	4.1	46.8	175	21
	Sendai	0.2	1.2	85.6	616	62
	Yamagata	0.6	3.3	131.6	215	23
	Fukushima	0.2	1.2	155.8	616	61
	Tochigi	1.3	7.0	25.4	102	17
	Utsunomiya	0.4	2.2	133.5	328	34
	Karuizawa	1.9	10.5	22.4	67	14
	Matsumoto	1.1	5.8	154.0	122	14
	Kofu	0.3	1.7	218.7	428	43
	Takayama	1.1	6.0	119.1	119	13
	Okayama	0.2	1.2	158.5	616	61
	Asozan	0.9	5.1	14.0	140	26
	Yufuin	0.4	2.0	107.3	349	36

※1 The solar radiation condition is calculated as the service life as cement-based materials with North face, drying at 20 ° C, melting in air in frozen water, the number of cycles at which the RDM becomes 90% is 300 cycles, and the number of cycles at which the RDM becomes 60% is 600 cycles.

※2 Service life is calculated as cement-based materials with water cement ratio of 45% and initial durability index of 90.

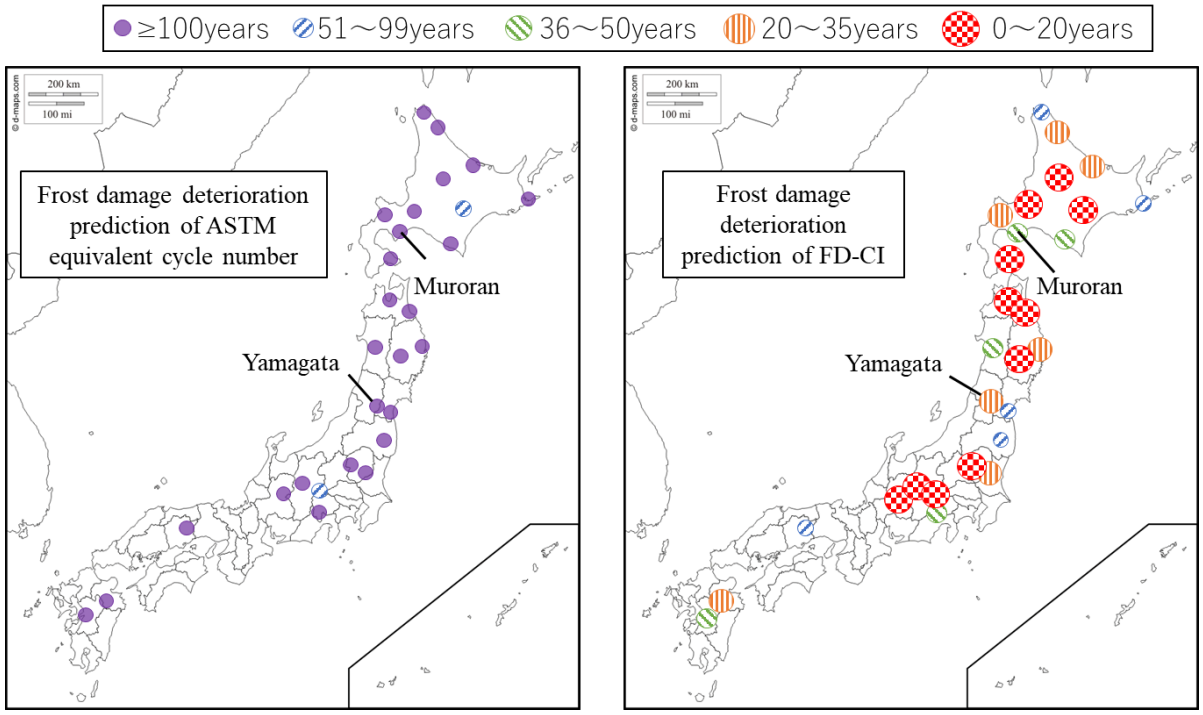

Figure 5.8 Map of service life calculated by ASTM Equivalent cycle number and by FD-CI

5.5. Estimation equation of carbonation speed due to maturity of of 150-15000 nm pores diameter

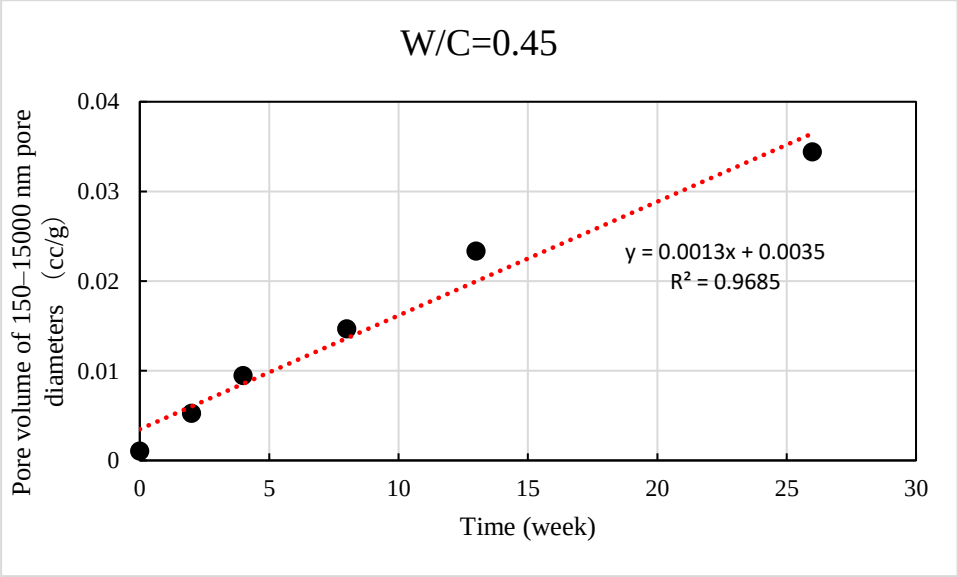

Figure 5.9 Pore volume change due to time

Figure 5.9 shows the relationship between pore volume of 150-15000 nm pore diameters and curing time. The pore volume increases with time duration. Figure 5.10 shows the relationship between pore volume of 150-15000nm diameters and carbonation speed. From Figure 5.10, the formula for estimating the carbonation speed due to pore structure change is obtained:

$$\mathrm{Ne}_{dc} = 41.064 PV_{dc} + 1.9799 \tag{44}$$

Combining equation (43) and equation (28) in Chapter 4, the estimation value of carbonation speed can be obtained as in Table 5.4.

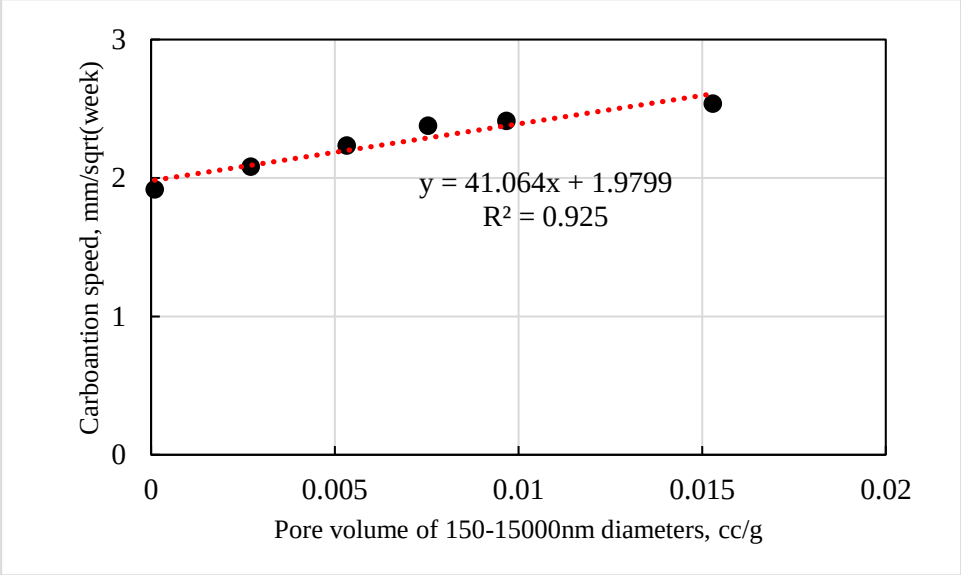

Figure 5.10 Relationship between pore volume of 150-15000nm diameters and carbonation speed

Table 5.4 Carbonation speed coefficients

Region		Sqrt of Mph (° D · day)	Estimation carbonation speed mm/sqrt(week)
Hokkaido	Wakkanai	3.77	2.08
	Kitami	6.14	2.12
	Asahikawa	9.05	2.19
	Abashiri	5.94	2.11
	Sapporo	8.73	2.18
	Obihiro	7.92	2.16
	Nemuro	2.63	2.06
	Suttsu	5.88	2.11
	Muroran	3.21	2.07
	Urakawa	2.31	2.06
	Hakodate	7.60	2.15
Honshu	Aomori	8.42	2.18
	Hachinohe	7.08	2.14
	Akita	10.03	2.23
	Morioka	9.24	2.20
	Miyako	6.84	2.13
	Sendai	9.25	2.20
	Yamagata	11.47	2.28
	Fukushima	12.48	2.32
	Tochigi	5.04	2.10
	Utsunomiya	11.55	2.29
	Karuizawa	4.73	2.09
	Matsumoto	12.41	2.32
	Kofu	14.79	2.44
	Takayama	10.91	2.26
	Okayama	12.59	2.33

5.6. Conclusions

In this study, the environmental indicator method has been used to as a forecasting method of frost damage degradation taking into consideration the influence of changes in pore structure during the summer on frost damage resistance and calculated the service life of cement-based materials for each region. When calculating the service life using environmental indicator method, the number of years is shorter than the service life calculated by ASTM Equivalent cycle number. It was found that there is a danger of frost damage deterioration and that it is necessary to take measures against freezing damage even in areas where the influence of winter season is small and the risk of frost damage deterioration was underestimated. In addition, the carbonation speed can be estimated due to pore structure change from the relationship between the pore volume of 150-15000 nm pore diameters and carbonation speed.

CHAPTER 6
CONCLUSIONS AND FUTURE WORK

CHAPTER 6 CONCLUSIONS AND FUTURE WORK

6.1. Introduction

In this study, by analyzing the influence of environmental conditions on the change of pore structure, quantifying the relationship of frost damage from pore structure change, conducting laboratory experiment and exposure to real environment, the environmental indicator method for forecasting frost damage deterioration calculated by ASTM Equivalent cycle number including winter environment and dry condition in summer is proposed.

6.2. Pore structure change due to temperature and humidity (Chapter 2)

In this chapter, in order to clarify the influence of curing conditions (temperature, curing period, moisture, water cement ratio) on pore structure change, coarsening by drying and densification by hydration reaction, the relations with the pore structure change of dry and wet repetition assuming an actual environment were arranged.

Under the condition where the relative humidity is low, the peak of pore size distribution shifts to larger diameter as the curing period progresses. It was confirmed that as the drying temperature was higher, the amount of pores with diameters of 40-2000 nm increased. Regardless of the water cement ratio, the tendency of the pore structure to coarsen with the age in all curing conditions except 20 ℃ 100% RH and 50 ℃ 100% RH was confirmed. Also, in underwater curing, since the amount of pores is small, it is considered to be densified.

Regardless of drying temperature and water cement ratio, the lower the relative humidity and the more the tendency of increasing the pore volume of the diameter of 40-2000 nm with the material age was confirmed. However, no increase in pore volume was observed at 20 °C. 75% RH, 20 °C. 100% RH, 50 °C. 100%RH. It was confirmed that as the water cement ratio was higher, the amount of pores with diameters of 40 to 2000 nm increased. Regardless of the water cement ratio, it was revealed that the upper limit of the diameter of 40 - 2000 nm pores reached the upper limit at 8 weeks of 35 ℃ 13%RH, and the upper limit value for

each water cement ratio is different. No increase in pore size of 40-2000 nm in diameter was observed in water curing, so it is considered that there is a maximum relative humidity at which pore structure change occurs.

6.3. The relationship between modified maturity and frost resistance (Chapter 3)

Chapter 3 formulates the pore structure change for each using curing conditions (temperature, curing period, water cement ratio) as elements, formulation of change in freezing harmfulness from the pore structure change which is the object of this research was carried out. Furthermore, using the proposed prediction formula, laboratory experiments and application of real environments were verified.

It was considered that there was a maximum humidity at which pore structure change occurred since no increase in pore size of 40-2000 nm in diameter was observed at relative humidity of 100% RH (underwater curing), regardless of the drying temperature. A prediction formula of pore structure change considering curing conditions (drying temperature, drying period, relative humidity, water cement ratio) proposed with the high correlation result was obtained.

The reference temperature at which the pore structure change occurs is a constant value regardless of the water cement ratio. However, at the reference humidity where the pore structure change occurs, results showing different values depending on the water cement ratio were obtained.

Based on experimental results with widely varying water cement ratio and temperature and humidity conditions, with the aim of expanding the application range of maturity function, which represents the pore structure change of mortar by drying, based on the equation of temperature and humidity time product.

Experimental results of increasing the humidity condition of this study revealed that it is not possible to represent the change in the pore volume of diameter from 40 to 2000 nm even with the temperature time function equation. Therefore the temperature humidity time product by multiplying the temperature time product by the element of the reference relative humidity was proposed. As a result, the datum temperature

and the datum relative humidity were reset and an empirical formula was obtained. The datum temperature at which the pore structure change occurs is 16 ° C regardless of the water cement ratio. In addition, it was revealed that the pore volume increases as the humidity decreases and the pore volume increases as the water cement ratio increases. A pore volume of 40 to 2000 nm in diameter and a time product of temperature and humidity were in good relation.

By using the equation expressing the temperature-humidity time product, it is possible to predict the amount of pores with a diameter of 40-2000 nm corresponding to the temperature, humidity and the water cement ratio. The datum humidity and the upper limit value were in a linear relationship with the water cement ratio, and could be expressed by a linear equation. Due to the pore structure change due to high-temperature drying in the summer, it was confirmed that the decrease in the durability index becomes larger as the annual temperature humidity time product is larger.

6.4. Effect of pore structure change on carbonation (Chapter 4)

In this chapter, in order to clarify the effect of curing conditions on pore structure change, the pore size range in which affect carbonation is investigated. It was confirmed that as the drying temperature was higher, the amount of pores with diameters of 150-15000 nm increased. Regardless of the water cement ratio, the tendency of the pore structure to coarsen with the age in all curing conditions.

No increase in pore volume was observed at 20 °C. 100% RH and 50 °C. 100%RH. It was confirmed that as the water cement ratio was higher, the amount of pores with diameters of 150-15000 nm increased.

It was considered that there was a maximum humidity at which pore structure change occurred since no increase in pore size of 150-15000 nm in diameter was observed at relative humidity of 100% RH (underwater curing), regardless of the drying temperature. A prediction formula of pore structure change considering curing conditions proposed with the high correlation result was obtained.

6.5. Service life prediction based on pore structure change (Chapter 5)

In this chapter, in predicting frost damage deterioration, the ASTM Equivalent cycle number representing the regional frost damage deterioration is used as meteorological conditions for frost damage deterioration of cement-based materials. In this study, the service life of cement-based materials is calculated for each region as forecasting method of frost damage by taking into consideration the effect of summer pore structure change on frost damage resistance; in addition to prediction of frost damage by conventional cycle number corresponding to ASTM using the proposal of environmental indicator method.

In the cycle Equivalent to ASTM, the Japanese climate data which was used in the previous research was changed and re-examination was carried out using the average month value of the Japan Meteorological Agency from 1981 to 2010. Regarding the pore structure change, the regional nature was examined by using the time product of temperature and humidity (the modified maturity function). In addition, a meteorological indicator to show the length of service life was proposed.

The relation between the annual extreme lowest temperature of the day in each region and the region coefficient shows a very good correlation in various parts of Honshu without the freezing duration, but the correspondence between them was bad. From these, it was confirmed that the regionality of the severity of the freezing and thawing action can be easily represented by the annual extreme of the daily lowest temperature.

In Hokkaido, Honshu, the higher the daily maximum temperature, the higher the temperature and humidity time product tended to be. In Hokkaido in particular, the relationship was a good result. From this, it is considered that the temperature in winter season in Hokkaido is low and outside the datum temperature and humidity of time humidity time product, the temperature in the summer seems to have influenced as it is.

It was confirmed that the decrease of the durability index was larger as the annual temperature and humidity time product was larger as the pore structure change due to high temperature drying in summer.

The service life using environmental indicator method for frost damage deterioration taking into consideration the influence of changes in pore structure during the summer on frost damage resistance was calculated. As a result, when comparing the conventional ASTM Equivalent cycle number and the environmental indicator method to service life, even in the area where influence of winter season has been small and the risk of frost damage deterioration was underestimated in the past, the service life becomes shorter considering the influence of summer has been found.

6.6. Future work

In this study, the environmental indicator method as a forecasting method of frost damage degradation was proposed and the service life of cement-based materials for each region was calculated. When calculating the service life using environmental indicator method, it was found that the number of years is shorter than the service life calculated by ASTM Equivalent cycle number. It is confirmed that there is a danger of frost damage deterioration and that it is necessary to take measures against frost damage even in areas where the influence of winter season is small and the risk of frost damage deterioration was underestimated.

The service life according to the number of cycles Equivalent to ASTM is more than 100 years in all areas, but considering drying by environmental indicator method, it will be less than 30 years in most areas. For this reason, it is important to consider the effect of drying in summer. Prediction formula of change in freezing resistance is influenced by humidity and difference of each freeze-thaw test method in laboratory experiment, micro cracks caused by drying shrinkage and frost damage deterioration in the actual environment may affect the change in frost resistance. Furthermore, it is necessary to consider the influence of the air amount on the change in frost resistance.

Since the number of cycles equivalent to ASTM and the calculation conditions of environmental indicator method are strict conditions as compared with actual conditions, it is necessary to study the correction method in the future.

Service life of cement-based materials is typically based on deterioration. In reality, existing cement-based materials are subjected to numerous of deterioration in their environments. Therefore, laboratory simulations and deterioration predictions should take into account these multiple deterioration mechanisms, when modelling service life, such as combining of both frost damage and carbonation.

REFERENCES

Abdel-Jawad, Yahia A. 2006. “The Maturity Method: Modifications to Improve Estimation of Concrete Strength at Later Ages.” *Construction and Building Materials* 20 (10):893–900. https://doi.org/10.1016/j.conbuildmat.2005.06.022.

Abell, A.B., K.L. Willis, and D.A. Lange. 1999. “Mercury Intrusion Porosimetry and Image Analysis of Cement-Based Materials.” *Journal of Colloid and Interface Science* 211 (1). Academic Press:39–44. https://doi.org/10.1006/JCIS.1998.5986.

ACI 116R. n.d. “Cement and Concrete Terminology (Reapproved 2005).”

Adolphs, J., M. J. Setzer, and P. Heine. 2002. “Changes in Pore Structure and Mercury Contact Angle of Hardened Cement Paste Depending on Relative Humidity.” *Materials and Structures* 35 (8):477–86. https://doi.org/10.1007/BF02483135.

Alexander, Mark, and Michael Thomas. 2015. “Service Life Prediction and Performance Testing — Current Developments and Practical Applications.” *Cement and Concrete Research* 78:155–64. https://doi.org/10.1016/j.cemconres.2015.05.013.

Aligizaki, Kalliopi K. 2006. *Pore Structure of Cement-Based Materials: Testing, Interpretation and Requirements*. Taylor & Francis.

Aono, Yoshimichi, Fumiaki Matsushita, Sumio Shibata, and Yukio Hama. 2007. “Nano-Structural Changes of C-S-H in Hardened Cement Paste during Drying at 50°C.” *Journal of Advanced Concrete Technology* 5 (3):313–23. https://doi.org/10.3151/jact.5.313.

Ashraf, Warda. 2016. “Carbonation of Cement-Based Materials: Challenges and Opportunities.” *Construction and Building Materials* 120:558–70. https://doi.org/10.1016/j.conbuildmat.2016.05.080.

ASTM C1074-11. 2011. *Standard Practice for Estimating Concrete Strength by the Maturity Method*.

Atarashi, Daiki, Yukio Hama, Masaru Shibuya, and Yoshimichi Aono. 2009. “Changes of Pore Structure and Frost Resistance of Mortar during Drying or Wetting-Drying.” *Cement Science and Concrete Technology* 63 (1):155–60. https://doi.org/10.14250/cement.63.155.

Bastidas-Arteaga, E., A. Chateauneuf, M. Sánchez-Silva, Ph. Bressolette, and F. Schoefs. 2010. “Influence of Weather and Global Warming in Chloride Ingress into Concrete: A Stochastic Approach.” *Structural Safety* 32 (4):238–49. https://doi.org/10.1016/J.STRUSAFE.2010.03.002.

Bastidas-Arteaga, Emilio, Franck Schoefs, Mark G. Stewart, and Xiaoming Wang. 2013. “Influence of Global Warming on Durability of Corroding RC Structures: A Probabilistic Approach.” *Engineering*

Structures 51 (June):259–66. https://doi.org/10.1016/J.ENGSTRUCT.2013.01.006.

Beaudoin, James J., and Basile T. Tamtsia. 2004. "Effect of Drying Methods on Microstructural Changes in Hardened Cement Paste: An A.C. Impedance Spectroscopy Evaluation." *Journal of Advanced Concrete Technology* 2 (1). Japan Concrete Institute:113–20. https://doi.org/10.3151/jact.2.113.

Borges, Paulo H.R., Juliana O. Costa, Neil B. Milestone, Cyril J. Lynsdale, and Roger E. Streatfield. 2010. "Carbonation of CH and C–S–H in Composite Cement Pastes Containing High Amounts of BFS." *Cement and Concrete Research* 40 (2):284–92. https://doi.org/10.1016/j.cemconres.2009.10.020.

Carino, Nicholas J., and Rajesh C. Tank. 1992. "Maturity Functions for Concretes Made with Various Cements and Admixtures." *ACI Materials Journal* 89 (2):188–96.

Chang, Honglei, Song Mu, Deqing Xie, and Penggang Wang. 2017. "Influence of Pore Structure and Moisture Distribution on Chloride 'Maximum Phenomenon' in Surface Layer of Specimens Exposed to Cyclic Drying-Wetting Condition." *Construction and Building Materials* 131:16–30. https://doi.org/10.1016/j.conbuildmat.2016.11.071.

Choi, Young Cheol, Jiyoung Kim, and Seongcheol Choi. 2017. "Mercury Intrusion Porosimetry Characterization of Micropore Structures of High-Strength Cement Pastes Incorporating High Volume Ground Granulated Blast-Furnace Slag." *Construction and Building Materials* 137:96–103. https://doi.org/10.1016/j.conbuildmat.2017.01.076.

Choo, B. S., and John Brian Newman. 2003. *Advanced Concrete Technology: Concrete Properties*. Butterworth-Heinemann.

Comité euro-international du béton. 1992. *Durable Concrete Structures : Design Guide.* Thomas Telford.

Cook, Raymond A., and Kenneth C. Hover. 1999. "Mercury Porosimetry of Hardened Cement Pastes." *Cement and Concrete Research* 29 (6):933–43. https://doi.org/10.1016/S0008-8846(99)00083-6.

Demis, Sotiris, Maria P. Efstathiou, and Vagelis G. Papadakis. 2014. "Computer-Aided Modeling of Concrete Service Life." *Cement and Concrete Composites* 47:9–18. https://doi.org/10.1016/j.cemconcomp.2013.11.004.

Diamond, Sidney. 2000. "Mercury Porosimetry: An Inappropriate Method for the Measurement of Pore Size Distributions in Cement-Based Materials." *Cement and Concrete Research* 30 (10):1517–25. https://doi.org/10.1016/S0008-8846(00)00370-7.

E. Kamada, O. Senbu, M. Tabata, and H Tanaka. 1996. "Statistical Investigation Concerning the Effects of Pore Structure on the Frost Resistance of Concrete." *Journal of Structural and Construction Engineering* No. 487:1–9.

Espinosa, Rosa Maria, and Lutz Franke. 2006. "Influence of the Age and Drying Process on Pore

Structure and Sorption Isotherms of Hardened Cement Paste." *Cement and Concrete Research* 36 (10):1969–84. https://doi.org/10.1016/j.cemconres.2006.06.010.

Galan, I., H. Beltagui, M. García-Maté, F.P. Glasser, and M.S. Imbabi. 2016. "Impact of Drying on Pore Structures in Ettringite-Rich Cements." *Cement and Concrete Research* 84:85–94. https://doi.org/10.1016/j.cemconres.2016.03.003.

Gallé, C. 2001. "Effect of Drying on Cement-Based Materials Pore Structure as Identified by Mercury Intrusion Porosimetry: A Comparative Study between Oven-, Vacuum-, and Freeze-Drying." *Cement and Concrete Research* 31 (10):1467–77. https://doi.org/10.1016/S0008-8846(01)00594-4.

Gallucci, E., X. Zhang, and K.L. Scrivener. 2013. "Effect of Temperature on the Microstructure of Calcium Silicate Hydrate (C-S-H)." *Cement and Concrete Research* 53:185–95. https://doi.org/10.1016/j.cemconres.2013.06.008.

Galobardes, Isaac, Sergio H. Cavalaro, Chris I. Goodier, Simon Austin, and Ángel Rueda. 2015. "Maturity Method to Predict the Evolution of the Properties of Sprayed Concrete." *Construction and Building Materials* 79:357–69. https://doi.org/10.1016/j.conbuildmat.2014.12.038.

Gao, Yun, Kai Wu, and Jinyang Jiang. 2016. "Examination and Modeling of Fractality for Pore-Solid Structure in Cement Paste: Starting from the Mercury Intrusion Porosimetry Test." *Construction and Building Materials* 124:237–43. https://doi.org/10.1016/j.conbuildmat.2016.07.107.

Hama, Y., Aono, Y., and Shibata, S. 2004. "Influence of Micro-Cracks on Frost Resistance of High Performance Concrete." In *JProceedings of International Conference on Durability of HPC and Final Workshop of CONLIFE,* 267–76.

Hama, Y., Kamada, E., Han, C. G. 1997. "An Experimental Study on Frost Resistance of Concrete Considering Drying Effects." In *Proceedings of the International RILEM Workshop on Resistance of Concrete to Freezing and Thawing with or without De-Icing Chemicals*, 207–14. Essen.

Hama, Y., Senbu, O., Tomosawa, F. 2002. "Effect of Curing Condition before Freezing and Thawing Test to Frost Resistance of High Performance Concrete." In *Proceedings of 6th International Symposium on High Strength/High Performance Concrete,* 1017–25.

Hama, Yukio, Kotaro Matsumura, Masayuki Tabata, Takashi Tomita, and Eiji Kamada. 1999. "Estimation of Frost Damage of Concrete Based on Meteorological Factors." *Journal of Structural and Construction Engineering (Transactions of AIJ)* 64 (523):9–16. https://doi.org/10.3130/aijs.64.9_5.

Hamami, A.A., Ph. Turcry, and A. Aït-Mokhtar. 2012. "Influence of Mix Proportions on Microstructure and Gas Permeability of Cement Pastes and Mortars." *Cement and Concrete Research* 42 (2):490–98. https://doi.org/10.1016/j.cemconres.2011.11.019.

Han, Min-Cheol, and Cheon-Goo Han. 2010. “Use of Maturity Methods to Estimate the Setting Time of Concrete Containing Super Retarding Agents.” *Cement and Concrete Composites* 32 (2):164–72. https://doi.org/10.1016/j.cemconcomp.2009.11.008.

Hasegawa, K., Hon E. 1979. “Influence of External Factors on Frost Damage of Concrete and Frost Damage Risk in Japan.”

Heede, Philip Van den, Michel De Keersmaecker, Alice Elia, Annemie Adriaens, and Nele De Belie. 2017. “Service Life and Global Warming Potential of Chloride Exposed Concrete with High Volumes of Fly Ash.” *Cement and Concrete Composites* 80:210–23. https://doi.org/10.1016/j.cemconcomp.2017.03.020.

Henriksen, C.F. 1993. “Prediction of Service Life and Choice of Repair Strategy.” In *Durability of Building Materials and Components 6, Proceedings of the Sixth International Conference Held in Omiya, Japan, Volume 2*, 1100–1106.

IUPAC. 1971. *Manual of Symbols and Terminology for Physicochemical Quantities and Units–Appendix II*. Elsevier. https://doi.org/10.1016/C2013-0-13261-8.

Jenni, A., R. Zurbriggen, L. Holzer, and M. Herwegh. 2006. “Changes in Microstructures and Physical Properties of Polymer-Modified Mortars during Wet Storage.” *Cement and Concrete Research* 36 (1):79–90. https://doi.org/10.1016/j.cemconres.2005.06.001.

Jin, Nan Ji, Inbae Seung, Yoon Sang Choi, and Jaeheum Yeon. 2017. “Prediction of Early-Age Compressive Strength of Epoxy Resin Concrete Using the Maturity Method.” *Construction and Building Materials* 152:990–98. https://doi.org/10.1016/j.conbuildmat.2017.07.066.

Jung, Woo-Yong, Young-Soo Yoon, and Young-Moo Sohn. 2003. “Predicting the Remaining Service Life of Land Concrete by Steel Corrosion.” *Cement and Concrete Research* 33 (5):663–77. https://doi.org/10.1016/S0008-8846(02)01034-7.

Khatri, R.P, and V Sirivivatnanon. 2004. “Characteristic Service Life for Concrete Exposed to Marine Environments.” *Cement and Concrete Research* 34 (5):745–52. https://doi.org/10.1016/S0008-8846(03)00086-3.

Kim, Kwang Yeom, Tae Sup Yun, and Kwang Pil Park. 2013. “Evaluation of Pore Structures and Cracking in Cement Paste Exposed to Elevated Temperatures by X-Ray Computed Tomography.” *Cement and Concrete Research* 50:34–40. https://doi.org/10.1016/j.cemconres.2013.03.020.

Kuosa, H., R.M. Ferreira, E. Holt, M. Leivo, and E. Vesikari. 2014. “Effect of Coupled Deterioration by Freeze–thaw, Carbonation and Chlorides on Concrete Service Life.” *Cement and Concrete Composites* 47:32–40. https://doi.org/10.1016/j.cemconcomp.2013.10.008.

Lachemi, M., K.M.A. Hossain, C. Anagnostopoulos, and A.R. Sabouni. 2007. “Application of Maturity Method to Slipforming Operations: Performance Validation.” *Cement and Concrete Composites* 29 (4):290–99. https://doi.org/10.1016/j.cemconcomp.2006.12.001.

Lamond, Joseph F., and J. H. Pielert. 2006. *Significance of Tests and Properties of Concrete and Concrete-Making Materials*. ASTM.

Liang, M.T., K.L. Wang, and C.H. Liang. 1999. “Service Life Prediction of Reinforced Concrete Structures.” *Cement and Concrete Research* 29 (9):1411–18. https://doi.org/10.1016/S0008-8846(99)00109-X.

Liao, Wei-Chong, B.J. Lee, and C.W. Kang. 2008. “A Humidity-Adjusted Maturity Function for the Early Age Strength Prediction of Concrete.” *Cement and Concrete Composites* 30 (6):515–23. https://doi.org/10.1016/j.cemconcomp.2008.02.006.

Malhotra, V. M., and Nicholas J. Carino. 2004. *Handbook on Nondestructive Testing of Concrete*. 2nd ed. CRC Press.

Marchand, Jacques, Michel. Pigeon, and M. Setzer. 1997. *Freeze-Thaw Durability of Concrete*. E & FN Spon.

Marques, Pedro Faustino, Carlos Chastre, and Ângela Nunes. 2013. “Carbonation Service Life Modelling of RC Structures for Concrete with Portland and Blended Cements.” *Cement and Concrete Composites* 37:171–84. https://doi.org/10.1016/j.cemconcomp.2012.10.007.

Martín-Pérez, B, H Zibara, R.D Hooton, and M.D.A Thomas. 2000. “A Study of the Effect of Chloride Binding on Service Life Predictions.” *Cement and Concrete Research* 30 (8):1215–23. https://doi.org/10.1016/S0008-8846(00)00339-2.

Marusin, Stella. 1981. “The Effect of Variation in Pore Structure on the Frost Resistance of Porous Materials.” *Cement and Concrete Research* 11 (1):115–24. https://doi.org/10.1016/0008-8846(81)90014-4.

Maruyama, Ippei, Naoki Sakamoto, Kunio Matsui, and Go Igarashi. 2017. “Microstructural Changes in White Portland Cement Paste under the First Drying Process Evaluated by WAXS, SAXS, and USAXS.” *Cement and Concrete Research* 91:24–32. https://doi.org/10.1016/j.cemconres.2016.10.002.

Meneghetti, F., and T. Meneghetti. 1985. “Non-Destructive Testing to Evaluatein Situ Maturity on Prestressed Reinforced Concrete Members.” *Materials and Structures* 18 (3):171–80. https://doi.org/10.1007/BF02472966.

Mindess, Sidney., J. Francis. Young, and David. Darwin. 2003. *Concrete*. Prentice Hall.

Moukwa, M., and P.-C. Aïtcin. 1988. “The Effect of Drying on Cement Pastes Pore Structure as Determined by Mercury Porosimetry.” *Cement and Concrete Research* 18 (5):745–52. https://doi.org/10.1016/0008-8846(88)90098-1.

Nakamura, Tohru, Yukio Hama, and Madoka Taniguchi. 2015. “Relationship between the Change of Volume of Pore Size 40-2000nm Diameter Macro Pore of Mortar in Dring Condition and Maturity.” *Journal of Structural and Construction Engineering (Transactions of AIJ)* 80 (713). Japan:981–89. https://doi.org/10.3130/aijs.80.981.

Nakamura, Tohru, Yukio Hama, and Mohamed Zakaria. 2015. “Influence of Environmental Conditions on Pore Structure Change in Mortar with Various Types of Cement.” In *Durability of Reinforced Concrete from Composition to Protection*, 155–67. Springer International Publishing. https://doi.org/10.1007/978-3-319-09921-7_14.

Neville, Adam M. 2012. *Properties of Concrete*. 5th ed. Harlow, England: Prentice Hall, Pearson.

Ngala, V.T., and C.L. Page. 1997. “Effects of Carbonation on Pore Structure and Diffusional Properties of Hydrated Cement Pastes.” *Cement and Concrete Research* 27 (7):995–1007. https://doi.org/10.1016/S0008-8846(97)00102-6.

Nurse, R. W. 1949. “Steam Curing of Concrete.” *Magazine of Concrete Research* 1 (2):79–88. https://doi.org/10.1680/macr.1949.1.2.79.

P. Kumar Mehta, and Paulo J.M. Monteiro. 2014. *Concrete: Microstructure, Properties, and Materials*. 4th ed. New York: McGraw-Hill Education.

Papadakis, V. G., M. N. Fardis, and C. G. Vayenas. 1992. “Effect of Composition, Environmental Factors and Cement-Lime Mortar Coating on Concrete Carbonation.” *Materials and Structures* 25 (5):293–304. https://doi.org/10.1007/BF02472670.

Parrott, L.J. 1981. “Effect of Drying History upon the Exchange of Pore Water with Methanol and upon Subsequent Methanol Sorption Behaviour in Hydrated Alite Paste.” *Cement and Concrete Research* 11 (5):651–58. https://doi.org/10.1016/0008-8846(81)90023-5.

———. 1992. “Variations of Water Absorption Rate and Porosity with Depth from an Exposed Concrete Surface: Effects of Exposure Conditions and Cement Type.” *Cement and Concrete Research* 22 (6):1077–88. https://doi.org/10.1016/0008-8846(92)90038-W.

Phung, Quoc Tri, Norbert Maes, Diederik Jacques, Els Bruneel, Isabel Van Driessche, Guang Ye, and Geert De Schutter. 2015. “Effect of Limestone Fillers on Microstructure and Permeability Due to Carbonation of Cement Pastes under Controlled CO2 Pressure Conditions.” *Construction and Building Materials* 82:376–90. https://doi.org/10.1016/j.conbuildmat.2015.02.093.

Phung, Quoc Tri, Norbert Maes, Diederik Jacques, Geert De Schutter, and Guang Ye. 2016. “Investigation of the Changes in Microstructure and Transport Properties of Leached Cement Pastes Accounting for Mix Composition.” *Cement and Concrete Research* 79:217–34. https://doi.org/10.1016/j.cemconres.2015.09.017.

Powers, T.C., Helmuth, R.A. 1953. “Theory of Volume Changes in Portland Cement Paste during Freezing.” In *Proc. Highway Research Board*, 285–97.

Powers, T. C. 1958. “Structure and Physical Properties of Hardened Portland Cement Paste.” *Journal of the American Ceramic Society* 41 (1):1–6. https://doi.org/10.1111/j.1151-2916.1958.tb13494.x.

Powers, T. C., and T. L. Brownyard. 1946. “Studies of the Physical Properties of Hardened Portland Cement Paste.” *ACI Journal Proceedings* 43 (9):469–504. https://doi.org/10.14359/15302.

Powers, T.C. 1949. “The Air Requirement of Frost Resistant Concrete.” In *Highway Research Board*, 184–211.

———. 1956. “Resistance of Concrete to Frost at Early Ages.” In *Proceedings RILEM Symposium on Winter Concreting*, 1–46.

———. 1965. “The Mechanism of Frost Action in Concrete.” In *Stanton Walker Lecture Series on the Materials Sciences*, 35.

Reinhardt, Hans-Wolf, and Michael Stegmaier. 2006. “Influence of Heat Curing on the Pore Structure and Compressive Strength of Self-Compacting Concrete (SCC).” *Cement and Concrete Research* 36 (5):879–85. https://doi.org/10.1016/j.cemconres.2005.12.004.

Richardson, Mark G. 2002. *Fundamentals of Durable Reinforced Concrete*. Spon Press.

Rostami, Vahid, Yixin Shao, Andrew J. Boyd, and Zhen He. 2012. “Microstructure of Cement Paste Subject to Early Carbonation Curing.” *Cement and Concrete Research* 42 (1):186–93. https://doi.org/10.1016/j.cemconres.2011.09.010.

Rostásy, F.S., R. Weiβ, and G. Wiedemann. 1980. “Changes of Pore Structure of Cement Mortars Due to Temperature.” *Cement and Concrete Research* 10 (2):157–64. https://doi.org/10.1016/0008-8846(80)90072-1.

Şahmaran, Mustafa, Erdoğan Özbay, Hasan E. Yücel, Mohamed Lachemi, and Victor C. Li. 2012. “Frost Resistance and Microstructure of Engineered Cementitious Composites: Influence of Fly Ash and Micro Poly-Vinyl-Alcohol Fiber.” *Cement and Concrete Composites* 34 (2):156–65. https://doi.org/10.1016/j.cemconcomp.2011.10.002.

Saul, A. G. A. 1951. “Principles Underlying the Steam Curing of Concrete at Atmospheric Pressure.” *Magazine of Concrete Research* 2 (6):127–40. https://doi.org/10.1680/macr.1951.2.6.127.

Šavija, Branko, and Mladena Luković. 2016. “Carbonation of Cement Paste: Understanding, Challenges, and Opportunities.” *Construction and Building Materials* 117:285–301. https://doi.org/10.1016/j.conbuildmat.2016.04.138.

Schutter, Geert De. 2004. “Applicability of Degree of Hydration Concept and Maturity Method for Thermo-Visco-Elastic Behaviour of Early Age Concrete.” *Cement and Concrete Composites* 26 (5):437–43. https://doi.org/10.1016/S0958-9465(03)00067-2.

Scrivener, Karen, Ruben Snellings, and Barbara Lothenbach. 2016. *A Practical Guide to Microstructural Analysis of Cementitious Materials*. Taylor & Francis.

Shah, Vineet, Karen Scrivener, Bishwajit Bhattacharjee, and Shashank Bishnoi. 2018. “Changes in Microstructure Characteristics of Cement Paste on Carbonation.” *Cement and Concrete Research* 109 (July). Pergamon:184–97. https://doi.org/10.1016/J.CEMCONRES.2018.04.016.

Shi, Zhenguo, Barbara Lothenbach, Mette Rica Geiker, Josef Kaufmann, Andreas Leemann, Sergio Ferreiro, and Jørgen Skibsted. 2016. “Experimental Studies and Thermodynamic Modeling of the Carbonation of Portland Cement, Metakaolin and Limestone Mortars.” *Cement and Concrete Research* 88:60–72. https://doi.org/10.1016/j.cemconres.2016.06.006.

Somerville, G., J. I. Glanville, and Adam M. Neville. 1997. *Prediction of Concrete Durability : Proceedings of STATS 21st Anniversary Conference*. E & FN Spon.

Song, Ha-Won, and Seung-Jun Kwon. 2007. “Permeability Characteristics of Carbonated Concrete Considering Capillary Pore Structure.” *Cement and Concrete Research* 37 (6):909–15. https://doi.org/10.1016/j.cemconres.2007.03.011.

Soutsos, Marios. n.d. *Concrete Durability : A Practical Guide to the Design of Durable Concrete Structures*.

Stewart, Mark G., Xiaoming Wang, and Minh N. Nguyen. 2011. “Climate Change Impact and Risks of Concrete Infrastructure Deterioration.” *Engineering Structures* 33 (4):1326–37. https://doi.org/10.1016/J.ENGSTRUCT.2011.01.010.

Taylor, H. F. W. (Harry F. W.). 1997. *Cement Chemistry*. T. Telford.

Tennis, Paul D, and Hamlin M Jennings. 2000. “A Model for Two Types of Calcium Silicate Hydrate in the Microstructure of Portland Cement Pastes.” *Cement and Concrete Research* 30 (6):855–63. https://doi.org/10.1016/S0008-8846(00)00257-X.

Tonoli, G.H.D., S.F. Santos, H. Savastano, S. Delvasto, R. Mejía de Gutiérrez, and M. del M. Lopez de Murphy. 2011. “Effects of Natural Weathering on Microstructure and Mineral Composition of Cementitious Roofing Tiles Reinforced with Fique Fibre.” *Cement and Concrete Composites* 33

(2):225–32. https://doi.org/10.1016/j.cemconcomp.2010.10.013.

Topçu, İlker Bekir, and Mehmet Uğur Toprak. 2005. “Fine Aggregate and Curing Temperature Effect on Concrete Maturity.” *Cement and Concrete Research* 35 (4):758–62. https://doi.org/10.1016/j.cemconres.2004.04.023.

Turcry, Philippe, Ahmed Loukili, Laurent Barcelo, and Jean Michel Casabonne. 2002. “Can the Maturity Concept Be Used to Separate the Autogenous Shrinkage and Thermal Deformation of a Cement Paste at Early Age?” *Cement and Concrete Research* 32 (9):1443–50. https://doi.org/10.1016/S0008-8846(02)00800-1.

Voigt, Thomas, Zhihui Sun, and Surendra P. Shah. 2006. “Comparison of Ultrasonic Wave Reflection Method and Maturity Method in Evaluating Early-Age Compressive Strength of Mortar.” *Cement and Concrete Composites* 28 (4):307–16. https://doi.org/10.1016/j.cemconcomp.2006.02.003.

Volz, Charles K., Richard L. Tucker, Ned H. Burns, and H.S. Lew. 1981. “Maturity Effects on Concrete Strength.” *Cement and Concrete Research* 11 (1):41–50. https://doi.org/10.1016/0008-8846(81)90007-7.

Waller, V., L. d’Aloïa, F. Cussigh, and S. Lecrux. 2004. “Using the Maturity Method in Concrete Cracking Control at Early Ages.” *Cement and Concrete Composites* 26 (5):589–99. https://doi.org/10.1016/S0958-9465(03)00080-5.

Washburn, Edward W. 1921. “The Dynamics of Capillary Flow.” *Physical Review* 17 (3). American Physical Society:273–83. https://doi.org/10.1103/PhysRev.17.273.

Winslow, Douglas, and Ding Liu. 1990. “The Pore Structure of Paste in Concrete.” *Cement and Concrete Research* 20 (2):227–35. https://doi.org/10.1016/0008-8846(90)90075-9.

Xuan, Dongxing, Baojian Zhan, and Chi Sun Poon. 2018. “A Maturity Approach to Estimate Compressive Strength Development of CO2-Cured Concrete Blocks.” *Cement and Concrete Composites* 85:153–60. https://doi.org/10.1016/j.cemconcomp.2017.10.005.

Y.Hama, E.Kamada, M.Tabata, and Y.Koh. 1993. “Study on Relationship between Environmental Conditions and Standard Method of Freezing-and-Thawing Test (ASTM C-666 A) on Frost Resistance of Concrete.” In *Durability of Building Materials and Components*, 1162–70.

Yikici, Tahsin Alper, and Hung-Liang (Roger) Chen. 2015. “Use of Maturity Method to Estimate Compressive Strength of Mass Concrete.” *Construction and Building Materials* 95:802–12. https://doi.org/10.1016/j.conbuildmat.2015.07.026.

Yoon, In-Seok, Oğuzhan Çopuroğlu, and Ki-Bong Park. 2007. “Effect of Global Climatic Change on Carbonation Progress of Concrete.” *Atmospheric Environment* 41 (34):7274–85.

https://doi.org/10.1016/J.ATMOSENV.2007.05.028.

Zeng, Qiang, Kefei Li, Teddy Fen-chong, and Patrick Dangla. 2012. “Pore Structure Characterization of Cement Pastes Blended with High-Volume Fly-Ash.” *Cement and Concrete Research* 42 (1):194–204. https://doi.org/10.1016/j.cemconres.2011.09.012.

Zhang, Jieying, Daniel Cusson, Paulo Monteiro, and John Harvey. 2008. “New Perspectives on Maturity Method and Approach for High Performance Concrete Applications.” *Cement and Concrete Research* 38 (12):1438–46. https://doi.org/10.1016/j.cemconres.2008.08.001.

Zhang, Peng, Folker H. Wittmann, Michael Vogel, Harald S. Müller, and Tiejun Zhao. 2017. “Influence of Freeze-Thaw Cycles on Capillary Absorption and Chloride Penetration into Concrete.” *Cement and Concrete Research* 100:60–67. https://doi.org/10.1016/j.cemconres.2017.05.018.

Zhang, Ping, Guanguo Liu, Chaoming Pang, Xile Yan, and Honggen Qin. 2017. “Influence of Pore Structures on the Frost Resistance of Concrete.” *Magazine of Concrete Research* 69 (6):271–79. https://doi.org/10.1680/jmacr.15.00471.

Zhang, Shuqiang, and Minhong Zhang. 2006. “Hydration of Cement and Pore Structure of Concrete Cured in Tropical Environment.” *Cement and Concrete Research* 36 (10):1947–53. https://doi.org/10.1016/j.cemconres.2004.11.006.

ACKNOWLEDGMENTS

It seems like just yesterday that I came to Muroran Institute of Technology when Sakura was blooming. I would like to call some people by name, without whose contributions, help and support I could not have finalised the research presented in this thesis. It is to them that I owe my deepest gratitude.

All of the experimental work was completed in the laboratory of the construction and building materials within the Department of Architecture, Civil and Environmental Engineering at Muroran Institute of Technology. I am gratefully acknowledged Muroran Institute of Technology for the financial support and the opportunity offered to me for pursuing a PhD degree.

The first person I am indebted massive thanks is Professor Hama. I would like to give my sincerest acknowledgement to him for his excellent guidance, patience, and providing me with an excellent atmosphere for doing research. He taught me to be patient, be logic, and pay more attention to the details during the research. His tireless efforts and constructive comments on this thesis are highly appreciated. In these three years, his suggestions, patience and encouragement supported me to pursue a doctorate. My thesis will not be finished without his sparkling ideas, mental support, fruitful discussions and patiently correction.

I also wished to express my appreciation to the vice supervisors, Prof. Mizoguchi and Prof. Sugata, who provided me their time, important opinions and valuable feedback for the revision of my doctoral thesis and the doctoral thesis defense presentation.

For the critical discussion on building materials topics, I would like to express my deep gratitude to Assist. Prof. Choi and Assoc. Prof. Kishimoto for the useful discussions, suggestions, guidance, support, and encouragement we had during seminar presentation in our laboratory. I am thankful to the post-doctor Kim from Korea for his suggestions and friendship.

I would also like to express a word of thankfulness to all Hama's laboratory members, Dr. Zhang, Dr.Hasegawa, Mr. Akio, Ms. Midori, Mr. Van, Mr. Yamagishi, Mr. Gota, Mr. Miwa, Mr. Shimakage, Mr. Kawamura, Mr. Matsumoto, Mr. Noguchi, Mr. Satou, Mr. Tamura, Ms. Kanako, my dear Vietnamese friends, especially to Otokoyama-Team (Mr. Ha) and all international friends, Dr. Reddy, Dr Madhu, Mrs. Shun, Dr. Owolabi, Ms. Wiwi, Dr. Guochin, Mr. Ding, Mr. Sha, Dr. Mona, Dr. Boom, Mr. Odd, Mr. Andrey, Mr. Rikky for their friendship, kindness, timely help and encouragement, especially to Miss Midori, my tutor and also my best friend; she helps every time I needed! Their friendship made my journey to finishing my study easier and my daily life rich and colorful. My warm thanks to PoreTeam members, Mr. Akio and Mr. Matsumoto for their help, technical and funny discussions, amusing talks, encouragement, and strong support.

I would like to thank Dr. Wakasugi, Dr. Kanazawa, Mr. Abe, Mr. Ao, Mr. Yamaguchi, Dr. Na, Mr. Hirata and Ms Nishikawa in Nippon Steel and Sumikin Cement Company, who provided me an opportunity to join their team as intern and gave me a lot of their guiding about SEM, XRD test, whom I have great regard and honour to work with.

I am really beholden beyond words to express my sense of gratitude to all the staffs of the centre for international relations at Muroran Institute of Technology, Mr. Endo, Ms. Noda, Ms. Chiba, Mr. Tajima, Mr. Baek, Ms. Ikeda and Japanese teacher, Assoc. Prof Ono and Assoc. Prof Yamaji for help and patiently teaching to make my life of studying abroad more perfect and make my doctoral study journey colorful and unforgettable forever.

I am grateful to my home university, Hanoi Architectural University in Vietnam, for allowing me to pursue my Ph.D. degree abroad. I would like to thank Assoc. Prof. Vương Ngọc Lưu, Assoc. Prof. Lê Quân, Assoc. Prof. Phạm Minh Hà, Assoc. Prof. Vũ Ngọc Anh, Assoc. Prof. Vũ Hoàng Hiệp, Assoc. Prof. Vũ Quốc Anh, Dr. Hoàng Văn Tùng, Dr. Nguyễn Việt Cường, Dr. Nguyễn Công Giang, Dr. Dương Quang Hùng, Dr. Đào Minh Hiếu for their introduction and recommendation and supported me to apply this PhD position in MIT.

Last but not least, I wish to acknowledge the love, support and understanding of my family, my parents, my parents-in-law, my brother-in-law and my younger sister and their son. I owe my loving thanks to my wife Nguyễn Thị Hiền and my daughter Nguyễn Thanh Hòa with her encouragement and understanding during the hard period of the PhD. We shared our joy, happiness, stress, and depression together. For being who they are, I love them so much!

Nguyễn Xuân Qúy

(Muroran, Hokkaido, Japan, March 2019)

LIST OF PUBLICATIONS

Journal papers:

1. Nguyen Xuan Quy, Junho Kim, Yukio Hama, Effect of 10-year outdoor exposure and curing conditions on the pore structure characteristics of hardened cement mortar, Journal of Advanced Concrete Technology, Vol. 16 (9), p.461-475, 2018. https://doi.org/10.3151/jact.16.461

Proceedings and International Conferences:

2. Nguyen Xuan Quy, Akio Sakaguchi, Hyeonggil Choi, Yukio Hama, Modelling the effects of Maturity on the change of Pore Structure of Mortar due to Drying Temperature and Humidity, Joint Seminar on Environmental Science and Disaster Mitigation Research (JSED 2017), Section B, p.111, Japan, 2017. (Written and Poster English Presentation)
3. Akio Sakaguchi, Yukio Hama, Shota Nagai, Nguyen Xuan Quy, Hyeonggil Choi, Maturity of Temperature and Humidity that presents the change of Pore Structure of Mortar by Drying condition, Proceedings of 10th International Symposium Between Korea, China and Japan on Performance Improvement of Conrete for Long Life Span Structure (PICLS 2016), Part 2, p.99, Korea, 2016.
4. Nguyen Xuan Quy, A study on Pore Structure Change and Carbonation of Mortar due to Drying-Wetting Cycles, Dokukon 2016 Muroran Institute of Technology Graduate School of Engineering Doctoral Student Research Presentation, Tokyo, Japan, 2016. (Poster English Presentation)
5. Nguyen Xuan Quy, Akio Sakaguchi, Kouta Matsumoto, Hyeonggil Choi, Yukio Hama, The Modified Maturity Function in Frost Damage Prediction of Cement-based Materials due to Environmental Conditions, Proceedings of AIJ Hokkaido Architectural Research Conference, No.90, p.17, Japan, 2017. (Written and Oral English Presentation)
6. Nguyen Xuan Quy, Akio Sakaguchi, Hyeonggil Choi, Yukio Hama, Service Lifetime Prediction of Cement-Based Materials in Cold Weather Regions, Proceedings of 11th International Symposium Between Korea, China and Japan on Performance Improvement of Conrete for Long Life Span Structure (PICLS 2017), Part 4, p.189, Japan, 2017. (Written and Oral English Presentation Award)
7. Kouta Matsumoto, Nguyen Xuan Quy, Hyeonggil Choi, Yukio Hama, A study on the proposal of climate index for frost damage of concrete, Proceedings of the 13th Korea-Japan Joint Symposium on Building Materials and Construction, Vol.13, p.103-108, Korea, Aug. 2017, (Moohan Kim Award Best Paper in Japanese)
8. Nguyen Xuan Quy, Kouta Matsumoto, Yukio Hama, The effect of Environmental Conditions on Service Life of Mortar corresponding Meteorological Index, Joint Seminar on Environmental Science

and Disaster Mitigation Research (JSED 2018), Section B, p.151, Japan, 2018. (Written and Poster English Presentation)

9. Kouta Matsumoto, Nguyen Xuan Quy, Hyeonggil Choi, Yukio Hama, Study on maturity of temperature and humidity describe the change of pore structure by drying condition of mortar using different type of cement, Joint Seminar on Environmental Science and Disaster Mitigation Research (JSED 2018), Section A, p.83, Japan, 2018.
10. Kouta Matsumoto, Nguyen Xuan Quy, Yukio Hama, Pore structure and properties of mortar specimens using different types of cement exposed outdoor for 10 years, Proceedings of 12th International Symposium Between Korea, China and Japan on Performance Improvement of Conrete for Long Life Span Structure (PICLS 2018), Part 1, p.95, China, 2018. (Written and Oral English Presentation Award)
11. Takumi Noguchi, Kouta Matsumoto, Nguyen Xuan Quy, Yukio Hama, Mapping of FRPST damage climate indexes using mesh climate value, Proceedings of 12th International Symposium Between Korea, China and Japan on Performance Improvement of Conrete for Long Life Span Structure (PICLS 2018), Part 2, p.272, China, 2018.
12. 松本皓太, Nguyen Xuan Quy, 崔　亨吉, 濱　幸雄, 各種セメントに対応した乾燥によるモルタルの細孔構造変化を表す温湿度時間積, 日本建築学会北海道支部　第 90 回研究発表会、室蘭, 北海道、日本、2017.
13. 松本 皓太, 野口 巧巳, Nguyen Xuan Quy, 濱　幸雄, コンクリートの凍害劣化を対象とした環境指標の提案: その 1 乾燥の影響を考慮したコンクリートの凍害劣化予測, 自然環境下のコンクリート劣化に関するシンポジウムソンホソ, 自然環境下のコンクリート劣化研究委員会, JCI –C95, p.235-240, 日本、 2018.
14. 野口 巧巳, 松本 皓太, Nguyen Xuan Quy, 濱　幸雄, コンクリートの凍害劣化を対象とした環境指標の提案その 2 メッシュ気候値を用いた凍害環境指標のマップ化, 自然環境下のコンクリート劣化に関するシンポジウム, 自然環境下のコンクリート劣化研究委員会 , JCI –C95, p. 241-248, 日本、 2018.